CHAPTER 11

RADIATIVE PROPERTIES OF MOLECULAR GASES

11.1 FUNDAMENTAL PRINCIPLES

Radiative transfer characteristics of an opaque wall can often be described with good accuracy by the very simple model of gray and diffuse emission, absorption, and reflection. The radiative properties of a molecular gas, on the other hand, vary so strongly and rapidly across the spectrum that the assumption of a "gray" gas is almost never a good one [1]. In the present chapter a short development of the radiative properties of molecular gases is given. Other elaborate discussions can be found, for example, in the book by Goody and Yung [2], in the monograph by Tien [3], and in the very recent treatise of Taine and Soufiani [4].

Most of the earlier work was not in the area of heat transfer but rather was carried out by astronomers, who had to deal with light absorption within Earth's atmosphere, and by astrophysicists, who studied the spectra of stars. The study of atmospheric radiation was apparently initiated by Lord Rayleigh [5] and Langley [6] in the late nineteenth century. The radiation spectra of stars started to receive attention in the early twentieth century, for example by Eddington [7] and Chandrasekhar [8, 9]. The earliest measurements of radiation from hot gases were reported by Paschen, a physicist, in 1894 [10], but his work was apparently ignored by heat transfer engineers for many years [11].

The last few decades have seen much progress in the understanding of molecular gas radiation, in particular the radiation from water vapor and carbon dioxide, which is of great importance in the combustion of hydrocarbon fuels, and which also dominates atmospheric radiation with its thermodynamic implications on Earth's atmosphere. The combination of the two, i.e., the man-made strong increases in the atmosphere's CO_2 content, giving rise to "global warming," is perhaps *the* most pressing problem facing mankind today. Much of the pioneering work since the late 1920s was done by Hottel and coworkers [12–19] (measurements and practical calculations) and by Penner [20] and Plass [21, 22] (theoretical basis).

When a photon (or an electromagnetic wave) interacts with a gas molecule, it may be either absorbed, raising the molecule's energy level, or scattered, changing the direction of travel of the photon. Conversely, a gas molecule may spontaneously lower its energy level by the emission of an appropriate photon. As will be seen in the next chapter on particle properties (since every molecule is, of course, a very small particle), the scattering of photons by molecules is always negligible for heat transfer applications. There are three different types of radiative transitions that lead to a change of molecular energy level by emission or absorption of a photon: (*i*) transitions between nondissociated ("bound") atomic or molecular states, called *bound–bound transitions*, (*ii*) transitions from a "bound" state to a "free" (dissociated) one (absorption) or

from "free" to "bound" (emission), called *bound–free transitions*, and (*iii*) transitions between two different "free" states, *free–free transitions*.

The internal energy of every atom and molecule depends on a number of factors, primarily on the energies associated with electrons spinning at varying distances around the nucleus, atoms within a molecule spinning around one another, and atoms within a molecule vibrating against each other. Quantum mechanics postulates that the energy levels for atomic or molecular electron orbit as well as the energy levels for molecular rotation and vibration are quantized; i.e., electron orbits and rotational and vibrational frequencies can only change by certain discrete amounts. Since the energy contained in a photon or electromagnetic wave is directly proportional to frequency, quantization means that, in *bound–bound* transitions, photons must have a certain frequency (or wavelength) in order to be captured or released, resulting in discrete spectral lines for absorption and emission. Since, according to Heisenberg's *uncertainty principle*, the energy level of an atom or molecule cannot be fixed precisely, this phenomenon (and, as we shall see, some others as well) results in a slight broadening of these spectral lines.

Changing the orbit of an electron requires a relatively large amount of energy, or a high-frequency photon, resulting in absorption–emission lines at short wavelengths between the ultraviolet and the near-infrared (between $10^{-2}\,\mu$m and $1.5\,\mu$m). Vibrational energy level changes require somewhat less energy, so that their spectral lines are found in the infrared (between $1.5\,\mu$m and $10\,\mu$m), while changes in rotational energy levels call for the least amount of energy and, thus, rotational lines are found in the far infrared (beyond $10\,\mu$m). Changes in vibrational energy levels may (and often must) be accompanied by rotational transitions, leading to closely spaced groups of spectral lines that, as a result of line broadening, may partly overlap and lead to so-called *vibration–rotation bands* in the infrared. Similarly, electronic transitions in molecules (as opposed to atoms) are always accompanied by vibrational and rotational energy changes, generally in the ultraviolet to the near-infrared.

If the initial energy level of a molecule is very high (e.g., in very high-temperature gases), then the absorption of a photon may cause the breaking-away of an electron or the breakup of the entire molecule because of too strong vibration, i.e., a *bound–free* transition. The postabsorption energy level of the molecule depends on the kinetic energy of the separated part, which is essentially not quantized. Therefore, *bound–free* transitions result in a continuous absorption spectrum over all wavelengths or frequencies for which the photon energy exceeds the required ionization or dissociation energy. The same is true for the reverse process, emission of a photon in a *free–bound* transition (often called *radiative combination*).

In an ionized gas free electrons can interact with the electric field of ions resulting in a *free–free* transition (also known as *Bremsstrahlung*, which is German for *brake radiation*); i.e., the release of a photon lowers the kinetic energy of the electron (decelerates it), or the capture of a photon accelerates it (*inverse Bremsstrahlung*). Since kinetic energy levels of electrons are essentially not quantized, these photons may have any frequency or wavelength.

Bound–free and *free–free* transitions generally occur at very high temperatures (when dissociation and ionization become substantial). The continuum radiation associated with them is usually found at short wavelengths (ultraviolet to visible). Therefore, these effects are of importance only in extremely high-temperature situations. Most engineering applications occur at moderate temperature levels, with little ionization and dissociation, making *bound–bound* transitions most important. At combustion temperatures the emissive power has its maximum in the infrared (between $1\,\mu$m and $6\,\mu$m), giving special importance to vibration–rotation bands. In this book we will focus our discussion on the most important case of bound–bound transitions.

11.2 EMISSION AND ABSORPTION PROBABILITIES

There are three different processes leading to the release or capture of a photon, namely, *spontaneous emission*, *induced* or *stimulated emission* (also called *negative absorption*), and *absorption*. The

absorption and emission coefficients associated with these transitions may, at least theoretically, be calculated from quantum mechanics. Complete descriptions of the microscopic phenomena may be found in books on statistical mechanics [23,24] or spectroscopy [25,26]. An informative (rather than precise) synopsis has been given by Tien [3] that we shall essentially follow here.

Let there be n_u atoms or molecules (per unit volume) at a nondegenerate higher energy state u and n_l at a lower energy state l. "Nondegenerate" means that, if there are several states with identical energies (*degeneracy*), each state is counted separately. The difference of energy between the two states is $h\nu$. The number of transitions from state u to state l by release of a photon with energy $h\nu$ (spontaneous emission) must be proportional to the number of atoms or molecules at that level. Thus

$$\left(\frac{dn_u}{dt}\right)_{u\to l} = -A_{ul}n_u, \tag{11.1}$$

where the proportionality constant A_{ul} is known as the *Einstein coefficient for spontaneous emission*. Spontaneous emission is isotropic, meaning that the direction of the emitted photon is random, resulting in equal emission intensity in all directions. Quantum mechanics postulates that, in addition to spontaneous emission, incoming radiative intensity (or photon streams) with the appropriate frequency may induce the molecule to emit photons into the same direction as the incoming intensity (stimulated emission). Therefore, the total number of transitions from state u to state l may be written as

$$\left(\frac{dn_u}{dt}\right)_{u\to l} = -n_u\left(A_{ul} + B_{ul}\int_{4\pi} I_\nu\, d\Omega\right), \tag{11.2}$$

where I_ν is the incoming intensity, which must be integrated over all directions to account for all possible transitions, and B_{ul} is the *Einstein coefficient for stimulated emission*. Finally, part of the incoming radiative intensity may be absorbed by molecules at energy state l. Obviously, the absorption rate will be proportional to the strength of incoming radiation as well as the number of molecules that are at energy state l, leading to

$$\left(\frac{dn_l}{dt}\right)_{l\to u} = n_l B_{lu}\int_{4\pi} I_\nu\, d\Omega, \tag{11.3}$$

where B_{lu} is the *Einstein coefficient for absorption*. The three Einstein coefficients may be related to one another by considering the special case of equilibrium radiation. Equilibrium radiation occurs in an isothermal black enclosure, where the radiative intensity is everywhere equal to the blackbody intensity $I_{b\nu}$ and where the average number of molecules at any given energy level is constant at any given time, i.e., the number of transitions from all upper energy levels u to all lower states l is equal to the ones from l to u, or

$$g_u\left(\frac{dn_u}{dt}\right)_{u\to l} + g_l\left(\frac{dn_l}{dt}\right)_{l\to u} = -g_u n_u\left(A_{ul} + B_{ul}\int_{4\pi} I_{b\nu}\, d\Omega\right) + g_l n_l B_{lu}\int_{4\pi} I_{b\nu}\, d\Omega = 0, \tag{11.4}$$

where g_u and g_l are the degeneracies of the upper and lower energy state, respectively, i.e., the number of different arrangements with which a molecule can obtain this energy level. At local thermodynamic equilibrium the number of particles at any energy level is governed by Boltzmann's distribution law [23], leading to

$$n_l/n_u = e^{-E_l/kT}\Big/e^{-E_u/kT} = e^{h\nu/kT}, \tag{11.5}$$

where E_u and E_l are the energy levels associated with states u and l, respectively. Thus, the blackbody intensity may be evaluated from equation (11.4) as

$$I_{b\nu} = \frac{1}{4\pi}\frac{A_{ul}/B_{ul}}{(g_l B_{lu}/g_u B_{ul})\, e^{h\nu/kT} - 1}. \tag{11.6}$$

Comparison with Planck's law, equation (1.9), shows that all three Einstein coefficients are dependent upon another, namely,

$$A_{ul} = \frac{8\pi h\nu^3}{c_0^2} B_{ul}, \quad g_u B_{ul} = g_l B_{lu}. \tag{11.7}$$

The Einstein coefficients are universal functions for a given transition and, therefore, the relationships between them hold also if local thermodynamic equilibrium does not prevail (i.e., the energy level populations do not obey Boltzmann's distribution, equation (11.5).

The one remaining independent Einstein coefficient is clearly an indicator of how strongly a gas is able to emit and absorb radiation. This is most easily seen by examining the number of induced transitions (by absorption and emission) in a single direction (or within a thin pencil of rays). If

$$\frac{d}{d\Omega}\left(g\frac{dn}{dt}\right)_{l\leftrightarrow u} = (g_l n_l B_{lu} - g_u n_u B_{ul}) I_\nu \tag{11.8}$$

is the net number of photons removed from the pencil of rays per unit time and per unit volume, then—since each photon carries the energy $h\nu$—the change of radiative energy per unit time, per unit area and distance, and per unit solid angle is

$$-h\nu\frac{d}{d\Omega}\left(g\frac{dn}{dt}\right)_{l\leftrightarrow u} = -(g_l n_l B_{lu} - g_u n_u B_{ul}) h\nu I_\nu. \tag{11.9}$$

This relation is equivalent to equation (10.1), except that in reality the spectral line associated with a transition between an upper energy state u and a lower energy state l is "broadened," i.e., transitions occur across a (very small) range of frequencies, and equation (11.9) captures all of these transitions. Accounting for this slight spread in frequencies (and recalling the definition of intensity, Section 1.6), we have

$$\frac{d}{ds}\int_{\Delta\nu} I_\nu \, d\nu = -(g_l n_l B_{lu} - g_u n_u B_{ul}) h\nu I_\nu = -\int_{\Delta\nu} (g_l n_l B'_{lu} - g_u n_u B'_{ul}) h\nu I_\nu \, d\nu, \tag{11.10}$$

i.e., the Einstein probabilities are not defined for a single transition frequency, but rather are spread over a small but finite frequency range $\Delta\nu$ due to broadening, with [27]

$$A'_{ul} = A_{ul}\phi_\nu, \quad B'_{ul} = B_{ul}\phi_\nu, \quad B'_{lu} = B_{lu}\phi_\nu, \tag{11.11}$$

and $\phi_\nu(\nu)$ is a *normalized line shape function* (assumed here to be equal for all three probabilities),

$$\int_{\Delta\nu} \phi_\nu(\nu) \, d\nu = 1. \tag{11.12}$$

The exact shape of line broadening will be discussed in detail in Section 11.4. Using equation (11.11) we can rewrite equation (11.10) as

$$\frac{d}{ds}\int_{\Delta\nu} I_\nu \, d\nu = -(g_l n_l B_{lu} - g_u n_u B_{ul}) \int_{\Delta\nu} h\nu\phi_\nu I_\nu \, d\nu. \tag{11.13}$$

This relation gives the absorption of an entire line, and we define the *line strength* or *line intensity* as

$$S_\nu = (g_l n_l B_{lu} - g_u n_u B_{ul}) \int_{\Delta\nu} h\nu\phi_\nu \, d\nu = (g_l n_l B_{lu} - g_u n_u B_{ul}) h\nu. \tag{11.14}$$

In the last expression of equation (11.14) the (line-center) frequency has been taken out of the integral, since ν varies very little across a narrow spectral line. By the definition of the absorption

coefficient the line strength is the (linear) absorption coefficient integrated across a line. On a spectral basis across $\Delta\nu$, this becomes

$$S_\nu = \int_{\Delta\nu} \kappa_\nu \, d\nu, \quad \text{and} \quad \kappa_\nu = S_\nu \phi_\nu, \tag{11.15}$$

so that

$$\frac{dI_\nu}{ds} = -\kappa_\nu I_\nu, \tag{11.16}$$

which is, of course, identical to equation (10.1). The absorption coefficient as defined here is often termed the *effective absorption coefficient* since it incorporates stimulated emission (or negative absorption). Sometimes a *true absorption coefficient* is defined from

$$\int_{\Delta\nu} \kappa_\nu \, d\nu = g_l n_l B_{lu} h\nu. \tag{11.17}$$

Since stimulated emission and absorption always occur together and cannot be separated, it is general practice to incorporate stimulated emission into the absorption coefficient, so that only the effective absorption coefficient needs to be considered.[1] Examination of equation (11.14) shows that the absorption coefficient is proportional to molecular number density. Therefore, as mentioned earlier, a number of researchers take the number density out of the definition for κ_ν either in the form of density or pressure, by defining a *mass absorption coefficient* or a *pressure absorption coefficient*, respectively, as

$$\kappa_{\rho\nu} \equiv \frac{\kappa_\nu}{\rho}, \quad \kappa_{p\nu} \equiv \frac{\kappa_\nu}{p}, \tag{11.18}$$

and similarly for S_ν. If a mass or pressure absorption coefficient is used, then a ρ or p must, of course, be added to equation (11.16).[2]

The negative of equation (11.1) gives the rate at which molecules emit photons of strength $h\nu$ randomly into all directions (into a solid angle of 4π) and per unit volume. Thus, multiplying this equation by $-h\nu$ and dividing by 4π gives isotropic energy emitted per unit time, per unit solid angle, per unit area and distance along a pencil of rays or, in short, the change of intensity per unit distance due to spontaneous emission:

$$\frac{d}{ds}\int_{\Delta\nu} I_\nu \, d\nu = -h\nu \frac{d}{d\Omega}\left(\frac{dn}{dt}\right)_{u\to l} = g_u n_u A_{ul} h\nu/4\pi. \tag{11.19}$$

This is the emission of an entire line and, on a spectral basis across $\Delta\nu$ this becomes

$$\frac{dI_\nu}{ds} = g_u n_u A'_{ul} h\nu/4\pi = j_\nu, \tag{11.20}$$

and j_ν is called the *emission coefficient*, which is related to the absorption coefficient through equations (11.7), (11.14), and (11.15), leading to

$$j_\nu = \kappa_\nu \frac{2h\nu^3}{c_0^2} \frac{n_u}{n_l - n_u}, \tag{11.21}$$

[1] Since it is experimentally impossible to distinguish stimulated emission from absorption, its existence had initially been questioned. Equation (11.6) is generally accepted as proof that stimulated emission does indeed exist: Without it $B_{ul} \to 0$ and the blackbody intensity would be governed by Wien's distribution, equation (1.18), which is known to be incorrect.

[2] Thus, depending on what spectral variable is employed (wavelength λ, wavenumber η, or frequency ν), a spectrally integrated absorption coefficient may appear in nine different variations. Often the only way to determine which definition has been used is to carefully check the units given.

At local thermodynamic equilibrium energy levels are populated according to Boltzmann's distribution, equation (11.5), and the emission coefficient and equation (11.20) reduce to

$$\frac{dI_\nu}{ds} = j_\nu = \kappa_\nu I_{b\nu}, \tag{11.22}$$

which represents the augmentation of directional intensity due to spontaneous emission, as given by equation (10.10).

11.3 ATOMIC AND MOLECULAR SPECTRA

We have already seen that the emission or absorption of a photon goes hand in hand with the change of rotational and/or vibrational energy levels in molecules, or with the change of electron orbits (in atoms and molecules). This change, in turn, causes a change in radiative intensity resulting in *spectral lines*. In this section we discuss briefly how the position of spectral lines within a vibration–rotation band can be calculated, since it is these bands that are of great importance to the heat transfer engineer. More detailed information as well as discussion of electronic spectra, and bound–free and free–free transitions may be found in more specialized books on quantum mechanics [24,25,28] or spectroscopy [26,29–31], in the book on atmospheric radiation by Goody and Yung [2], or in the monographs on gas radiation properties by Tien [3] and Taine and Soufiani [4].

Since every particle moves in three-dimensional space, it has three degrees of freedom: It can move in the forward–backward, left–right, and/or upward–downward directions. If two or more particles are connected with each other (diatomic and polyatomic molecules), then each of the atoms making up the molecule has three degrees of freedom. However, it is more convenient to say that a molecule consisting of N atoms has three degrees of freedom for translation, and $3N - 3$ degrees of freedom for relative motion between atoms. These $3N - 3$ degrees of internal freedom may be further separated into rotational and vibrational degrees of freedom. This fact is illustrated in Fig. 11-1 for a diatomic molecule and for linear and nonlinear triatomic molecules. The diatomic molecule has three internal degrees of freedom. Obviously, it can rotate around its center of gravity within the plane of the paper or, similarly, perpendicularly to the paper (with the rotation axis lying in the paper). It could also rotate around its own axis; however, neither one of the atoms would move (except for rotating around itself). Thus, the last degree of freedom must be used for vibrational motion between the two atoms as indicated in the figure. The situation gets rapidly more complicated for molecules with increasing number of atoms. For linear triatomic molecules (e.g., CO_2, N_2O, HCN) there are, again, only two rotational modes. Since there are six internal degrees of freedom, there are four vibrational modes, as indicated in Fig. 11-1. However, two of these vibrational modes are identical, or *degenerate* (except for taking place in perpendicular planes). In contrast, a nonlinear triatomic molecule has three rotational modes: In this case rotation around the horizontal axis in the plane of the paper is legitimate, so that there are only three vibrational degrees of freedom. Depending on the axis of rotation, a polyatomic molecule may have different moments of inertia for each of the three rotational modes. If symmetry is such that all three moments of inertia are the same, the molecule is classified as a *spherical top* (e.g., CH_4). It is called a *symmetric top*, if two are the same (e.g., NH_3, CH_3Cl, C_2H_6, SF_6), and an *asymmetric top*, if all three are different (e.g., H_2O, O_3, SO_2, NO_2, H_2S, H_2O_2).

Rotational Transitions

To calculate the allowed rotational energy level from quantum mechanics using *Schrödinger's wave equation* (see, for example, [23,24]), we generally assume that the molecule consists of point

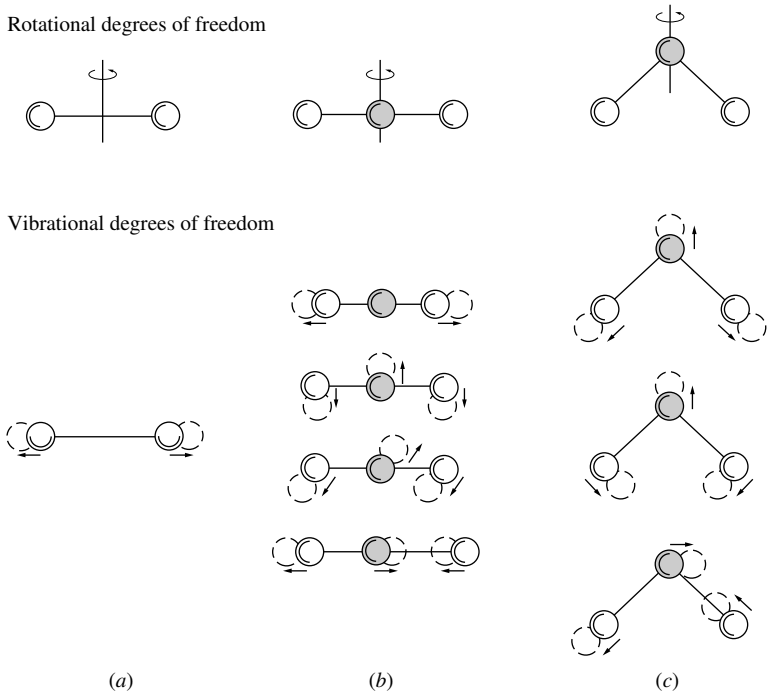

FIGURE 11-1
Rotational and vibrational degrees of freedom for (*a*) diatomic, (*b*) linear triatomic, and (*c*) nonlinear triatomic molecules.

masses connected by rigid massless rods, the so-called *rigid rotator model*. The solution to this wave equation dictates that possible energy levels for a linear molecule are limited to

$$E_j = \frac{\hbar^2}{2I} j(j+1) = hc_0 B j(j+1), \quad j = 0, 1, 2, \ldots \ (j \text{ integer}), \tag{11.23}$$

where $\hbar = h/2\pi$ is the modified Planck's constant, I is the moment of inertia of the molecule, j is the rotational quantum number, and the abbreviation B has been introduced for later convenience. Allowed transitions are $\Delta j = \pm 1$ and 0 (the latter being of importance for a simultaneous vibrational transition); this expression is known as the *selection rule*. In the case of the absorption of a photon ($j \to j+1$ transition) the wavenumbers of the resulting spectral lines can then be determined[3] as

$$\begin{aligned} \eta = (E_{j+1} - E_j)/hc_0 &= B(j+1)(j+2) - Bj(j+1) \\ &= 2B(j+1), \qquad\qquad j = 0, 1, 2, \ldots . \end{aligned} \tag{11.24}$$

The results of this equation produce a number of equidistant spectral lines (in units of wavenumber or frequency), as shown in the sketch of Fig. 11-2.

The rigid rotator model turns out to be surprisingly accurate, although for high rotation rates ($j \gg 0$) a small correction factor due to the centrifugal contribution (stretching of the "rod") may be considered. Not all linear molecules exhibit rotational lines, since an electric dipole moment is required for a transition to occur. Thus, diatomic molecules such as O_2 and N_2 never undergo rotational transitions, while symmetric molecules such as CO_2 show a rotational spectrum only if accompanied by a vibrational transition [3]. Evaluation of the spectral lines of nonlinear polyatomic molecules is always rather complicated and the reader is referred to specialized treatises such as the one by Herzberg [30].

[3]In our discussion of surface radiative transport we have used wavelength λ as the spectral variable throughout, largely to conform with the majority of other publications. However, for gases frequency ν or wavenumber η are considerably more convenient to use [see, for example, equation (11.24)]. Again, to conform with the majority of the literature, we shall use wavenumber throughout this part.

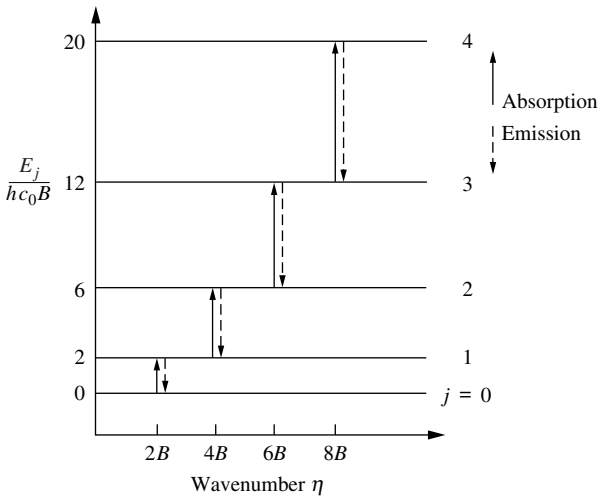

FIGURE 11-2
Spectral position and energy levels for a rigid rotator.

Vibrational Transitions

The simplest model of a vibrating diatomic molecule assumes two point masses connected by a perfectly elastic massless spring. Such a model leads to a harmonic oscillation and is, therefore, called the *harmonic oscillator*. For this case the solution to Schrödinger's wave equation for the determination of possible vibrational energy levels is readily found to be

$$E_v = h\nu_e(v + \tfrac{1}{2}), \quad v = 0, 1, 2, \ldots \ (v \text{ integer}), \tag{11.25}$$

where ν_e is the equilibrium frequency of harmonic oscillation or *eigenfrequency*, and v is the vibrational quantum number. The selection rule for a harmonic oscillator is $\Delta v = \pm 1$ and, thus, one would expect a single spectral line at the same frequency as the harmonic oscillation, or at a wavenumber

$$\eta = (E_{v+1} - E_v)/hc_0 = (\nu_e/c_0)(v + 1 - v) = \nu_e/c_0, \tag{11.26}$$

as indicated in Fig. 11-3. Unfortunately, the assumption of a harmonic oscillator leads to considerably less accurate results than the one of a rigid rotator. This fact is easily appreciated by looking at Fig. 11-4, which depicts the molecular energy level of a diatomic molecule *vs.* interatomic distance: When atoms move toward each other repulsive forces grow more and more rapidly, while the opposite is true when the atoms move apart. The heavy line in Fig. 11-4 shows the minimum and maximum distances between atoms for any given vibrational energy state

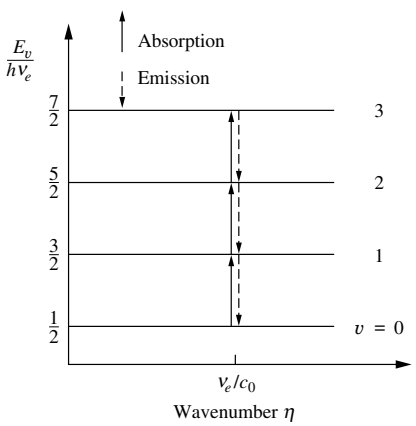

FIGURE 11-3
Spectral position and energy levels for a harmonic oscillator.

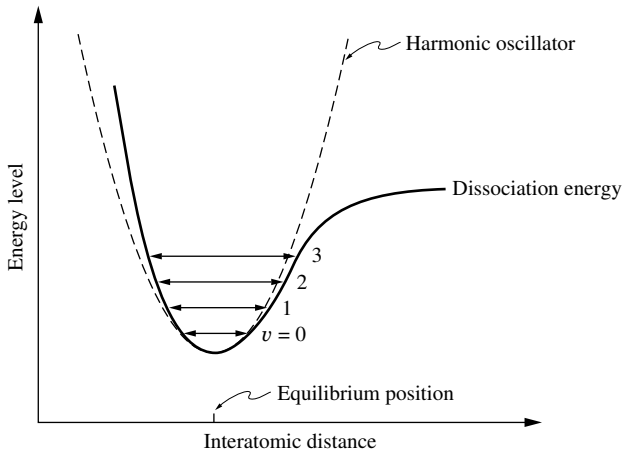

FIGURE 11-4
Energy level *vs.* interatomic distance.

(showing also that the molecule may dissociate if the energy level becomes too high). In a perfectly elastic spring, force increases linearly with displacement, leading to a symmetric quadratic polynomial for the displacement limits as also indicated in the figure. If a more complicated spring constant is included in the analysis, this results in additional terms in equation (11.25); and the selection rule changes to $\Delta v = \pm 1, \pm 2, \pm 3, \ldots$, producing several approximately equally spaced spectral lines. The transition corresponding to $\Delta v = \pm 1$ is called the *fundamental*, or the *first harmonic*, and usually is by far the strongest one. The transition corresponding to $\Delta v = \pm 2$ is called the *first overtone* or *second harmonic*, and so on. For example, CO has a strong fundamental band at $\eta_0 = 2143\,\text{cm}^{-1}$ and a much weaker first overtone band at $\eta_0 = 4260\,\text{cm}^{-1}$ (see the data in Table 11.3 in Section 11.10).

In the literature the vibrational state of a molecule is identified by the values of the vibrational quantum numbers. For example, the vibrational state of a nonlinear, triatomic molecule, such as H_2O, with its three different vibrational modes, is identified as $(v_1 v_2 v_3)$. The case is a little bit more complicated for molecules with degeneracies. For example, the linear CO_2 molecule has three different vibrational modes, the second one being doubly degenerate (see Fig. 11-1); its vibrational state is defined by $\left(v_1 {v_2}^{l_2} v_3\right)$ or $(v_1 v_2 l_2 v_3)$, where $0 \le l_2 \le v_2$ is an angular momentum quantum number, describing the rotation of the molecule caused by different vibrations in perpendicular planes. More details on these issues are given by Taine and Soufiani [4] and by Herzberg [30].

Combined Vibrational–Rotational Transitions

Since the energy required to change the vibrational state is so much larger than that needed for rotational changes, and since both transitions can (and indeed often must) occur simultaneously, this requirement leads to many closely spaced lines, also called a vibration–rotation band, centered around the wavenumber $\eta = \nu_e / c_0$, which is known as the *band origin* or *band center*.

For the simplest model of a rigid rotator combined with a harmonic oscillator, assuming both modes to be independent, the combined energy level at quantum numbers j, v is given by

$$E_{vj} = h\nu_e(v + \tfrac{1}{2}) + B_v j(j+1), \quad v, j = 0, 1, 2, \ldots. \tag{11.27}$$

Since the small error due to the assumption of a totally rigid rotator can result in appreciable total error when a large collection of simultaneous vibration–rotation transition is considered, allowance has been made in the above expression for the fact that B_v (or the molecular moment of inertia) may depend on the vibrational energy level. The allowed transitions ($\Delta v = \pm 1$ combined with $\Delta j = \pm 1, 0$) lead to three separate branches of the band, namely P ($\Delta j = -1$), Q

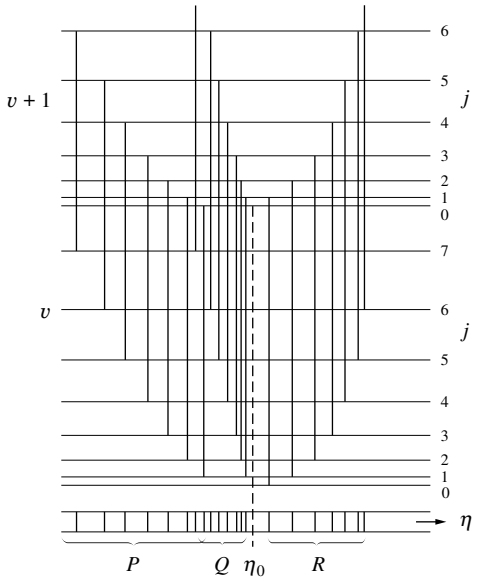

FIGURE 11-5
Typical spectrum of vibration–rotation bands.

($\Delta j = 0$) and R ($\Delta j = +1$) branches, with spectral lines at wavenumbers

$$\eta_P = \eta_0 - (B_{v+1} + B_v)j + (B_{v+1} - B_v)j^2, \qquad j = 1, 2, 3, \ldots \tag{11.28a}$$

$$\eta_Q = \eta_0 + (B_{v+1} - B_v)j + (B_{v+1} - B_v)j^2, \qquad j = 1, 2, 3, \ldots \tag{11.28b}$$

$$\eta_R = \eta_0 + 2B_{v+1} + (3B_{v+1} - B_v)j + (B_{v+1} - B_v)j^2, \qquad j = 0, 1, 2, \ldots \tag{11.28c}$$

where j is the rotational state before the transition. It is seen that there is no line at the band origin. If $B_{v+1} = B_v = \text{const}$, then the Q-branch vanishes and the two remaining branches yield equally spaced lines on both sides of the band center. If $B_{v+1} < B_v$ (larger moment of inertia I at higher vibrational level), then the R-branch will, for sufficiently large j, fold back toward and beyond the band origin. In that case all lines within the band are on one side of a limiting wavenumber. Those bands, where this occurs close to the band center (i.e., for small j where the line strength is strong), are known as *bands with a head*. A sketch of a typical vibration–rotation band spectrum is shown in Fig. 11-5. Note that in linear molecules the Q-branch often does not occur as a result of forbidden transitions [3]. Many more complicated combined transitions are possible, since every molecule has a number of rotational and vibrational energy modes, any number of which could undergo a transition simultaneously. An example is given in Fig. 11-6, which shows a calculated spectrum of the 4.3 μm CO_2 band (a collection of many different vibrational transitions together with their rotational lines), generated from the HITRAN database [32]. It is apparent that this band has no Q-branch.

Electronic Transitions

Electronic energy transitions, i.e., changing the orbital radius of an electron, requires a substantially larger amount of energy than vibrational and rotational transitions, with resulting photons in the ultraviolet and visible parts of the spectrum. Transitions of interest in heat transfer applications (i.e., at wavelengths above 0.25 μm) generally occur only at very high temperatures (above several thousand degrees Kelvin) and/or in the presence of large numbers of free electrons (such as fluorescent lights). At extreme temperatures atoms and molecules may also become ionized through a bound–free absorption event, or an ion and electron can recombine (free–bound emission). In addition, a free electron colliding with a molecule may absorb or emit a photon (free–free transition). If the gas is monatomic, radiation can alter only electronic energy states. Still, this results in some 914 lines for monatomic nitrogen and 682 for

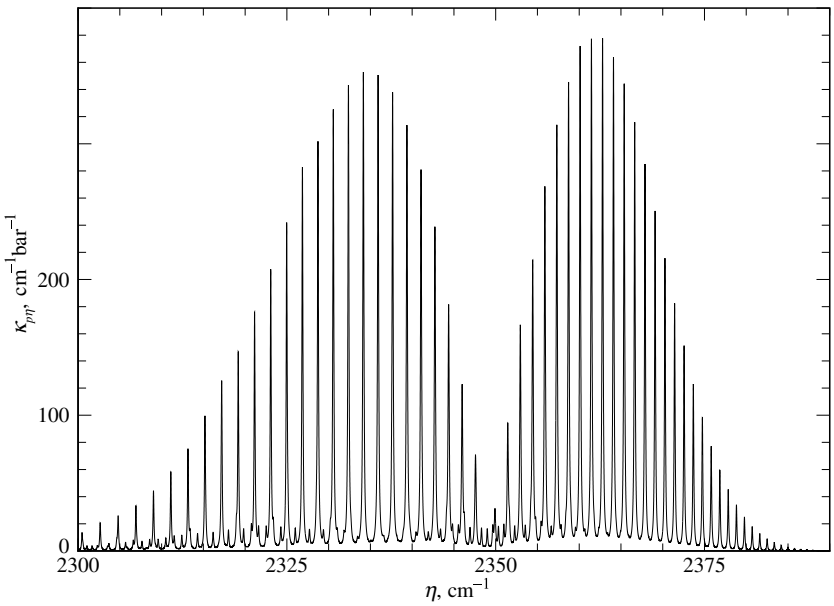

FIGURE 11-6
Pressure-based spectral absorption coefficient for small amounts of CO_2 in nitrogen; 4.3 μm band at p = 1.0 bar, T = 296 K.

monatomic oxygen [33], contributing to heat transfer in high-temperature applications, such as the air plasma in front of a hypersonic spacecraft entering Earth's atmosphere. As an example Fig. 11-7 shows the absorption coefficient of atomic nitrogen at T = 10,860 K, as encountered in the shock layer of the Stardust spacecraft [34]. Many of the monatomic lines are extremely strong (with absorption coefficients near 10^6 m^{-1}), and continuum radiation (bound–free and free–free transitions) is substantial. In this part of the spectrum otherwise radiatively inert molecules, e.g., diatomic nitrogen, also emit and absorb photons, leading to simultaneous electronic–vibration–rotation bands. For comparison, the absorption coefficient for N_2 is also included in Fig. 11-7, consisting of 5 electronic bands, each containing many vibration–rotation subbands. At temperatures above 10,000 K N_2 is nearly completely dissociated, making its absorption coefficient small in comparison to that of monatomic N. At lower temperatures, nearly all molecules are at the lowest electronic energy level, and only the bands with $\eta > 50{,}000\,\text{cm}^{-1}$, or $\lambda < 0.2\,\mu$m remain (of no importance in most engineering applications).

Strength of Spectral Lines within a Band

In equation (11.14) we related the spectral absorption coefficient to the Einstein coefficients B_{lu} and B_{ul} before knowing how such a transition takes place. We now want to develop equation (11.14) a little further to learn how the strength of individual lines (and, through it, the absorption coefficient) varies across vibration–rotation bands, and how they are affected by variations in temperature and pressure.

For a combined vibrational (from vibrational quantum number v to $v \pm 1$) and rotational (from rotational quantum number j to j or $j \pm 1$) transition, the *line intensity* or *line strength* may be rewritten in terms of wavenumber (i.e., after division by c_0) as

$$S_\eta = (n_l g_l B_{lu} - n_u g_u B_{ul}) h\eta, \tag{11.29}$$

where η is the associated transition wavenumber from equations (11.28). Using equations (11.5)

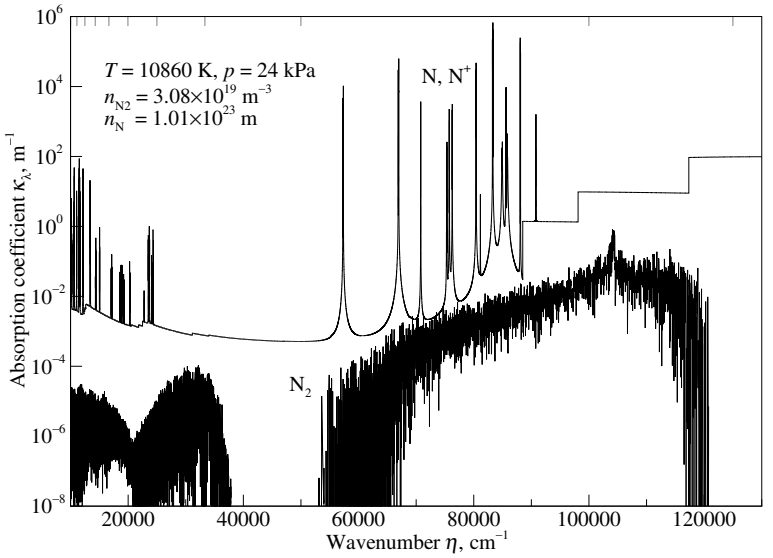

FIGURE 11-7
Linear spectral absorption coefficient of monatomic and diatomic nitrogen in a hypersonic boundary air plasma.

and (11.7) this becomes

$$S_\eta = \frac{n_l g_u A_{ul}}{8\pi c_0 \eta^2}\left(1 - e^{-hc_0\eta/kT}\right). \tag{11.30}$$

The number of molecules at the lower energy state, n_l, may be related to the total number of particles per unit volume, n, through [23]

$$\frac{n_l}{n} = \frac{e^{-E_l/kT}}{Q(T)}, \qquad n = \frac{p}{kT}, \tag{11.31}$$

where $Q(T)$ is the *rovibrational partition function* (a summation over all the possible rotational and vibrational energy levels of the molecule). Substituting this into equation (11.30) and relating the Einstein coefficient to matrix elements of the molecule's electric dipole moment [20], $\mathfrak{R}_{ul}$, leads to

$$S_\eta = \frac{8\pi^3\eta}{3hc_0 k}|\mathfrak{R}_{ul}|^2 \frac{p}{Q(T)T}\left(1 - e^{-hc_0\eta/kT}\right)e^{-E_l/kT}. \tag{11.32}$$

The rovibrational partition function $Q(T)$ and dipole elements $|\mathfrak{R}_{ul}|^2$ can, at least in principle, be calculated from quantum mechanics through very lengthy and complex calculations. For example, much of Penner's book [20] is devoted to this subject.

To gain some insight into the relative strengths of lines within a vibration–rotation band, we will look at the case of a rigid rotator–harmonic oscillator, with the additional assumptions that the bandwidth is small compared with the wavenumber at the band center and that only the P and R branches are important. For such a case the evaluation of the $|\mathfrak{R}_{ul}|^2$ is relatively straightforward [20], and equation (11.32) may be restated as

$$S_{Pj} = Cj\, e^{-hc_0 B_v j(j+1)/kT}, \qquad j = 1, 2, 3, \ldots \tag{11.33a}$$

$$S_{Rj} = C(j+1)\, e^{-hc_0 B_v j(j+1)/kT}, \quad j = 0, 1, 2, \ldots \tag{11.33b}$$

where $E_{rj} = hc_0 B_v j(j+1)$ is the rotational contribution to the lower energy state from equation (11.23) (i.e., before transition for absorption of a photon; after transition for emission), and C collects the coefficients in equation (11.32), as well as the vibrational contribution to the

lower energy state. Examination of equations (11.33) shows that line strength first increases linearly with increasing j (as long as $hc_0B_v j(j+1)/kT \ll 1$), levels off around $j \simeq \sqrt{kT/hc_0B_v}$, then drops off exponentially with large values of j. It is apparent that the band widens with temperature, and lines farther away from the band center become most important. An example is given in Fig. 11-6 for the calculated spectrum of the 4.3 μm CO_2 band, generated from the HITRAN database [32]. At room temperature the 4.3 μm band is dominated by the $00^00 \rightarrow 00^01$ vibrational transition, centered at 2349 cm^{-1}. It is clear that this band has no Q-branch, and that the line strengths of the P- and R-branches closely follow equation (11.33).

Temperature and pressure dependence As seen from equation (11.32) the linear line strength S_η is directly proportional to the pressure of the absorbing/emitting gas; therefore, pressure-based line strength $S_{p\eta}$ and density-based line strength $S_{\rho\eta}$ are functions of temperature only. The temperature dependence comes from three contributions: *(i)* from the partition function $Q(T)$, *(ii)* from the stimulated emission term, $\exp(-hc_0\eta/kT)$, and *(iii)* from the lower energy state E_l. Evaluation of the partition function is extremely difficult, and approximations need to be made. To a good degree of accuracy rotational and vibrational contributions can be separated, i.e., $Q(T) \simeq Q_v(T)Q_r(T)$. The vibrational partition function can then be determined, assuming a harmonic oscillator, as [30]

$$Q_v(T) = \prod_k \left(1 - e^{-hc_0\eta_k/kT}\right)^{-g_k}, \tag{11.34}$$

where the product is over all the different vibrational modes with their harmonic oscillation wavenumbers η_k [$= \nu_e/c_0$ in equation (11.25)], and g_k is the degeneracy of the vibrational mode. The rotational partition function depends on the symmetry of the molecule and on the moments of inertia for rotation around two (linear molecule) or three (nonlinear molecule) axes. For moderate to high temperatures, i.e., when $2IkT/\hbar^2 \gg 1$ [23, 30],

$$\text{Linear molecules } (I_x = I_y = I): \quad Q_r(T) = \frac{1}{\sigma}\frac{2IkT}{\hbar^2} \propto T, \tag{11.35a}$$

$$\text{Nonlinear molecules:} \quad Q_r(T) = \frac{1}{\sigma}\prod_{i=x,y,z}\left(\frac{2I_ikT}{\hbar^2}\right)^{1/2} \propto T^{3/2}, \tag{11.35b}$$

where σ is a *symmetry number*, or the number of distinguishable rotational modes. Examining the separate contributions to the temperature dependence we note that, at moderate temperatures, the rotational partition function causes the line strength to decrease with temperature as $1/T$ or $1/T^{3/2}$, while the influences of the vibrational partition function and of stimulated emission are very minor (but may become important for $T > 1000$ K). The influence of the lower energy state E_l can be negligible or dramatic, depending on the size of E_l: for small values of E_l (low vibrational levels) $\exp(-E_l/kT) \simeq 1$ and further raising the temperature will not change this value. On the other hand, large values of E_l (associated with high vibrational levels) make line strengths very small at low temperatures, but produce sharply increasing line strengths at elevated temperatures (when more molecules populate the higher vibrational levels), giving rise to so-called "hot lines" and "hot bands." An example of the temperature dependence of the spectral absorption coefficient (including effects of line broadening and spacing) will be given in the next section, in Fig. 11-11.

11.4 LINE RADIATION

In the previous two sections we have seen that quantum mechanics postulates that a molecular gas can emit or absorb photons at an infinite set of distinct wavenumbers or frequencies. We already observed that no spectral line can be truly monochromatic; rather, absorption or emission occurs over a tiny but finite range of wavenumbers. The results are *broadened spectral lines* that have their maxima at the wavenumber predicted by quantum mechanics. In this

section we will briefly look at line strengths, the causes of line broadening and at *line shapes*, i.e., the variation of line strength with wavenumber for an isolated line. More detailed accounts may be found in more specialized works [2,3,20,26]. The effects of line overlap, which usually occurs in vibration–rotation bands in the infrared, will be discussed in Section 11.8, "Narrow Band Models."

Numerous phenomena cause broadening of spectral lines. The four most important ones are *natural line broadening*, *collision broadening*, *Stark broadening*, and *Doppler broadening*, with collision and, to a lesser extent, Doppler broadening dominating in most engineering applications. These models have been developed for isolated lines, i.e., interaction between overlapping lines is not considered, and was found to be accurate for low-to-moderate pressures. However, at elevated pressures (roughly 10 bar) collisional interference (or line mixing) effects should be accounted for [35,36].

Natural Line Broadening

Every excited molecule will have its energy levels decay spontaneously to a lower state by emitting a photon, even if the molecule is completely undisturbed. According to Heisenberg's uncertainty principle no energy transition can occur with precisely the same amount of energy, thus causing the energy of emitted photons to vary slightly and the spectral lines to be broadened. The mechanism of decay for that of spontaneous emission is the same as that for collision broadening as discussed in the next section, resulting in identical line shapes. However, the average time for spontaneous decay is much larger than the average time between molecular collisions. Therefore, natural line broadening is generally not important from an engineering point of view, and its effect is invariably small compared to collision broadening. Its small effect may be accounted for by adding a line half-width γ_N to the collision line half-width γ_C discussed below.

Collision Broadening

As the name indicates, *collision broadening* of spectral lines is attributable to the frequency of collisions between gas molecules. The shape of such a line can be calculated from the electron theory of Lorentz* or from quantum mechanics [2,37] as

$$\kappa_\eta = \frac{S}{\pi}\frac{\gamma_C}{(\eta-\eta_0)^2+\gamma_C^2} = S\phi_{L\eta}(\gamma_C, \eta-\eta_0), \quad S \equiv \int_{\Delta\eta} \kappa_\eta \, d\eta, \tag{11.36}$$

where S is the line-integrated absorption coefficient or line strength, γ_C is the so-called line half-width in units of wavenumber (half the line width at half the maximum absorption coefficient), and η_0 is the wavenumber at the line center. The *line shape function* is a normalized Lorentz profile, such that

$$\int_{\Delta\eta} \phi_{L\eta}(\eta)\, d\eta = 1. \tag{11.37}$$

The line shape function is not dimensionless, but has the units of reciprocal spectral variable. In equation (11.37) this is reciprocal wavenumber (or cm), since κ_η is expressed in terms of wavenumber. The shape of a collision-broadened line is identical to that of natural line broadening, and the combined effect is generally termed *Lorentz broadening* with a line half-width γ_L. The spectral distribution of a Lorentz line is shown in Fig. 11-8 (together with the shape of Doppler- and Voigt-broadened lines). Since molecular collisions are proportional to the

*A biographical footnote for Hendrik A. Lorentz may be found in Section 2.6.

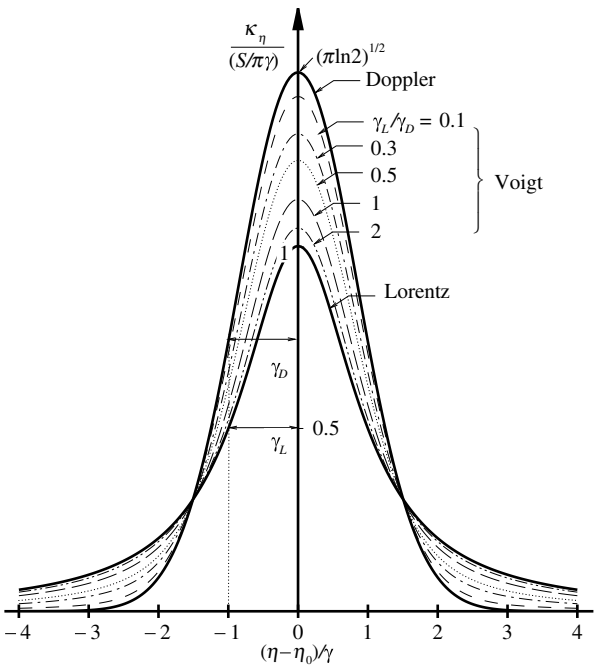

FIGURE 11-8
Spectral line shape for Lorentz (collision), Doppler, and Voigt broadening (for equal line strength and half-width).

number density of molecules ($n \propto \rho \propto p/T$) and to the average molecular speed ($v_{av} \propto \sqrt{T}$), it is not surprising that the half-width for a pure gas can be calculated from kinetic theory [2] as

$$\gamma_C = \frac{2}{\sqrt{\pi}} \frac{D^2 p}{c_0 \sqrt{mkT}} = \gamma_{C0} \left(\frac{p}{p_0}\right) \left(\frac{T_0}{T}\right)^n , \tag{11.38}$$

where D is the effective diameter of the molecule, m is its mass, p is total gas pressure, T is absolute temperature, and the subscript "0" denotes a reference state. The collisional diameter depends on the temperature of the gas and the value for the exponent n must, in general, be found from experiment. If the absorbing–emitting gas is part of a mixture, the fact that collisions involving only nonradiating gases do not cause broadening, and that the nonradiating gases have different molecular diameters, must be accounted for, and equation (11.38) must be generalized to

$$\gamma_C = \sqrt{\frac{2}{\pi}} \sum_i \frac{\sigma_i^2 p_i}{c_0 \sqrt{kT}} \left(\frac{1}{m} + \frac{1}{m_i}\right)^{1/2} = \sum_i \gamma_{C0,i} \left(\frac{p_i}{p_0}\right) \left(\frac{T_0}{T}\right)^{n_i} , \tag{11.39}$$

where p_i and m_i are partial pressure and molecular mass of the various broadening gases (including the radiating gas), respectively, and σ_i is the effective collisional diameter with species i. Temperature-dependent broadening coefficients for some absorbing gases have been tabulated by Rosenmann *et al.* [38] (CO_2), Delaye *et al.* [39] (H_2O), and Hartmann *et al.* [40], all for mixtures containing N_2, O_2, CO_2, and H_2O.

Stark Broadening

Stark broadening occurs if the radiative transition occurs in the presence of a strong electric field. The electrical field may be externally applied, but it is most often due to an internal field, such as the presence of ions and free electrons in a high-temperature plasma. At low-enough pressures Stark broadened lines are symmetric and have Lorentzian shape, equation (11.36). Line widths depend strongly on free electron number density, n_e, and free electron temperature,

T_e, and may be calculated as [26,41]

$$\gamma_S = \gamma_{S0}\left(\frac{T_e}{T_0}\right)^n\left(\frac{n_e}{n_0}\right), \tag{11.40}$$

where again the subscript "0" denotes a reference state. The Stark effect can also result in a shift in the line's spectral position.

Doppler Broadening

According to the Doppler effect a wave traveling toward an observer appears slightly compressed (shorter wavelength or higher frequency) if the emitter is also moving toward the observer, and slightly expanded (longer wavelength or lower frequency) if the emitter is moving away. This is true whether the wave is a sound wave (for example, the pitch of a whistle of a train passing an observer) or an electromagnetic wave. Thus,

$$\eta_{\text{obs}} = \eta_{\text{em}}\left(1 + \frac{\mathbf{v}\cdot\hat{\mathbf{s}}}{c}\right), \tag{11.41}$$

where $\mathbf{v}$ is the velocity of the emitter and $\hat{\mathbf{s}}$ is a unit vector pointing from the emitter to the observer. Assuming local thermodynamic equilibrium, so that Maxwell's velocity distribution applies, the probability for a relative velocity $v = \mathbf{v}\cdot\hat{\mathbf{s}}$ between an emitting/absorbing molecule and an observer is

$$p(v) = \left(\frac{m}{2\pi kT}\right)^{1/2}\exp\left(-\frac{mv^2}{2kT}\right), \tag{11.42}$$

where m is the mass of the radiating molecule. For small v this leads to a *Doppler shift* in observed wavenumber of

$$\eta - \eta_0 = \eta_0\frac{v}{c}. \tag{11.43}$$

Substituting equation (11.43) into (11.42) one can calculate the line profile as [20]

$$\kappa_\eta = S\,\phi_{D\eta}(\gamma_D, \eta-\eta_0) = S\frac{\sqrt{\ln 2}}{\gamma_D\sqrt{\pi}}\exp\left[-(\ln 2)\left(\frac{\eta-\eta_0}{\gamma_D}\right)^2\right], \tag{11.44}$$

where γ_D is the Doppler line half-width, given by

$$\gamma_D = \frac{\eta_0}{c_0}\sqrt{\frac{2kT}{m}\ln 2}. \tag{11.45}$$

Note that, unlike during collision and natural line broadening, the Doppler line width depends on its spectral position. The different line shapes are compared in Fig. 11-8. For equal overall strength, the Doppler line is much more concentrated near the line center.

Combined Effects

In most engineering applications collision broadening, which is proportional to $p/\sqrt{T}$, is by far the most important broadening mechanism. Only at very high temperatures (when, owing to the distribution of the Planck function, transitions at large η are most important; and/or through the opposing temperature dependencies of γ_L and γ_D) and/or low pressures may Doppler broadening, with its proportionality to $\eta\sqrt{T}$, become dominant. Figure 11-9 shows typical line half-widths for CO_2 and water vapor in their 2.7 μm bands as a function of temperature. It is seen that at low pressures ($p = 0.1$ bar) Doppler broadening always dominates. At higher pressures ($p \geq 1$ bar) collision broadening dominates, unless extremely high temperatures ($T > 2000$ K)

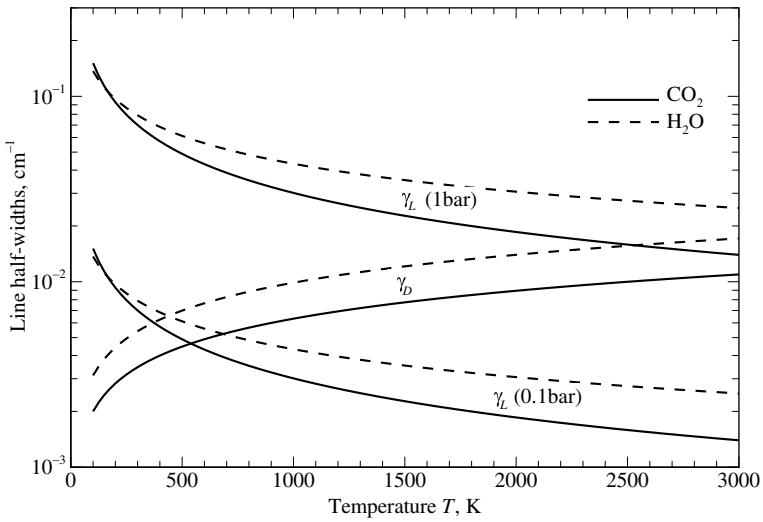

FIGURE 11-9
Lorentz and Doppler line half-widths for the 2.7 μm bands of CO_2 and H_2O.

are encountered. Even then the lines retain their Lorentz shape in the all-important line wings (since in gas columns line centers tend to be opaque, regardless of line shape, radiative behavior is usually governed by the strengths of the line wings). A study by Wang and Modest [42] quantifies the conditions under which combined pressure–Doppler broadening must be considered. Combined broadening behavior is also encountered in low-pressure plasmas, where both Doppler and Stark broadening can be substantial, especially for monatomic gases.

If combined effects need to be considered, it is customary to assume collision and Doppler broadening to be independent of one another (which is not strictly correct). In that case a collision-broadened line would be displaced by the Doppler shift, equation (11.43), and averaged over its probability, equation (11.42). This leads to the *Voigt profile* [2],

$$\kappa_\eta = \frac{S\gamma_L}{\pi^{3/2}} \int_{-\infty}^{+\infty} \frac{e^{-x^2}dx}{\left(\eta - \eta_0 - \dfrac{x\gamma_D}{\sqrt{\ln 2}}\right)^2 + \gamma_L^2}, \quad x = v\sqrt{\frac{m}{2kT}}. \tag{11.46}$$

No closed-form solution exists for the Voigt profile. It has been tabulated in the meteorological literature in terms of the parameter $2\gamma_L/\gamma_D$. How the shape of the Voigt profile changes from pure Doppler broadening ($\gamma_L/\gamma_D = 0$) to pure collision broadening ($\gamma_L/\gamma_D \to \infty$) is also shown in Fig. 11-8 (for constant line half-widths). Several fast algorithms for the calculation of the Voigt profile have also been reported [43–46]. A Fortran subroutine `voigt` is given in Appendix F, that calculates the Voigt κ_η as a function of S, γ_L, γ_D, and $|\eta - \eta_0|$ based on the Humlíček algorithm [46].

Example 11.1. The half-width of a certain spectral line of a certain gas has been measured to be 0.05 cm^{-1} at room temperature (300 K) and 1 atm. When the line half-width is measured at 1 atm and 3000 K, it turns out that the width has remained unchanged. Estimate the contributions of Doppler and collision broadening in both cases.

Solution
As a first approximation we assume that the widths of both contributions may be added to give the total line half-width (this is a fairly good approximation if one makes a substantially larger contribution than the other). Therefore, we may estimate

$$\gamma_{C1} + \gamma_{D1} \approx \gamma_1 = \gamma_2 \approx \gamma_{C2} + \gamma_{D2}$$

and, from equations (11.38) and (11.45),

$$\frac{\gamma_{C2}}{\gamma_{C1}} = \sqrt{\frac{T_1}{T_2}} = \frac{1}{\sqrt{10}}, \quad \frac{\gamma_{D2}}{\gamma_{D1}} = \sqrt{\frac{T_2}{T_1}} = \sqrt{10}.$$

Eliminating the Doppler widths from these equations we obtain

$$\gamma_2 = \frac{\gamma_{C1}}{\sqrt{10}} + \sqrt{10}\gamma_{D1} = \frac{\gamma_{C1}}{\sqrt{10}} + \sqrt{10}(\gamma_1 - \gamma_{C1}),$$

$$\frac{\gamma_{C1}}{\gamma_1} = \frac{\sqrt{10}}{9}\left(\sqrt{10} - \frac{\gamma_2}{\gamma_1}\right) = 0.76,$$

and

$$\frac{\gamma_{C2}}{\gamma_2} = \frac{1}{9}\left(\sqrt{10}\,\frac{\gamma_1}{\gamma_2} - 1\right) = 0.24.$$

We see that at room temperature, collision broadening is about three times stronger than Doppler broadening, while exactly the reverse is true at 3000 K.

Radiation from Isolated Lines

Combining equations (11.16) and (11.22) gives the complete equation of transfer for an absorbing–emitting (but not scattering) medium,

$$\frac{dI_\eta}{ds} = \kappa_\eta(I_{b\eta} - I_\eta), \tag{11.47}$$

where the first term of the right-hand side represents augmentation due to emission and the second term is attenuation due to absorption. Let us assume we have a layer of an isothermal and homogeneous gas of thickness L. Then neither $I_{b\eta}$ nor κ_η is a function of location and the solution to the equation of transfer is

$$I_\eta(X) = I_\eta(0)\,e^{-\kappa_\eta X} + I_{b\eta}\left(1 - e^{-\kappa_\eta X}\right), \tag{11.48}$$

where the *optical path length* X is equal to L if a linear absorption coefficient is used (*geometric path length*), or equal to L multiplied by partial density (*density path length*) or pressure (*pressure path length*) of the radiating gas if either mass or pressure absorption coefficient is used. Thus, the difference between entering and exiting intensity, integrated over the entire spectral line, is

$$I(X) - I(0) = \int_{\Delta\eta} [I_\eta(X) - I_\eta(0)]\,d\eta \approx [I_{b\eta} - I_\eta(0)] \int_{\Delta\eta} \left(1 - e^{-\kappa_\eta X}\right) d\eta, \tag{11.49}$$

where the assumption has been used that neither incoming nor blackbody intensity can vary appreciably over the width of a single spectral line. The integrand of the factor

$$W = \int_{\Delta\eta} \left(1 - e^{-\kappa_\eta X}\right) d\eta \tag{11.50}$$

is the fraction of incoming radiation absorbed by the gas layer at any given wavenumber, and it is also the fraction of the total emitted radiation that escapes from the layer (not undergoing self-absorption). W is commonly called the *equivalent line width* since a line of width W with infinite absorption coefficient would have the identical effect on absorption and emission; the dependence of the increase of W with increasing optical path X is sometimes called the *curve of growth*. The equivalent line width for a Lorentz line may be evaluated by substituting equation (11.36) into equation (11.50) to yield

$$W = 2\pi\gamma_L x\,e^{-x}[I_0(x) + I_1(x)] = 2\pi\gamma_L L\,(x), \tag{11.51}$$

where

$$\gamma_L \equiv \gamma_C + \gamma_N, \qquad x \equiv SX/2\pi\gamma_L, \tag{11.52}$$

the I_0 and I_1 are modified Bessel functions, and $L(x)$ is called the Ladenburg–Reiche function, after the authors who originally developed it [47]. For simpler evaluation, equation (11.51) may be approximated as reported by [2] as

$$L(x) \simeq x\left[1 + \left(\frac{\pi x}{2}\right)^{5/4}\right]^{-2/5}, \tag{11.53}$$

with a maximum error of approximately 1% near $x = 1$. Asymptotic values for W are easily obtained as

$$W = SX, \qquad x \ll 1, \tag{11.54a}$$

$$W = 2\sqrt{SX\gamma_L}, \qquad x \gg 1. \tag{11.54b}$$

Comparing equation (11.52) with equation (11.36), evaluated at half-height ($|\eta - \eta_0| = \gamma_L$), shows that x is the nondimensional *optical thickness* of the gas layer, $\kappa_\eta X$, at that location. Therefore, the parameter x gives an indication of the strength of the line. For a weak line ($x \ll 1$) little absorption takes place so that every position in the gas layer receives the full irradiation, resulting in a linear absorption rate (with distance). In the case of a strong line ($x \gg 1$) the radiation intensity has been appreciably weakened before exiting the gas layer, resulting in locally lesser absorption and causing the square-root dependence of equation (11.54*b*).

11.5 NONEQUILIBRIUM RADIATION

There are many radiation applications, in which local thermal equilibrium cannot be assumed, such as in the plasma generated during atmospheric entry of spacecraft, ballistic ranges, high-speed shock tubes, arc jets, etc. When a gas is not in thermal equilibrium, its state cannot be described by a single temperature [48], and the populations of internal energy states do not follow Boltzmann distributions, equation (11.5). The thermodynamic state may then be described using a multitemperature approach (i.e., a Boltzmann distribution is assumed for each internal mode with a specific temperature) [49]. Alternatively, level population distributions may be calculated directly, taking into account collisional and radiative processes. This is known as the Collisional–Radiative model (CR) [50, 51] or, if infinitely fast reaction rates are assumed, the Quasi-Steady State (QSS) approximation [49]. Most often the more closely spaced energy levels for translation, rotation, vibration, and free electrons are assumed to have individual equilibrium distributions with up to four different temperatures (T_t, T_r, T_v, T_e), while the widely spaced electronic energy levels are modeled using the QSS/CR approach. Once all energy state distributions have been determined, the emission is given by equation (11.20). Relating it to the absorption coefficient one may define a nonequilibrium Planck function, from equation (11.21), as (in terms of wavenumbers)

$$I_{b\eta}^{\text{ne}} = \frac{j_\eta}{\kappa_\eta} = 2hc_0^2\eta^3\frac{n_u}{n_l - n_u}. \tag{11.55}$$

An example is given in Fig. 11-10, showing the nonequilibrium Planck function for diatomic CN (a strongly radiating ablation product from thermal protection systems) [52]. In this graph a two-temperature model was adopted with $T_t = T_r = 15{,}000$ K and $T_v = T_{el} = T_e = 10{,}000$ K (with electronic energy levels in equilibrium at T_{el}), and only Doppler broadening was considered. The ultraviolet CN band ($1 \leftrightarrow 3$ electronic transition) is shown, including many vibration–rotation subbands. For example, the lines labeled $\Delta v = v_u - v_l = -2$ imply that the vibrational energy of the upper (electronic) level is two levels lower than that of the lower (electronic) energy state, and so on. The nonequilibrium Planck function displays line structure similar to that of the

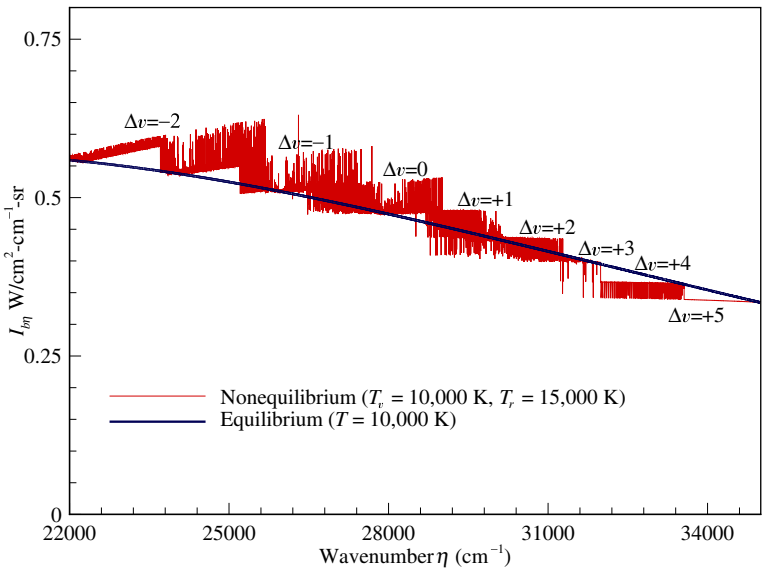

FIGURE 11-10
Nonequlibrium Planck function for CN for a two-temperature model (electronic, vibrational, and electron states at equilibrium with T_v, rotational and translational states with T_r).

absorption coefficient. This can be better understood by looking at the special case of negligible stimulated emission and no line overlap (both good approximations for the present case). Then [cf. equation (11.31)]

$$\frac{I_{b\eta}^{\text{ne}}(T_v, T_r)}{I_{b\eta}(T_v)} = \frac{n_u}{n_l} e^{hc_0\eta'/kT_v} = \frac{[Q_{vr,l}/Q_{vr,u}]^{\text{ne}}(T_v, T_r)}{[Q_{vr,l}/Q_{vr,u}](T_v)} \exp\left[\frac{E_{ru} - E_{rl}}{k}\left(\frac{1}{T_v} - \frac{1}{T_r}\right)\right], \tag{11.56}$$

where Q_{vr} is the rovibrational partition function (depending on temperature only), and E_r is the rotational energy level. Note that u and l refer to the upper and lower states of the total transition, always determined by the electronic level, i.e., $E_{ru} - E_{rl}$ is the rotational energy change for a given transition (spectral line), which can be negative (lines below the equilibrium Planck function in Fig. 11-10).

As can be appreciated from the discussion in this section, and on electronic transitions in Section 11.3, radiation in high-temperature nonequilibrium plasmas is considerably more complicated than usually encountered in engineering, and is beyond the scope of the present text. The reader is referred to the literature dedicated to such problems [49, 53].

11.6 HIGH-RESOLUTION SPECTROSCOPIC DATABASES

During the past 40 years or so, due to the advent of high-resolution spectroscopy (mostly FTIR spectrometers), it has become possible to measure strengths and positions of individual spectral lines. A first collection of spectral data was assembled in the late 1960s by the Air Force Cambridge Research Laboratories for atmospheric scientists, including low-temperature data for the major constituents of the Earth's atmosphere, and was published in 1973 as an Air Force report [54]. With contributions from many researchers across the world this grew into the HITRAN database (an acronym for HIgh resolution TRANsmission molecular absorption), first published in 1987 [55]. The database is maintained by the Harvard–Smithsonian Center for Astrophysics, with periodic updates [32, 56–59]. The latest version at present is HITRAN

2008 [32], which includes detailed information on 39 species with a total of about 2.7 million lines.

As the popularity of HITRAN grew, the need for a database valid at elevated temperatures became obvious. A first attempt was made by the group around Taine in France, who augmented HITRAN 1986 data for water vapor and carbon dioxide through theoretical calculations [60,61]. A development by the HITRAN group resulted in a first version of HITEMP (1995) [62] for H_2O, CO_2, CO, and OH, using theoretical models. Comparison with experiment [63–66] indicated that HITEMP 1995 greatly overpredicted CO_2 emissivities above 1000 K, while agreement for H_2O was acceptable. More accurate and extensive calculations for CO_2 were carried out in Russia, resulting in several versions of the CDSD-1000 database [67,68] (with the 2008 version containing 4 million lines), which were shown to agree well with experiment. The latest version of CDSD, called CDSD-4000 [69], aims to be accurate up to 4000 K, and has 628 million lines, requiring 23 GB of storage. Several extensive high-temperature collections were developed for H_2O: the Ames database [70] includes 300 million lines, SCAN [71] contains 3 billion, and the BT2 collection [72] has 500 million lines; building up on the Ames database, Perez et al. [73] rejected lines from the Ames collection that remain weak below 3000 K, and combined it with well-established lines from HITRAN 2001 and HITEMP 1995, culminating in a manageable collection with 1.3 million lines. Finally, in 2010 a new version of HITEMP was released [74], designed for temperatures up to 3000 K. Citing best agreement against experimental data, HITEMP 2010 incorporates and extends CDSD 2008 for CO_2 (11 million lines) and a slimmed-down version of BT2 for H_2O (111 million lines). HITEMP 2010 also includes data for three diatomic gases (CN, CO, and OH) with their relatively few lines. Approximate high-temperature data for methane (up to 2000 K) are available from [75]. An example calculation is given in Fig. 11-11, showing a small part of the artificial spectrum of the 4.3 μm CO_2 band, generated from the HITRAN database [32], assuming Lorentz broadening, and containing more than 1,500 spectral lines. The top frame of Fig. 11-11 shows the pressure-based absorption coefficient of CO_2 at low partial pressure in air at a total pressure of 10 mbar. Because of the relatively low total pressure, the lines are fairly narrow, resulting in little overlap. If the total pressure is raised to 1 bar, shown in the center frame, lines become strongly broadened, leading to substantial line overlap, and a smoother variation in the absorption coefficient (with considerably lower maxima and higher minima). At the high temperatures usually encountered during combustion the spectral lines narrow considerably [see equation (11.38)], decreasing line overlap; at the same time the strengths of the lines that were most important at low temperature decrease according to equation (11.35) and finally, at high temperatures "hot lines," that were negligible at room temperature, become more and more important. To be valid up to 3000 K HITEMP 2010 [74] lists more than 22,000 spectral lines for this small wavenumber range. The result is a fairly erratic looking absorption coefficient as depicted in the bottom frame of Fig. 11-11. If high temperatures are combined with low total pressures (not shown), the spectral behavior of the absorption coefficient resembles high-frequency electronic noise. Fortunately, heat transfer calculations in media at low total pressure are rare (they are important, though, in meteorological applications dealing with the low-pressure upper atmosphere).

Similar efforts have been made by the plasma radiation community. RAD/EQUIL is perhaps the earliest attempt, including contributions from atomic lines and continua, and approximate models for molecules, but only for thermodynamic equilibrium conditions [76]. The NonEQuilibrium AIr Radiation (NEQAIR) model [77] was originally developed for the study of radiative properties of nonequilibrium, low density air plasmas. The updated NEQAIR96 model [78] includes spectral line data for spontaneous emission, stimulated emission, and absorption for 14 monatomic and diatomic species, as well as bound–free and free–free transition data for atoms. Nonequilibrium electronic level populations are determined using the QSS approximation (cf. Section 11.5). Since the creation of NEQAIR various improvements have been made by Laux [79] and others, leading to the SPECAIR database [80]. In Japan the SPRADIAN database was assembled [81], which was recently updated in cooperation with KAIST [82]. A new High-

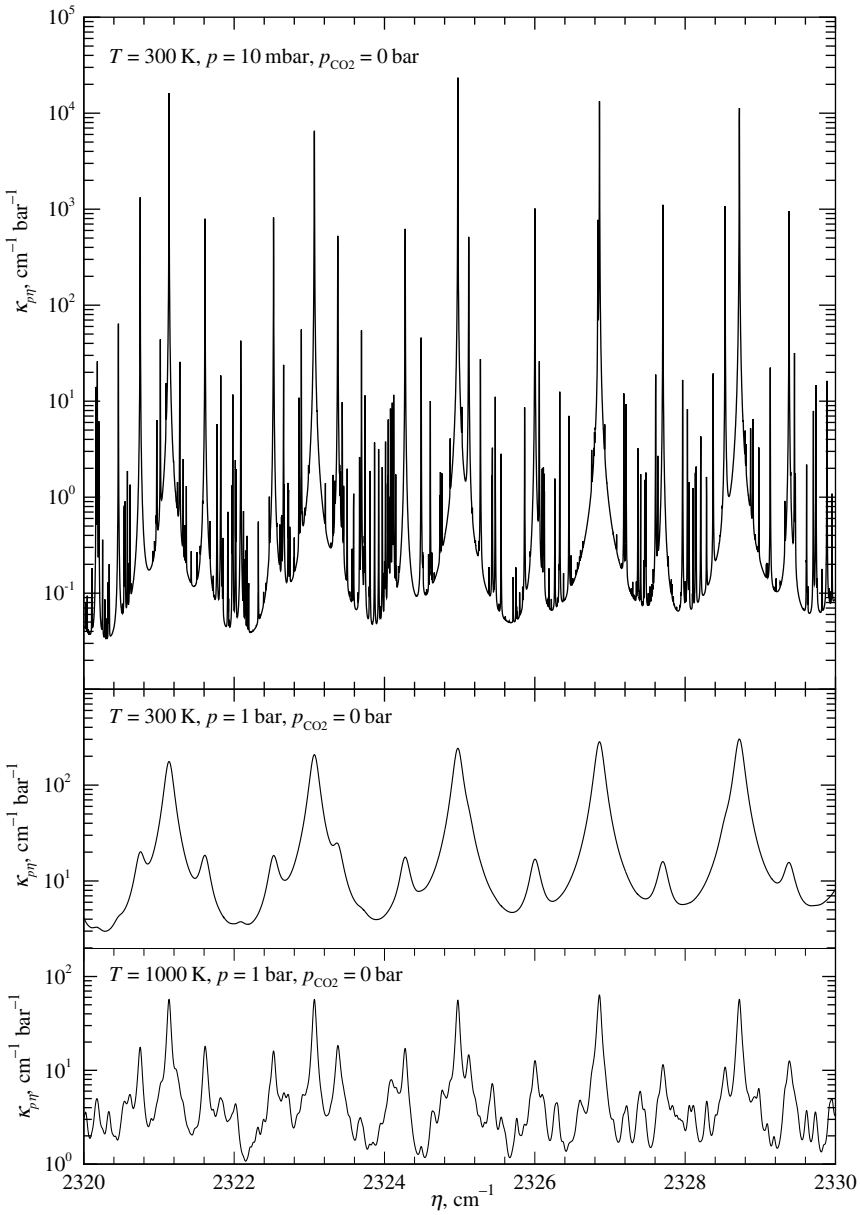

FIGURE 11-11
Spectral absorption coefficient for small amounts of CO_2 in nitrogen, across a small portion of the CO_2 4.3 μm band; top frame: $p = 10$ mbar, $T = 300$ K; center frame: $p = 1$ bar, $T = 300$ K; bottom frame: $p = 1$ bar, $T = 1000$ K.

temperature Aerothermodynamic RAdiation model (HARA) developed by Johnston [50, 83] utilizes comprehensive and updated atomic line data obtained from the National Institute of Standards and Technology (NIST) online database [84] and the Opacity Project [85], as well as atomic bound-free cross-sections from the TOPbase [86]. Since the above databases are generally stand-alone programs, incorporating several other tools, such as primitive RTE solvers, Sohn et al. [87] extracted the relevant data from NEQAIR96 to form an efficient radiative property module. This database has very recently been updated for high-speed retrieval rates and to incorporate the state-of-the-art data in HARA [88].

11.7 SPECTRAL MODELS FOR RADIATIVE TRANSFER CALCULATIONS

A single spectral line at a certain spectral position is fully characterized by its strength (the intensity, or integrated absorption coefficient) and its line half-width (plus knowledge of the broadening mechanism, i.e., collision and/or Doppler broadening). However, a vibration–rotation band has many closely spaced spectral lines that may overlap considerably. While the absorption coefficients for individual lines may simply be added to give the absorption coefficient of an entire band at any spectral position,

$$\kappa_\eta = \sum_j \kappa_{\eta j}, \tag{11.57}$$

the resulting function tends to gyrate violently across the band (as seen in Figs. 11-6 and 11-11), unless the lines overlap very strongly. This tendency, plus the fact that there may be literally millions of spectral lines, makes radiative transfer calculations a truly formidable task, if the exact relationship is to be used in the spectral integration for total intensity [equation (10.28)], total radiative heat flux [equation (10.52)], or the divergence of the heat flux [equation (10.59)]. This has prompted the development of a number of approximate spectral models. Exact and approximate methods may be loosely put into four groups (in order of decreasing complexity and accuracy): (1) line-by-line calculations, (2) narrow band calculations, (3) wide band calculations, and (4) global models.

Line-By-Line Calculations With the advent of powerful computers and the necessary high-resolution spectroscopic databases, a number of spectrally resolved or "line-by-line calculations" have been performed, a few for actual heat transfer calculations, e.g., [89–91], some to prepare narrow band model correlations, e.g., [92, 93], and others to validate global spectral models, e.g., [94–96]. Such calculations rely on very detailed knowledge of every single spectral line, taken from one of the high-resolution spectroscopic databases described in Section 11.6. Because of strongly varying values of the absorption coefficient (see Fig. 11-11), the spectral radiative transfer problem must be solved for up to one million wavenumbers, followed by integration over the spectrum. While such calculations may be the most accurate to date, they require vast amounts of computer resources. This is and will remain undesirable, even with the availability of powerful computers, since radiative calculations are usually only a small part of a sophisticated, overall fire/combustion code. In addition, high-resolution gas property data (resolution of better than $0.01\,\mathrm{cm}^{-1}$), which are required for accurate line-by-line calculations, are generally found from theoretical calculations and mostly still remain to be validated against experimental data. In particular, temperature and pressure dependence of spectral line broadening is very complicated and simply not well enough understood to extrapolate room temperature data to the high temperatures important in combustion environments. For these reasons it is fair to assume that, for the foreseeable future, line-by-line calculations will only be used as benchmarks for the validation of more approximate spectral models.

Narrow Band Models When calculating spectral radiative fluxes from a molecular gas one finds that the gas absorption coefficient (and with it, the radiative intensity) varies much more rapidly across the spectrum than other quantities, such as blackbody intensity, etc. It is, therefore,

in principle possible to replace the actual absorption coefficient (and intensity) by smoothened values appropriately averaged over a narrow spectral range. A number of such "narrow band models" were developed some 40–50 years ago, and will be examined in the following section. In principle, narrow band calculations can be as accurate as line-by-line calculations, provided an "exact" narrow band average can be found. The primary disadvantages of such narrow band models are that they are difficult to apply to nonhomogeneous gases and the fact that heat transfer calculations, based on narrow band data and using general solution methods, are limited to nonscattering media within a black-walled enclosure.

An alternative to the "traditional" narrow band models is the so-called "correlated *k*-distribution." In this method it is observed that, over a narrow spectral range, the rapidly oscillating absorption coefficient κ_η attains the same value many times (at slightly different wavenumbers η), each time resulting in identical intensity I_η and radiative flux (provided the medium is homogeneous, i.e., has an absorption coefficient independent of position). Since the actual wavenumbers are irrelevant (across the small spectral range), in the correlated *k*-distribution method the absorption coefficient is reordered, resulting in a smooth dependence of absorption coefficient *vs*. artificial wavenumber (varying across the given narrow range). This, in turn, makes spectral integration very straightforward. *k*-distributions are relatively new, and are still undergoing development. While attractive, they also are difficult to apply to nonhomogeneous media.

Wide Band Models Wide band models make use of the fact that, even across an entire vibration–rotation band, blackbody intensity does not vary substantially. In principle, wide band correlations are found by integrating narrow band results across an entire band, resulting in only slightly lesser accuracy. Wide band model calculations have been very popular in the past, due to the facts that the necessary calculations are relatively simple and that much better spectral data were not available. However, it is well recognized that wide band correlations have a typical correlational accuracy of ±30%, and in some cases may be in error by as much as 70%; substantial additional but unquantified errors may be expected due to experimental inaccuracies. One of the attractions of the correlated *k*-distributions is that they can be readily adapted to wide band calculations.

Global Models In heat transfer calculations it is generally only the (spectrally integrated) total radiative heat flux or its divergence that are of interest. Global models attempt to calculate these total fluxes directly, using spectrally integrated radiative properties. Most early global methods employ the total emissivities and absorptivities of gas columns, but more recently full-spectrum correlated *k*-distributions have also been developed.

During the remainder of this chapter we will discuss the smoothing of spectral radiative properties of molecular gases over narrow bands and wide bands, as well as the evaluation of total properties. Actual heat transfer calculations using these data will be deferred until Chapter 20 (i.e., until after the discussion of particulate properties and of solution methods for the radiative transfer equation). Global models require manipulation of the RTE and, thus, will also be deferred to Chapter 20.

11.8 NARROW BAND MODELS

Examination of the formal solution to the equation of radiative transfer, equation (10.28), shows that all spectral integrations may be reduced to four cases, namely,

$$\int_0^\infty \kappa_\eta I_{(b)\eta}\, d\eta \quad \text{and} \quad \int_0^\infty I_{(b)\eta} \left[1 - \exp\left(-\int_0^X \kappa_\eta\, dX\right)\right] d\eta, \tag{11.58}$$

where $I_{(b)\eta}$ denotes that either $I_{b\eta}$ or I_η can occur, and X is the optical path length introduced in equation (11.48). It is clear from inspection of Fig. 1-5 that the Planck function will never vary appreciably over the spectral range of a few lines, considering that adjacent lines are very closely spaced (measured in fractions of cm^{-1}). Local radiation intensity I_η, on the other hand,

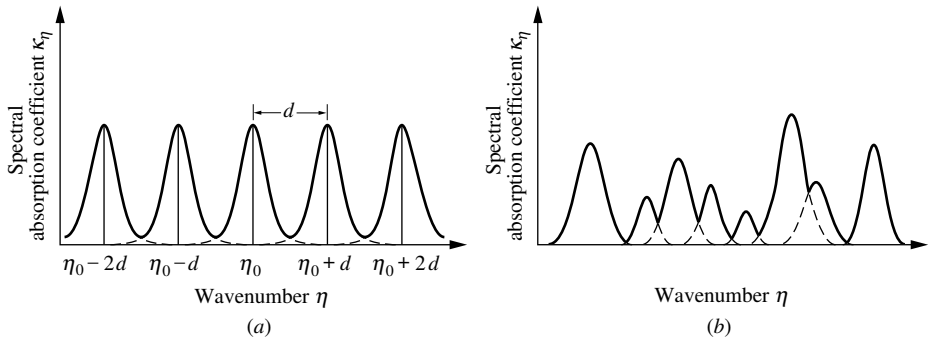

FIGURE 11-12
Typical spectral line arrangement for (*a*) Elsasser and (*b*) statistical model.

may vary just as strongly as the absorption coefficient, since emission within the gas takes place at those wavenumbers where κ_η is large [see equation (10.10)]. However, if we limit our consideration to nonscattering media bounded by black (or no) walls, the formal solution of the radiative equation of transfer, equation (10.29), shows that all spectral integrations involve only the Planck function, and not the local intensity. For such a restricted scenario[4] we may simplify expressions (11.58), with extremely good accuracy, to

$$\int_0^\infty I_{b\eta} \left\{ \frac{1}{\Delta\eta} \int_{\eta-\Delta\eta/2}^{\eta+\Delta\eta/2} \kappa_\eta \, d\eta' \right\} d\eta \tag{11.59a}$$

and

$$\int_0^\infty I_{b\eta} \left\{ \frac{1}{\Delta\eta} \int_{\eta-\Delta\eta/2}^{\eta+\Delta\eta/2} \left[1 - \exp\left(- \int_0^X \kappa_\eta \, dX \right) \right] d\eta' \right\} d\eta. \tag{11.59b}$$

The expressions within the large braces are local averages of the spectral absorption coefficient and of the spectral emissivity, respectively, indicated by an overbar:[5]

$$\overline{\kappa}_\eta(\eta) = \frac{1}{\Delta\eta} \int_{\eta-\Delta\eta/2}^{\eta+\Delta\eta/2} \kappa_\eta \, d\eta', \tag{11.60}$$

$$\overline{\epsilon}_\eta(\eta) = \frac{1}{\Delta\eta} \int_{\eta-\Delta\eta/2}^{\eta+\Delta\eta/2} \left[1 - \exp\left(- \int_0^X \kappa_\eta \, dX \right) \right] d\eta'. \tag{11.61}$$

One can expect the spectral variation of $\overline{\kappa}$ and $\overline{\epsilon}$ to be relatively smooth over the band, making spectral integration of radiative heat fluxes feasible.

To find spectrally averaged or "narrow band" values of the absorption coefficient and the emissivity, some information must be available on the spacing of individual lines within the group and on their relative strengths. A number of models have been proposed to this purpose, of which the two extreme ones are the *Elsasser model*, in which equally spaced lines of equal intensity are considered, and the *statistical models*, in which the spectral lines are assumed to have random spacing and/or intensity. A typical spectral line arrangement for these two extreme models is shown in Fig. 11-12. The main distinction between the two models is the difference in line overlap. Both models will predict the same narrow band parameters for optically thin situations or nonoverlap conditions (since overlap has no effect), as well as for optically very strong situations (since no beam can penetrate through the gas, regardless of the overlapping

[4]If the Monte Carlo method is employed as the solution method, this restriction is not necessary, since integration over local intensity is avoided even for reflecting walls/scattering media; see Section 21.3.

[5]It should be understood that the definition of $\overline{\kappa}$ in equation (11.60) is not sufficient since $\overline{\epsilon} \neq 1 - \exp(-\overline{\kappa}s)$. This fact will be demonstrated in Example 11.2.

characteristics). Under intermediate conditions the Elsasser model will always predict a higher emissivity/absorptivity than the statistical models, since regular spacing always results in less overlap (for the same average absorption coefficient) [3]. The deviation between the models is never more than 20%. In the following we will limit our discussion to lines of Lorentz shape, since collision broadening generally dominates at the relatively high pressures encountered in heat transfer applications. Discussion on models for Doppler and Voigt line shapes can be found in the meteorological literature, e.g., [2].

The Elsasser Model

We saw earlier in this chapter that diatomic molecules and linear polyatomic molecules have only two, identical rotational modes, resulting in a single set of lines (consisting of two or three branches, as shown in Fig. 11-2 and Fig. 11-5). For these gases one may expect spectral lines with nearly constant spacing and slowly varying intensity, in particular if the Q-branch is unimportant (or "forbidden") and if the folding back of the R-branch gives also only a small contribution.

Summing up the contributions from infinitely many Lorentz lines on both sides of an arbitrary line with center at η_0, we get

$$\kappa_\eta = \sum_{i=-\infty}^{\infty} \frac{S}{\pi} \frac{\gamma_L}{(\eta - \eta_0 - id)^2 + \gamma_L^2}, \tag{11.62}$$

where d is the (constant) spacing between spectral lines.[6] This series may be evaluated in closed form, as was first done by Elsasser, resulting in [97]

$$\kappa_\eta = \frac{S}{d} \frac{\sinh 2\beta}{\cosh 2\beta - \cos(z - z_0)}, \tag{11.63}$$

where

$$\beta \equiv \pi\gamma_L/d, \qquad z \equiv 2\pi\eta/d. \tag{11.64}$$

From equation (11.60), the average absorption coefficient is simply

$$\overline{\kappa}_\eta = \frac{S}{d}. \tag{11.65}$$

This also follows without integration from the fact that S is each line's contribution to the integrated absorption coefficient [see equation (11.36)], and that the lines are spaced d wavenumbers apart, i.e., for every d wavenumbers S is added to the integrated absorption coefficient. The spectrally averaged emissivity may be evaluated from equation (11.61) as

$$\overline{\epsilon}_\eta = 1 - \frac{1}{2\pi} \int_{-\pi}^{\pi} \exp\left(-\frac{2\beta x \sinh 2\beta}{\cosh 2\beta - \cos z}\right) dz, \tag{11.66}$$

where, since the absorption coefficient is a periodic function, one full period was chosen for the averaging wavenumber range and, thus, the arbitrary location z_0 could be eliminated. As one may see from its definition, equation (11.64), β is the *line overlap parameter:* β gives an indication of how much the individual lines overlap each other, and x, already defined in equation (11.52), is the *line strength parameter*. At this point we may also define another nondimensional parameter, the *narrow band optical thickness* $\tau = \overline{\kappa}X$, so that we now have three characterizing parameters, namely,

$$x = \frac{SX}{2\pi\gamma_L}, \quad \beta = \pi\frac{\gamma_L}{d}, \quad \tau = \frac{S}{d}X = 2\beta x. \tag{11.67}$$

[6] Since we are using wavenumber here, the value for d is measured in units of wavenumbers, cm^{-1}. If we were to use frequency or wavelength, the definition and units of d would correspondingly change.

Equation (11.66) cannot be solved in closed form, but an accurate approximate expression, known as the Godson approximation, has been given [2]:

$$\bar{\epsilon}_\eta \approx \text{erf}\left(\frac{\sqrt{\pi}}{2}\frac{W}{d}\right) = \text{erf}\left(\frac{\sqrt{\pi}}{2}\frac{S}{d}X\,e^{-x}[I_0(x)+I_1(x)]\right) = \text{erf}\left(\sqrt{\pi}\beta L(x)\right) \tag{11.68}$$

where erf is the *error function* and is tabulated in standard mathematical texts [98]. The Godson approximation is reasonably accurate for small-to-moderate line overlap ($\beta < 1$). For larger values of β, and for hand calculations it is desirable to have simpler expressions. We can distinguish among three different limiting regimes:

$$\begin{aligned} &\text{weak lines } (x \ll 1): \\ &\text{strong overlap } (\beta > 1): \end{aligned} \qquad \bar{\epsilon}_\eta = 1 - \exp\left(-\frac{S}{d}X\right) = 1 - e^{-\tau}, \tag{11.69a}$$

$$\text{strong lines } (x \gg 1): \qquad \bar{\epsilon}_\eta = \text{erf}\left(\sqrt{\pi\frac{S}{d}\frac{\gamma_L}{d}X}\right) = \text{erf}\left(\sqrt{\tau\beta}\right), \tag{11.69b}$$

$$\text{no overlap } (\beta \ll 1): \qquad \bar{\epsilon}_\eta = \frac{W}{d} = 2\beta L(x), \tag{11.69c}$$

where the W/d in equation (11.69*c*) can possibly be further simplified using equations (11.54*a*) and (11.54*b*). These relations are summarized in Table 11.1.

The Statistical Models

In the statistical models it is assumed that the spectral lines are not equally spaced and of equal strength but, rather, are of random strength and are randomly distributed across the narrow band. This assumption can be expected to be an accurate representation for complex molecules for which lines from different rotational modes overlap in an irregular fashion. In several early studies Goody [99] and Godson [100] showed that any narrow band model with randomly placed spectral lines, with arbitrary strengths and line shape (i.e., Lorentzian or other) leads to the same expression for the spectrally averaged emissivity,

$$\bar{\epsilon}_\eta = 1 - \exp\left(-\frac{\overline{W}}{d}\right), \tag{11.70}$$

where $\overline{W}$ is an average over the N lines contained in the spectral interval,

$$\overline{W} = \frac{1}{N}\sum_{i=1}^{N} W_i, \tag{11.71}$$

and d is the average line spacing, defined as

$$d = \frac{\Delta\eta}{N}. \tag{11.72}$$

A number of statistical models have been developed, in which lines are placed at random across $\Delta\eta$ with random strengths picked from different probability distributions. We will limit our brief discussion to three different models, which excel due to their simplicity and/or their success to model actual spectral distributions.

The simplest statistical model is the *uniform statistical model*, in which all lines have equal strengths, or

$$\text{Uniform statistical model:} \qquad S = \overline{S} = \text{const.} \tag{11.73}$$

A more realistic representation must allow for varying lines strengths, given by a *probability density function* $p(S)$. The properties of the narrow band are then found by averaging line properties with the probability density function. A frequently used such probability distribution is the exponential form proposed by Goody [99],

$$\text{Goody model:} \qquad p(S) = \frac{1}{\overline{S}} \exp\left(-\frac{S}{\overline{S}}\right), \quad 0 \le S < \infty, \tag{11.74}$$

which is popular due to its simplicity. However, Malkmus [101] recognized that in many cases this exponential intensity distribution severely underpredicts the number of low-strength lines. He modified the physically plausible $1/S$ distribution proposed by Godson [100] to obtain an exponential-tailed $1/S$ distribution, now known as the Malkmus model:

$$\text{Malkmus model:} \qquad p(S) = \frac{1}{S} \exp\left(-\frac{S}{\overline{S}}\right), \quad 0 \le S < \infty. \tag{11.75}$$

All three distribution functions, equations (11.73), (11.74), and (11.75), have identical average line strengths $\overline{S}$.

Finding the average equivalent line width $\overline{W}$ for the uniform statistical model is trivial, since every equivalent line width from equation (11.73) is identical, and $\overline{W} = W$ (single line). For the Goody and Malkmus model the sum in equation (11.71) can, for a large statistical sample, be replaced by an integral:

$$\overline{W} \underset{N\to\infty}{\longrightarrow} \int_0^\infty p(S)W(S)\,dS = \int_0^\infty p(S) \int_{-\infty}^{+\infty} \left(1 - e^{-\kappa_\eta(S)X}\right) d\eta\, dS. \tag{11.76}$$

Substituting equations (11.74) and (11.75) and carrying out the integrations leads to, for Lorentz lines,

$$\text{Uniform statistical model:} \quad \frac{\overline{W}}{d} = 2\pi\frac{\overline{\gamma}_L}{d} L\left(\frac{\overline{S}X}{2\pi\overline{\gamma}_L}\right) = 2\beta L(x) = 2\beta L(\tau/2\beta), \tag{11.77}$$

$$\text{Goody model:} \quad \frac{\overline{W}}{d} = \frac{\overline{S}}{d}X \Big/ \left(1 + \frac{\overline{S}X}{\pi\overline{\gamma}_L}\right)^{1/2} = \tau \Big/ (1 + \tau/\beta)^{1/2}, \tag{11.78}$$

$$\text{Malkmus model:} \quad \frac{\overline{W}}{d} = \frac{\pi\overline{\gamma}_L}{2d}\left[\left(1 + \frac{4\overline{S}X}{\pi\overline{\gamma}_L}\right)^{1/2} - 1\right] = \frac{\beta}{2}\left[(1 + 4\tau/\beta)^{1/2} - 1\right], \tag{11.79}$$

where $L(x)$ is the Ladenburg–Reiche function given by equation (11.51). In these models the *narrow band parameters* $\overline{\gamma}_L/d$ and $\overline{S}/d$ are either found by fitting experimental data, or from high-resolution spectral data, such as the HITRAN database [32]. In the latter case, it is desirable to have the models yield exact results in the limits of weak lines ($x \ll 1$) as well as strong lines ($x \gg 1$). In the weak line limit we have, for all three models,

$$\text{weak lines } (x \ll 1): \quad \frac{\overline{W}}{d} \to \frac{\overline{S}}{d}X = 2\beta x = \tau, \tag{11.80}$$

while the models lead to slightly different strong line limits, i.e.,

$$\text{strong lines } (x \gg 1):$$

$$\text{Uniform statistical:} \quad \frac{\overline{W}}{d} \to \frac{2\sqrt{\overline{\gamma}_L \overline{S}X}}{d} = 2\beta(2x/\pi)^{1/2} = 2(\tau\beta/\pi)^{1/2}, \tag{11.81a}$$

$$\text{Goody/Malkmus:} \quad \frac{\overline{W}}{d} \to \frac{\sqrt{\pi\overline{\gamma}_L \overline{S}X}}{d} = \beta(2x)^{1/2} = (\tau\beta)^{1/2}. \tag{11.81b}$$

TABLE 11.1
Summary of effective line widths and narrow band emissivities for Lorentz lines.

	Weak line $x \ll 1$	Strong line $x \gg 1$	No overlap $\beta \ll 1$	All regimes
Single line, W	SX	$2\sqrt{SX\gamma_L}$		$2\pi\gamma_L L(\tau/2\beta)$
$\dfrac{W}{d}$	τ	$2\sqrt{\tau\beta/\pi}$		$2\beta L(\tau/2\beta)$
Elsasser model				
$\dfrac{W}{d}$	τ	$2\sqrt{\tau\beta/\pi}$		$2\beta L(\tau/2\beta)$
$\bar{\epsilon}_\eta$	$1-e^{-\tau}$	$\operatorname{erf}\left(\sqrt{\tau\beta}\right)$	$\dfrac{W}{d}$	$\operatorname{erf}\left(\dfrac{\sqrt{\pi}}{2}\dfrac{W}{d}\right)$
Statistical models				
$\dfrac{\overline{W}}{d}$ (S = const)	τ	$2\sqrt{\tau\beta/\pi}$		$2\beta L(\tau/2\beta)$
$\dfrac{\overline{W}}{d}$ (Goody)	τ	$\sqrt{\tau\beta}$		$\tau\Big/\sqrt{1+\tau/\beta}$
$\dfrac{\overline{W}}{d}$ (Malkmus)	τ	$\sqrt{\tau\beta}$		$\frac{\beta}{2}\left[\sqrt{1+4\tau/\beta}-1\right]$
$\bar{\epsilon}_\eta$	$1-e^{-\tau}$	$1-\exp\left(-\overline{W}/d\right)$	$\dfrac{\overline{W}}{d}$	$1-\exp\left(-\overline{W}/d\right)$

Definitions:

$$x=\frac{\overline{S}X}{2\pi\overline{\gamma}_L};\quad \beta=\pi\frac{\overline{\gamma}_L}{d};\quad \tau=\frac{\overline{S}}{d}X=2\beta x;\quad L(x)\simeq x\left[1+\left(\frac{\pi x}{2}\right)^{5/4}\right]^{-2/5}$$

Satisfying these two conditions requires [2]

$$\frac{\overline{S}}{d}=\frac{1}{\Delta\eta}\sum_{i=1}^{N}S_i,\qquad \frac{\overline{\gamma}_L}{d}=\frac{C_\gamma}{\Delta\eta}\frac{\left[\sum_{i=1}^{N}(S_i\gamma_{Li})^{1/2}\right]^2}{\sum_{i=1}^{N}S_i},\tag{11.82}$$

with $C_\gamma = 1$ for the uniform statistical model, and $C_\gamma = 4/\pi$ for the Goody and Malkmus models; the latter two models will always have some weak lines, resulting in a smaller value for $\overline{W}/d$, even in the strong line limit (based on *average* line strength). The results from the statistical models have also been summarized in Table 11.1.

The narrow band emissivities from all four models are compared in Fig. 11-13 as a function of the optical path of an average spectral line (i.e., average absorption coefficient $\overline{S}/2\pi\overline{\gamma}_L$ multiplied by distance X). Note that all predictions are relatively close to each other, although the statistical models may predict up to 20% lower emissivities for optically thick situations. The Goody and Malkmus models more or less coincide for small values of β, giving somewhat lower emissivities than the uniform statistical model because of their different strong line behavior. For optically thin situations ($x < 1$) the uniform statistical and Goody's model move toward the Elsasser model, with lower emissivities predicted by the Malkmus model. Note that the Elsasser lines were drawn from numerical evaluations of equation (11.66), not from equation (11.68), which would show serious error for the $\beta = 1$ line.

Example 11.2. The following data are known at a certain spectral location for a pure gas at 300 K and 0.75 atm: The mean line spacing is 0.6 cm^{-1}, the mean line half-width is 0.03 cm^{-1}, and the mean line strength (or integrated absorption coefficient) is 0.08 $\text{cm}^{-2}\,\text{atm}^{-1}$. What is the mean spectral emissivity for geometric path lengths of 1 cm and 1 m, if the gas is diatomic (such as CO), or if the gas is polyatomic (such as water vapor)?

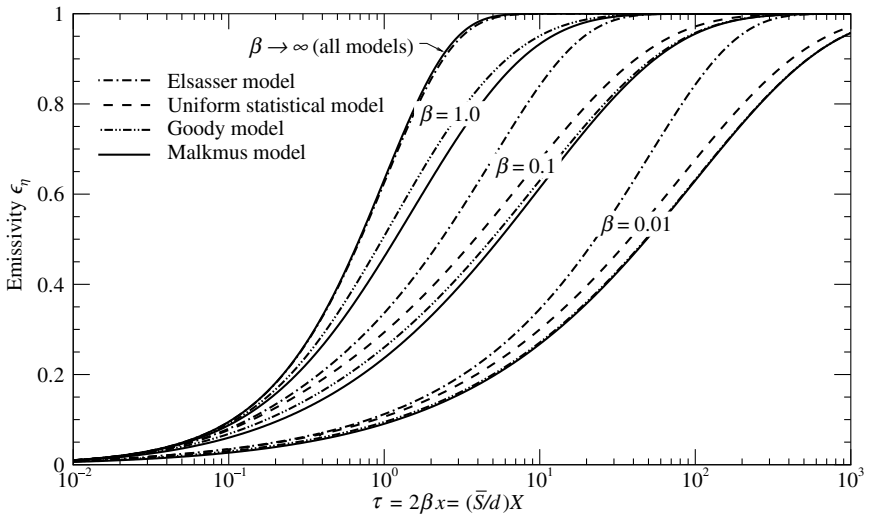

FIGURE 11-13
Mean spectral emissivities for Lorentz lines as a function of average optical depth $(\bar{S}/d)X$.

Solution
Since the units of the given line strength tell us that a pressure absorption coefficient has been used, we need to employ a pressure path length $X = ps$. For a path length of 1 cm we get $X = 0.75\,\text{atm} \times 1\,\text{cm} = 0.75\,\text{cm atm}$ and $x = SX/2\pi\gamma = 0.08\,\text{cm}^{-2}\,\text{atm}^{-1} \times 0.75\,\text{cm atm}/(2\pi\,0.03\,\text{cm}^{-1}) = 1/\pi$, while the overlapping parameter turns out to be $\beta = \pi\gamma/d = \pi \times 0.03\,\text{cm}^{-1}/0.6\,\text{cm}^{-1} = \pi/20$, and $\tau = 2\beta x = 2(\pi/20)(1/\pi) = 0.1$. For a diatomic gas for which the Elsasser model should be more accurate, we can use either equation (11.68) or (since $\beta \ll 1$) equation (11.69*c*). Evaluating the Ladenburg–Reiche function from (11.53) gives

$$L\left(\frac{1}{\pi}\right) = \frac{1}{\pi}\left[1 + 0.5^{5/4}\right]^{-2/5} = 0.2766,$$

and

$$\bar{\epsilon}_\eta = \text{erf}\left(\sqrt{\pi}\frac{\pi}{20}0.2766\right) = \text{erf}\,(0.0770) = 0.0867 \simeq 2\frac{\pi}{20}0.2766 = 0.0869 = 8.7\%.$$

If the gas is polyatomic we may want to use one of the statistical models. Choosing the Malkmus model, equation (11.79), we obtain

$$\bar{\epsilon}_\eta = 1 - \exp\left\{-\frac{1}{2}\frac{\pi}{20}\left[\left(1 + \frac{4 \times 0.1}{(\pi/20)}\right)^{1/2} - 1\right]\right\} = 0.0670.$$

If the path length is a full meter, we have $X = 75\,\text{cm atm}$ and $x = 100/\pi$ while β is still $\beta = \pi/20$ and now $\tau = 10$. Thus we are in the strong-line region. For the diatomic gas, from equation (11.69*b*) $\bar{\epsilon}_\eta = \text{erf}[\sqrt{10(\pi/20)}] = \text{erf}(1.2533) = 0.924$. For the polyatomic gas, again using equation (11.79), we get $\bar{\epsilon}_\eta = 0.692$.

In the first two cases, using the simple relation $\bar{\epsilon} = 1 - \exp(-\bar{\kappa}s)$ actually would have given fairly good results (0.095) because the gas is optically thin resulting in essentially linear absorption at every wavenumber. For the larger path we would have gotten $1 - e^{-10} \approx 1$. Thus, using an average value for the absorption coefficient makes the gas opaque at *all* wavenumbers rather than only near the line centers.

Example 11.3. For a certain polyatomic gas the line-width-to-spacing ratio and the average absorption coefficient for a vibration–rotation band in the infrared are known as

$$\left(\frac{S}{d}\right)_\eta \approx \left(\frac{S}{d}\right)_0 e^{-2|\eta-\eta_0|/\omega}, \quad \left(\frac{S}{d}\right)_0 = 10\,\text{cm}^{-1}, \tag{11.83}$$

$$\omega = 50\,\text{cm}^{-1}, \quad \frac{\gamma}{d} \approx 0.1 \approx \text{const.}$$

Find an expression for the averaged spectral emissivity and for the *total band absorptance*, defined by

$$A \equiv \int_{\text{band}} \epsilon_\eta \, d\eta = \int_0^\infty \left(1 - e^{-\kappa_\eta X}\right) d\eta,$$

for a path length of 20 cm.

Solution

Calculating the optical thickness $\tau_0 = (S/d)_0 X = 10 \times 20 = 200$, the overlap parameter $\beta = \pi/10$, and the line strength $x_0 = \tau_0/2\beta = 1000/\pi$, we find that this band falls into the "strong-line" regime everywhere except in the (unimportant) far band wings. Since we have a polyatomic molecule with exponential decay of intensity, one of the statistical models should provide the best answer. As seen from Fig. 11-13, all three statistical models give very similar results, and the (more appropriate) Goody and Malkmus models go to the same strong line limit, equation (11.81*b*), or

$$\bar{\epsilon}_\eta = 1 - e^{-\overline{W}/d} \approx 1 - \exp\left(-\sqrt{\tau\beta}\right),$$

since $\tau/\beta \gg 1$. Substituting yields the spectral emissivity,

$$\bar{\epsilon}_\eta = 1 - \exp\left(-\sqrt{\tau_0\beta}\, e^{-|\eta-\eta_0|/\omega}\right).$$

Integrating this equation over the entire band gives the total band absorptance,

$$A = \int_0^\infty \left[1 - \exp\left(-\sqrt{\tau_0\beta}\, e^{-|\eta-\eta_0|/\omega}\right)\right] d\eta.$$

Realizing that this integral has two symmetric parts and setting $\ln z = -(\eta - \eta_0)/\omega$, we have

$$A = 2\omega \int_0^1 \left[1 - \exp\left(-\sqrt{\tau_0\beta} z\right)\right] \frac{dz}{z}.$$

This integral may be solved in terms of exponential integrals[7] as given, for example, in Abramowitz and Stegun [98]. This leads to

$$A = 2\omega\left(E_1(\sqrt{\tau_0\beta}) + \ln(\sqrt{\tau_0\beta}) + \gamma_E\right) = 264.7\,\text{cm}^{-1},$$

where $\gamma_E = 0.57721\ldots$ is Euler's constant.

Most available narrow band property data, such as the RADCAL database [102,103], have been correlated with the Goody model. The correlation by Malkmus is a relative latecomer, but is today recognized as the best model for polyatomic molecules. While commonly used in the atmospheric sciences this correlation was widely ignored by the heat transfer community for many years. Taine and coworkers [92,93,104] have generated artificial narrow band properties from HITRAN 1992 line-by-line data. Employing the Malkmus model with a resolution of $25\,\text{cm}^{-1}$ they observed a maximum 10% error between line-by-line and narrow band absorptivities. Using two narrow spectral ranges of H_2O and CO_2 Lacis and Oinas [105] showed that (for a resolution of $10\,\text{cm}^{-1}$, and for total gas pressures above 0.1 atm) the correlational accuracy of the Malkmus model can be improved to better than 1% if the model parameters are found through least square fits of the HITRAN 1992 line-by-line data. Soufiani and Taine [106] have assembled the Malkmus-correlated EM2C narrow band database ($25\,\text{cm}^{-1}$ resolution) for various gases, using the HITRAN 1992 database together with some proprietary French high-temperature extensions. However, to date very few experimental narrow band data have been correlated with the Malkmus model: Phillips has measured and correlated the 2.7 μm H_2O band [107] and the 4.3 μm CO_2 band [108], both between room temperature and 1000 K. Both the RADCAL and the EM2C databases are included in Appendix F.

More recently, two generalizations of the Malkmus model have been developed, a multiscale model for nonhomogeneous gases [109] (see also below) and a generalized model more appropriate for Doppler-dominated regimes [110].

[7] Exponential integrals are discussed in some detail in Appendix E.

Gas Mixtures

Experimental data for narrow band properties, such as line overlap (γ/d) and average absorption coefficient (S/d), are usually given from correlations of measurements performed on a homogeneous column involving a single absorbing gas species. In practical applications, on the other hand, radiative properties of mixtures that contain several absorbing gas species, such as CO_2, H_2O, CO, etc., are generally required. Over large portions of the spectrum spectral lines from different species do not overlap each other, and the expressions given in Table 11.1 remain valid. However, there are regions of the spectrum where spectral line overlap is substantial and must be accounted for. For example, the two most important combustion gases, water vapor and CO_2, both have strong bands in the vicinity of 2.7 μm. Mixture values for (γ/d) and (S/d) are found from their definitions, equation (11.82), by setting

$$\sum_i S_i = \sum_n \sum_i S_{ni}; \qquad \sum_i \sqrt{S_i \gamma_i} = \sum_n \sum_i \sqrt{S_{ni} \gamma_{ni}}, \tag{11.84}$$

where the subscript n identifies the gas species. Comparing equation (11.82) for the mixture and its individual components readily leads to

$$\left(\frac{S}{d}\right)_{\text{mix}} = \sum_n \left(\frac{S}{d}\right)_n; \qquad \left(\frac{\gamma}{d}\right)_{\text{mix}} \left(\frac{S}{d}\right)_{\text{mix}} = \left[\sum_n \sqrt{\left(\frac{\gamma}{d}\right)_n \left(\frac{S}{d}\right)_n}\right]^2. \tag{11.85}$$

Expressions in Table 11.1 together with equation (11.85) can then be used to evaluate the transmissivity of a gas mixture. Other expressions for mixture values of (γ/d) and (S/d) have been discussed by Liu and coworkers [111].

Taine and Soufiani [4] pointed out that there is no physical reason why there should be any significant correlation between the spectral variation of absorption coefficients of different gas species. If one treats the absorption coefficients of the M species as statistically independent random variables, the transmissivity of a mixture can be evaluated as the product of the individual species' transmissivities,

$$\overline{\tau}_{\eta,\text{mix}} = 1 - \overline{\epsilon}_{\eta,\text{mix}} = \prod_{m=1}^{M} \overline{\tau}_{\eta,m}. \tag{11.86}$$

For example, comparing the mixture transmissivity of a room temperature water vapor–carbon dioxide mixture for the overlapping 2.7 μm region, calculated directly from the HITRAN database and from equation (11.86), they found them to be virtually indistinguishable.

Nonhomogeneous Gases

Up to this point in calculating narrow band emissivities we have tacitly assumed that the gas is isothermal, and has constant total and partial pressure of the absorbing gas everywhere, i.e., we replaced the integral $\int_0^X \kappa \, dX$ in equation (11.61) by κX. We now want to expand our results to include nonhomogeneous gases. For the Elsasser model the solution to equation (11.66) is possible, but too cumbersome to allow a straightforward solution if properties are path-dependent. For the more important statistical models the same is true, especially if not only line strength, S, but also the line overlap parameter, β, varies along the path. Instead, one resorts to approximations. The best known and most widely used approximation is known as the Curtis–Godson two parameter scaling approximation [2, 112], which has been fairly successful. Other scaling approximations have been developed, e.g., the one by Lindquist and Simmons [113]. In the Curtis–Godson approximation the values of τ and β used in equation (11.66), or (11.68) (Elsasser model) and equations (11.70) plus (11.77) through (11.79) (statistical models) are replaced by path-averaged values $\widetilde{\tau}$ and $\widetilde{\beta}$. The proper values (scaling) for $\widetilde{\tau}$ and

$\widetilde{\beta}$ are found by satisfying both the optically thin and optically thick limits. Thus, we find from equations (11.54*a*) and (11.54*b*), for a single line "*i*",

$$x \ll 1: \qquad W_i = \int_0^X S_i(X)\, dX, \tag{11.87}$$

$$x \gg 1: \qquad W_i = 2\sqrt{\int_0^X S_i(X)\, \gamma_{Li}(X)\, dX}. \tag{11.88}$$

For many lines, from equation (11.71),

$$x \ll 1: \qquad \overline{W} = \frac{1}{N}\sum_{i=1}^{N} \int_0^X S_i(X)\, dX = \int_0^X \overline{S}(X)\, dX. \tag{11.89}$$

Now, from equation (11.69*a*) or (11.80),

$$\widetilde{\tau} = \frac{\overline{W}}{d} = \int_0^X \left(\frac{\overline{S}}{d}\right) dX. \tag{11.90}$$

For strong lines we obtain

$$x \gg 1: \qquad \overline{W} = \frac{2}{N}\sum_{i=1}^{N} \sqrt{\int_0^X S_i(X)\, \gamma_{Li}(X)\, dX}. \tag{11.91}$$

If one assumes S_i and γ_{Li} to be separable, i.e., they can be written as, e.g., $S_i(X) = S_{i0} f_s(X)$, where S_{i0} is a different constant for each line, and $f_s(X)$ is a function of the path (but the same for each line), one can—after some manipulation—rewrite equation (11.91) as [4]

$$x \gg 1: \qquad \overline{W}^2 = \left(\frac{2}{N}\right)^2 \int_0^X \left[\sum_{i=1}^{N} \sqrt{S_i(X)\, \gamma_{Li}(X)}\right]^2 dX. \tag{11.92}$$

Comparing with equation (11.54*b*) [or (11.81)], and utilizing equation (11.82) we obtain

$$\left(\frac{\overline{W}}{d}\right)^2 = \frac{4/\pi}{C_\gamma}\widetilde{\tau}\widetilde{\beta} = \frac{4}{d^2}\int_0^X \overline{S}(X)\, \gamma_L(X)\, dX \tag{11.93}$$

or

$$\widetilde{\beta} = \frac{1}{\widetilde{\tau}} \int_0^X \frac{\overline{S}}{d}\beta\, dX. \tag{11.94}$$

Equations (11.68) and (11.77) through (11.79) may now be used with $\widetilde{\tau}$ and $\widetilde{\beta}$ to calculate narrow band emissivities for nonhomogeneous paths.

The accuracy of various scaling approximations was tested by Hartmann and coworkers [93, 104] for various nonhomogeneous conditions in CO_2–N_2 and H_2O–N_2 mixtures. It was found that the Malkmus model together with the Curtis–Godson scaling approximation generally gave the most accurate results, except in the presence of strong (total) pressure gradients. More recently a multiscale Malkmus model was developed by Bharadwaj and Modest [109] to improve its accuracy for nonhomogeneous paths. In this scheme it is assumed that high-temperature spectral lines (coming from elevated vibrational energy levels, i.e., with larger lower level energy E_l) are uncorrelated from lower temperature lines. This implies that transmissivities of the individual "scales" are multiplicative [equation (11.86)]. Separating the gas accordingly into

scales and applying equation (11.75) to each scale m as well as the Curtis–Godson approximation leads to

$$\frac{\overline{W}}{d} = \sum_m \frac{\tilde{\beta}_m}{2} \left[\left(1 + \frac{4\tilde{\tau}_m}{\tilde{\beta}_m} \right)^{1/2} - 1 \right], \tag{11.95}$$

with $\tilde{\tau}_m$ and $\tilde{\beta}_m$ from equations (11.90) and (11.94). Bharadwaj and Modest also outlined how scales are to be defined, whether using experimental data or data from spectroscopic databases. Testing the method with various nonhomogeneous CO_2–H_2O–N_2 mixtures, they found the 2-scale Malkmus model to be a factor of 2 to 5 more accurate than the standard Curtis–Godson approach.

11.9 NARROW BAND *k*-DISTRIBUTIONS

As in the case of "traditional" narrow band models (i.e., Elsasser and statistical models), we will start by looking at a homogeneous medium (constant temperature, pressure, and concentrations), i.e., a medium whose absorption coefficient is a function of wavenumber alone. In such a medium the spectral intensity depends on geometry, the Planck function, $I_{b\eta}$, emittance of bounding surfaces, ϵ_η, the absorption and scattering coefficients of suspended particles, $\kappa_{p\eta}$ and $\sigma_{s\eta}$, and finally the absorption coefficient of any absorbing gas. Over a small spectral interval, such as a few tens of wavenumbers, the Planck function and nongaseous radiation properties remain essentially constant. Thus, across such a small spectral interval the intensity varies with gas absorption coefficient alone. On the other hand, Fig. 11-11 shows that the gas absorption coefficient varies wildly even across a very narrow spectrum, attaining the same value for κ_η many times, each time producing the identical intensity field within the medium. Thus, carrying out line-by-line calculations across such a spectrum would be rather wasteful, repeating the same calculation again and again. It would, therefore, be advantageous to reorder the absorption coefficient field into a smooth, monotonically increasing function, assuring that each intensity field calculation is carried out only once.

This reordering idea was first reported in the Western literature by Arking and Grossman [114], but they give credit to Kondratyev [115], who in turn credits a 1939 Russian paper. Other early publications on *k*-distributions are by Goody and coworkers [116], Lacis and Oinas [105], and Fu and Liou [117], all in the field of meteorology (atmospheric radiation). In the heat transfer area most of the work on *k*-distributions again is due to the group around Taine and Soufiani in France [106, 118–120].

The narrow band average of any spectral quantity that depends only on the gaseous absorption coefficient, such as intensity $\bar{I}_\eta$, transmissivity $\overline{\tau}_\eta$, etc., can be rewritten in terms of a *k*-distribution $f(k)$ as follows (here expressed for transmissivity $\overline{\tau}_\eta$):

$$\overline{\tau}_\eta(X) = \frac{1}{\Delta\eta} \int_{\Delta\eta} e^{-\kappa_\eta X} \, d\eta = \int_0^\infty e^{-kX} f(k) \, dk. \tag{11.96}$$

The nature of *k*-distributions and how to evaluate them is best illustrated by looking at a very small part of the spectrum with very few lines. Figure 11-14*a* shows a fraction of the CO_2 15 μm band at 1 bar and 296 K and, to minimize irregularity, with only the strongest 10 lines considered (two of them having their centers slightly outside the depicted spectral range). It is seen that the absorption coefficient goes through a number of minima and maxima; between any two of these the integral may be rewritten as

$$\int e^{-\kappa_\eta X} \, d\eta = \int_{\kappa_{\eta,\min}}^{\kappa_{\eta,\max}} e^{-\kappa_\eta X} \left| \frac{d\eta}{d\kappa_\eta} \right| d\kappa_\eta.$$

The absolute value sign comes from the fact that, where $d\kappa_\eta/d\eta < 0$, we have changed the direction of integration (always from $\kappa_{\eta,\min}$ to $\kappa_{\eta,\max}$). Therefore, integration over the entire

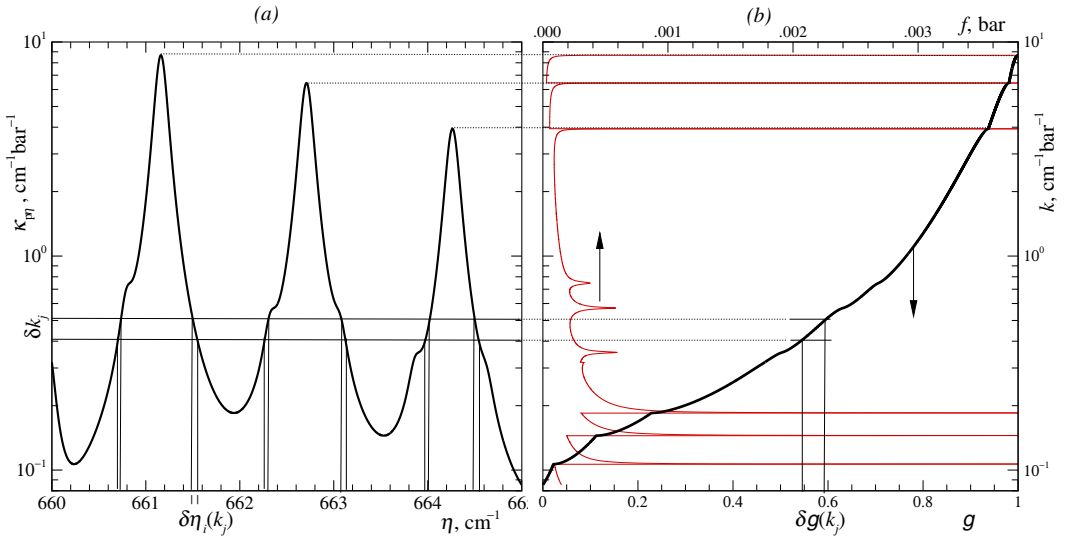

FIGURE 11-14
Extraction of *k*-distributions from spectral absorption coefficient data: *(a)* simplified absorption coefficient across a small portion of the CO_2 15 μm band (p = 1.0 bar, T = 296 K); *(b)* corresponding *k*-distribution $f(k)$ and cumulative *k*-distribution $k(g)$.

range $\Delta\eta$ gives $f(k)$ as a weighted sum of the number of points where $\kappa_\eta = k$,

$$f(k) = \frac{1}{\Delta\eta} \sum_i \left| \frac{d\eta}{d\kappa_\eta} \right|_i . \tag{11.97}$$

Mathematically, this can be put into a more elegant form as

$$f(k) = \frac{1}{\Delta\eta} \int_{\Delta\eta} \delta(k - \kappa_\eta)\, d\eta, \tag{11.98}$$

where $\delta(k - \kappa_\eta)$ is the *Dirac-delta function* defined by

$$\delta(x) = \lim_{\delta\epsilon \to 0} \begin{cases} 0, & |x| > \delta\epsilon, \\ \dfrac{1}{2\delta\epsilon}, & |x| < \delta\epsilon, \end{cases} \tag{11.99a}$$

or

$$\int_{-\infty}^{\infty} \delta(x)\, dx = 1. \tag{11.99b}$$

The *k*-distribution of the absorption coefficient in Fig. 11-14*a* is shown as the thin solid line in Fig. 11-14*b*. Even for this minuscule fraction of the spectrum with only three dominant lines, $f(k)$ shows very erratic behavior: wherever the absorption coefficient has a maximum or minimum $f(k) \to \infty$ since $|d\kappa_\eta/d\eta| = 0$ at those points (6 in the present case); and wherever a semistrong line produces a wiggle in the absorption coefficient $f(k)$ has a strong maximum. Thankfully, the *k*-distribution itself is not needed during actual calculations. Introducing the *cumulative k-distribution function* $g(k)$ as

$$g(k) = \int_0^k f(k)\, dk, \tag{11.100}$$

we may rewrite the transmissivity (or any other narrow band-averaged quantity) as

$$\overline{\tau}_\eta(X) = \int_0^\infty e^{-kX} f(k)\, dk = \int_0^1 e^{-k(g)X} dg, \tag{11.101}$$

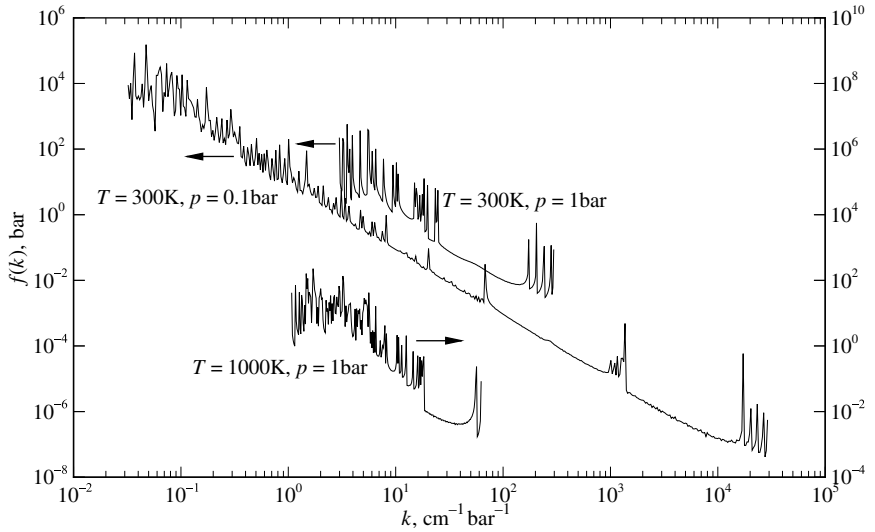

FIGURE 11-15
CO_2 k-distributions for the three cases depicted in Fig. 11-11.

with $k(g)$ being the inverse function of $g(k)$, which is shown in Fig. 11-14*b* as the thick solid line. Sticking equation (11.100) into (11.98) leads to

$$g(k) = \int_0^k f(k)\,dk = \frac{1}{\Delta\eta}\int_{\Delta\eta}\int_0^k \delta(k-\kappa_\eta)\,dk\,d\eta = \frac{1}{\Delta\eta}\int_{\Delta\eta} H(k-\kappa_\eta)\,d\eta, \tag{11.102}$$

where $H(k)$ is *Heaviside's unit step function,*

$$H(x) = \begin{cases} 0, & x < 0, \\ 1, & x > 0. \end{cases} \tag{11.103}$$

Thus, $g(k)$ represents the fraction of the spectrum whose absorption coefficient lies below the value of k and, therefore, $0 \le g \le 1$ [this can also be seen by setting $X = 0$ in equations (11.96) or (11.101), leading to $\overline{\tau}_\eta = 1$]. g acts as a nondimensional wavenumber (normalized by $\Delta\eta$), and the reordered absorption coefficient $k(g)$ is a smooth, monotonically increasing function, with minimum and maximum values identical to those of $\kappa_\eta(\eta)$.

In actual reordering schemes values of k are grouped over small ranges $k_j \le k < k_j + \delta k_j = k_{j+1}$, as depicted in Fig. 11-14, so that

$$dg(k_j) = f(k_j)\delta k_j \simeq \frac{1}{\Delta\eta}\sum_i \left|\frac{\delta\eta}{\delta\kappa_\eta}\right|_i \delta k_j = \frac{1}{\Delta\eta}\sum_i \delta\eta_i(k_j), \tag{11.104}$$

where the summation over i collects all the occurrences where $k_j < \kappa_\eta < k_{j+1}$, as also indicated in the figure. If the absorption coefficient is known from line-by-line data, the k-distribution is readily calculated from equation (11.104).

The k-distributions for the three cases in Fig. 11-11 are shown in Fig. 11-15. Because of the many maxima and minima in the absorption coefficient these functions show very erratic behavior, as expected. Numerically, one can never obtain the singularities $f(k) \to \infty$, and they appear as sharp peaks [strongly dependent on the spacing used for η and δk in equation (11.104)]. Inaccurate evaluation of $f(k)$ (such as its peaks) has little influence on $k(g)$, which is much easier to determine accurately. This, and the fact that $g(k)$ represents the fraction of wavenumbers with $k_\eta \le k$, suggests a very simple method to evaluate $f(k)\delta k$ and $g(k)$: the wavenumber range $\Delta\eta$ is broken up into N intervals $\delta\eta$ of equal width. The absorption coefficient at the center of each

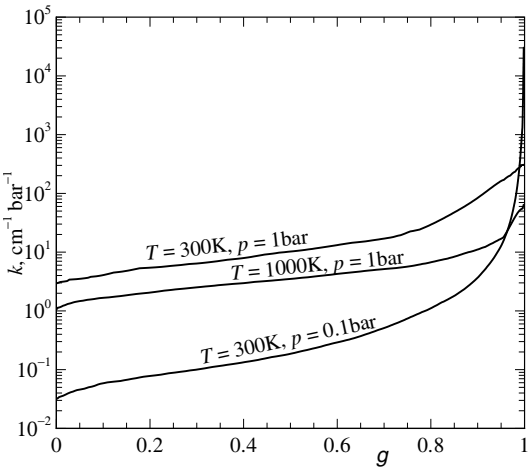

FIGURE 11-16
k-values as a function of cumulative k-distribution g for the three CO_2 cases depicted in Fig. 11-11.

interval is evaluated and, if $k_j \le \kappa_\eta < k_{j+1}$, the value of $f(k_j)\delta k_j$ is incremented by $1/N$. After all intervals have been tallied $f(k_j)\delta k_j$ contains the fraction of wavenumbers with $k_j \le \kappa_\eta < k_{j+1}$, and

$$g(k_{j+1}) = \sum_{j'=1}^{j} f(k_{j'})\delta k_{j'} = g(k_j) + f(k_j)\delta k_j. \tag{11.105}$$

The $k(g)$ for the three cases in Fig. 11-11 are shown in Fig. 11-16.

Program `nbkdistdb` in Appendix F is a Fortran code that calculates such a $g(k)$ distribution directly from a spectroscopic database, while `nbkdistsg` determines a single k-distribution from a given array of wavenumber–absorption coefficient pairs. As an example for the determination of k-distributions, the instructions to `nbkdistdb` show how to obtain the distributions of Figs. 11-15 and 11-16.

The k-distribution can be found more easily if accurate narrow band transmissivity data are available: inspection of equation (11.96) shows that $\overline{\tau}_\eta$ is the Laplace transform of $f(k)$, i.e.,

$$f(k) = \mathscr{L}^{-1}\{\overline{\tau}_\eta(X)\}, \tag{11.106}$$

where $\mathscr{L}^{-1}$ indicates inverse Laplace transform. This was first recognized by Domoto [121], who also found an analytical expression for the k-distribution based on the Malkmus model, equation (11.79):

$$f(k) = \frac{1}{2}\sqrt{\frac{\overline{\kappa}\beta}{\pi k^3}}\exp\left[\frac{\beta}{4}\left(2 - \frac{\overline{\kappa}}{k} - \frac{k}{\overline{\kappa}}\right)\right], \quad \overline{\kappa} = \frac{S}{d}. \tag{11.107}$$

The cumulative k-distribution can also be determined analytically as

$$g(k) = \frac{1}{2}\,\mathrm{erfc}\left[\frac{\sqrt{\beta}}{2}\left(\sqrt{\frac{\overline{\kappa}}{k}} - \sqrt{\frac{k}{\overline{\kappa}}}\right)\right] + \frac{1}{2}\,e^{\beta}\,\mathrm{erfc}\left[\frac{\sqrt{\beta}}{2}\left(\sqrt{\frac{\overline{\kappa}}{k}} + \sqrt{\frac{k}{\overline{\kappa}}}\right)\right], \tag{11.108}$$

where erfc is the *complementary error function* [98] and, by convention, $\mathrm{erfc}(-\infty) = 2$.

Example 11.4. A certain diatomic gas is found to have an absorption coefficient that obeys Elsasser's model across a narrow band of width $\Delta\eta = 10\,\mathrm{cm}^{-1}$. The gas conditions are such that mean absorption coefficient (S/d) and overlap parameter β are known for the $N = \Delta\eta/d$ lines across the narrow band. Determine the narrow band k-distribution of the gas.

Solution

From equation (11.64) the absorption coefficient may be written as

$$\kappa_\eta = \frac{S}{d}\frac{\sinh 2\beta}{\cosh 2\beta - \cos\left(2\beta\dfrac{\eta-\eta_c}{\gamma}\right)}, \quad \eta_l < \eta < \eta_l + \Delta\eta, \tag{11.109}$$

where η_l is the minimum wavenumber of the narrow band and η_c is the line center position of any one line in the band. Because of the periodic nature of an Elsasser band (see Fig. 11-12*a*), there will be exactly $2N$ wavelengths where

$$k_{\min} = \frac{S}{d}\frac{\sinh 2\beta}{\cosh 2\beta + 1} < k = \kappa_\eta < k_{\max} = \frac{S}{d}\frac{\sinh 2\beta}{\cosh 2\beta - 1}$$

with identical $|d\kappa_\eta/d\eta|$ each time. Therefore, from equation (11.97) or (11.98)

$$f(k) = \frac{1}{\Delta\eta}\int \delta(k-\kappa_\eta)\left|\frac{d\eta}{d\kappa_\eta}\right|_{k=\kappa_\eta} d\kappa_\eta = \frac{2N}{\Delta\eta}\left|\frac{d\eta}{d\kappa_\eta}\right|_{k=\kappa_\eta}.$$

But

$$\left|\frac{d\kappa_\eta}{d\eta}\right| = \frac{S}{d}\frac{\sinh 2\beta}{\left[\cosh 2\beta - \cos\left(2\beta\dfrac{\eta-\eta_c}{\gamma}\right)\right]^2}\frac{2\beta}{\gamma}\sin\left(2\beta\frac{\eta-\eta_c}{\gamma}\right) = \frac{\kappa_\eta^2}{\dfrac{S}{d}\sinh 2\beta}\frac{2\beta}{\gamma}\sin\left(2\beta\frac{\eta-\eta_c}{\gamma}\right),$$

and

$$\sin\left(2\beta\frac{\eta-\eta_c}{\gamma}\right) = \sin\left(\cos^{-1}\left[\cosh 2\beta - \frac{S}{d}\frac{\sinh 2\beta}{\kappa_\eta}\right]\right) = \sqrt{1-\left[\cosh 2\beta - \frac{S}{d}\frac{\sinh 2\beta}{\kappa_\eta}\right]^2}.$$

Therefore,

$$\begin{aligned} f(k) &= \frac{2}{d}\frac{\gamma}{2\beta}\frac{\dfrac{S}{d}\sinh 2\beta}{k^2}\Bigg/\sqrt{1-\left[\cosh 2\beta - \frac{S}{d}\frac{\sinh 2\beta}{k}\right]^2} \\ &= \frac{1}{\pi}\frac{\dfrac{S}{d}\sinh 2\beta}{k\sqrt{k^2-\left(k\cosh 2\beta - \dfrac{S}{d}\sinh 2\beta\right)^2}}. \end{aligned}$$

Integrating $f(k)$ according to equation (11.101) we obtain (using integration tables),

$$g(k) = 1 - \frac{1}{\pi}\cos^{-1}\left[\cosh 2\beta - \frac{S}{d}\frac{\sinh 2\beta}{k}\right]$$

or, after inversion,

$$k = \frac{S}{d}\frac{\sinh 2\beta}{\cosh 2\beta - \cos\pi(1-g)}. \tag{11.110}$$

This is, of course, just equation (11.109) with $2\beta(\eta-\eta_c)/\gamma$ replaced by $\pi(1-g)$: the k-distribution recognizes that, in the Elsasser scheme, the same structure is repeated $2N$ times (of that N times as a mirror image), and a single half-period is stretched across the entire reordered range $0 \le g \le 1$. The present k-distribution can also be obtained by precalculating an array of absorption coefficients across $\Delta\eta$ from equation (11.109) and using subroutine `nbkdistsg` in Appendix F.

Comparing equation (11.101) with the first expression in equation (11.96), we note that the integration in equation (11.101) is equivalent in difficulty to the integration over half of a single line. Given that a narrow spectral range can contain thousands of little overlapping lines, we conclude that the CPU time savings over line-by-line calculations can be enormous! However, the generation of the necessary k-distributions from the large number of spectral lines contained in the various spectroscopic databases is tedious and time consuming. A first database of

narrow band *k*-distributions for CO_2 and H_2O was offered by Soufiani and Taine [106] as part of their EM2C narrow band database. It contains *k*-distribution data for fairly wide spectral intervals (larger than $100\,cm^{-1}$; 17 bands for CO_2 and 44 for H_2O), and are valid for atmospheric pressure and temperatures up to 2500 K. Each *k*-distribution is defined by 7 *k*-values, to be used with a 7-point Gaussian quadrature for spectral integration. Like their Malkmus parameter counterparts they are generated from the HITRAN 1992 database plus proprietary extensions (cf. p. 333). A more accurate, highly compact database, also for CO_2 and H_2O, was generated by Wang and Modest [122], valid for total pressures between 0.1 bar and 30 bar, and temperatures between 300 K and 2500 K. The spectrum is divided into 248 narrow bands for all gases (allowing the determination of mixture *k*-distributions from those of individual species). Nested Gauss–Chebychev quadrature with up to 128 quadrature points is used to guarantee 0.5% accuracy for all absorption coefficient and emissivity calculations, and to allow for variable order spectral quadrature. The original Wang and Modest database employed the CDSD-1000 database [67] (for CO_2) and HITEMP 1995 [62] (for H_2O). This Narrow Band K-Distribution for InfraRed (NBKDIR) database has since then been augmented to include additional species (CO, CH_4, and C_2H_4), and is continuously updated to incorporate the newest spectroscopic data; at the time of print all *k*-distributions have been obtained from HITEMP 2010 [74] (H_2O, CO_2, and CO) and HITRAN 2008 [32], (CH_4 and C_2H_4). Both EM2C and NBKDIR are included in Appendix F.

Gas Mixtures

k-distributions for mixtures can, in principle, be calculated directly, simply by adding the linear, spectral absorption coefficients of all components in the mixture before applying the reordering process, equation (11.104). Since assembling *k*-distributions is a tedious, time-consuming affair, it is desirable to obtain them from databases. However, determining an exact *k*-distribution for a mixture from those of individual species is in general impossible, because *k*-distributions never retain any information pertaining to the spectral location of individual absorption lines. Only in two simple situations is exact manipulation of *k*-distributions feasible: (1) a gas "mixing" with itself, i.e., changing the concentration of the absorbing gas species, and (2) adding a gray (across the given narrow band) material to the nongray absorbing gas.

Variable Mole Fraction of a Single Absorbing Gas Consider a gas whose absorption coefficient is linearly dependent on its partial pressure, i.e., a gas whose line broadening is unaffected by its own partial pressure. This is always true for molecules that have the same size as the surrounding broadening gas (such as CO_2 in air), and for all gases whenever Doppler broadening dominates. Then

$$\kappa_{x\eta}(T,p,x;\eta) = x\kappa_\eta(T,p;\eta), \tag{11.111}$$

where κ_η is the absorption coefficient of the pure gas and x is its mole fraction in a mixture. Comparing the two *k*-distributions

$$f(T,p;k) = \frac{1}{\Delta\eta}\int_{\Delta\eta}\delta(k-\kappa_\eta)\,d\eta, \tag{11.112}$$

$$f_x(T,p,x;k_x = xk) = \frac{1}{\Delta\eta}\int_{\Delta\eta}\delta(k_x-\kappa_{x\eta})\,d\eta, \tag{11.113}$$

we see that they both are populated by exactly the same spectral locations (i.e., $k_x = \kappa_{x\eta}$ wherever $k = \kappa_\eta$), so that

$$f_x(T,p,x;k_x)\,d(xk) = f(T,p;k)\,dk$$

or

$$f_x(T,p,x;k_x) = \frac{1}{x}f(T,p;k_x/x). \tag{11.114}$$

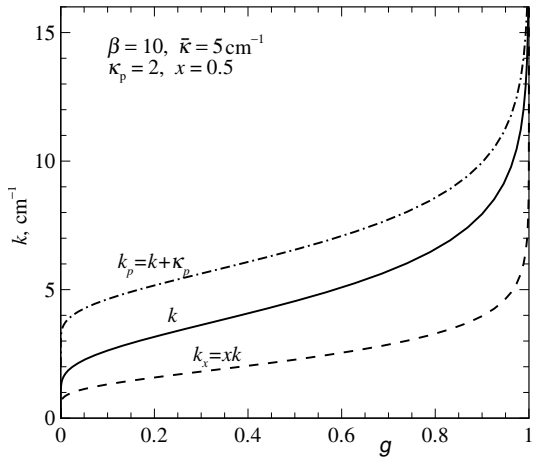

FIGURE 11-17
Scalability of narrow band k-distributions: k: pure gas; k_x: gas with mole fraction $x = 0.5$; k_p: gas mixed with gray medium of $\kappa_p = 2\,\mathrm{cm}^{-1}$.

Integrating equation (11.114) leads to

$$g(T,p;k) = \int_0^k f(T,p;k)\,dk = \int_0^{k_x} f_x(T,p,x;k_x)\,dk_x = g_x(T,p,x;k_x), \tag{11.115}$$

i.e., the k *vs.* g behavior is independent of mole fraction. In a k *vs.* g plot the lines are simply vertically displaced by a multiplicative factor of x, or

$$k_x(g) = xk(g), \tag{11.116}$$

as demonstrated in Fig. 11-17 for a k-distribution based on the Malkmus model, equation (11.108) (using an unrealistically large overlap parameter of $\beta = 10$ for better visibility).

Single Absorbing Gas Mixed with Gray Medium Consider a gas that is mixed with a gray medium (say, particles), with constant absorption coefficient κ_p. Then

$$\kappa_{p\eta}(T,p,\kappa_p;\eta) = \kappa_\eta(T,p,\eta) + \kappa_p. \tag{11.117}$$

Proceeding as in the previous paragraph we obtain

$$\begin{aligned} f_p(T,p,\kappa_p;k_p) &= \frac{1}{\Delta\eta}\int_{\Delta\eta} \delta(k_p - [\kappa_{x\eta} + \kappa_p])\,d\eta \\ &= \frac{1}{\Delta\eta}\int_{\Delta\eta} \delta([k_p - \kappa_p] - \kappa_{x\eta})\,d\eta \\ &= f(T,p;k = k_p - \kappa_p) \end{aligned} \tag{11.118}$$

and

$$g(T,p;k) = g_p(T,p,\kappa_p;k_p = k + \kappa_p), \tag{11.119}$$

i.e., the k *vs.* g behavior is also independent of any gray additions. In a k *vs.* g plot the lines are simply vertically displaced by a constant amount of κ_p,

$$k_p(g) = \kappa_p + k(g), \tag{11.120}$$

as also shown in Fig. 11-17.

Multispecies Mixtures Several approximate mixing models for k-distributions have been proposed that rely on assumptions about the statistical relationships between the absorption lines of the individual species, mostly by Solovjov and Webb [123] (full spectrum models only),

such as their convolution, superposition, multiplication, and hybrid approaches, and by Modest and Riazzi [124], exploiting the uncorrelatedness between species. All of these approaches produce a single mixture k-distribution, but rely on different assumptions and methodologies to achieve their goal. It was found that the approach of Modest and Riazzi results in negligible errors for all conditions tested (low to moderate pressures). Very recently, Pal and Modest [125] found that their methodology works equally well at very high pressures (up to 30 bar), even though broadened spectral lines overlap much more strongly. Consequently, we will present here only the Modest and Riazzi mixing scheme.

Earlier it was shown how the idea of uncorrelated absorption coefficients can be used to obtain the transmissivity of a mixture, as given by equation (11.86). Through simple mathematical manipulation, it is possible to extend this logic to the mixing of cumulative k-distributions. We begin by recalling that the definition of the transmissivity, in terms of the k-distribution for a single absorbing species, is also the definition of the Laplace transform of $f(k)$ [121], equation (11.106). Using this and the product of transmissivities model, the transmissivity of a mixture of M species may be expressed as the product of the Laplace transforms of the component k-distributions, or

$$\bar{\tau}_{\eta,\text{mix}} = \mathscr{L}[f_{\text{mix}}(k)] = \prod_{m=1}^{M} \bar{\tau}_{\eta,m} = \prod_{i=m}^{M} \mathscr{L}[f_m(k)]. \tag{11.121}$$

In terms of the cumulative k-distributions, the transmissivity of an individual component is given by

$$\bar{\tau}_m = \int_0^1 e^{-k_m L} dg_m, \tag{11.122}$$

and for a binary mixture this becomes

$$\bar{\tau}_{\text{mix}} = \mathscr{L}[f_{\text{mix}}(k)] = \int_0^1 e^{-k_1 L} dg_1 \int_0^1 e^{-k_2 L} dg_2 = \int_{g_1=0}^1 \int_{g_2=0}^1 e^{-[k_1(g_1)+k_2(g_2)]L} dg_2\, dg_1. \tag{11.123}$$

Using the integral property of the Laplace transform we obtain

$$\begin{aligned} \mathscr{L}\left[\int_0^k f_{\text{mix}}(k)\right] = \mathscr{L}[g_{\text{mix}}(k)] &= \left(\int_{g_1=0}^1 \int_{g_2=0}^1 e^{-[k_1(g_1)+k_2(g_2)]L} dg_2\, dg_1\right) \frac{1}{L} \\ &= \int_{g_1=0}^1 \int_{g_2=0}^1 \frac{e^{-[k_1(g_1)+k_2(g_2)]L}}{L} dg_2\, dg_1, \end{aligned} \tag{11.124}$$

or, when the inverse transform is taken, with H being the Heaviside step function,

$$g_{\text{mix}}(k_{\text{mix}}) = \int_{g_1=0}^1 \int_{g_2=0}^1 H[k_{\text{mix}} - (k_1 + k_2)] dg_2\, dg_1 = \int_{g_1=0}^1 g_2(k_{\text{mix}} - k_1)\, dg_1. \tag{11.125}$$

In the second, once integrated expression, it is assumed that $g_m(k < k_{m,\min}) = 0$ (i.e., *all* absorption coefficients are above $k_{m,\min}$) and $g_m(k > k_{m,\max}) = 1$ (i.e., *all* absorption coefficients are below $k_{m,\max}$). This relation may also be readily extended to a mixture of M species,

$$g_{\text{mix}}(k_{\text{mix}}) = \int_{g_1=0}^1 .... \int_{g_M=0}^1 H[k_{\text{mix}} - (k_1 + ... + k_M)] dg_M .... dg_1. \tag{11.126}$$

This integral may be evaluated by multiple Gaussian quadrature, leading to a single mixture k-distribution at specific k-values while using the component k-distributions stored at quadrature points with their associated weights. The k-values for this new mixture distribution must be

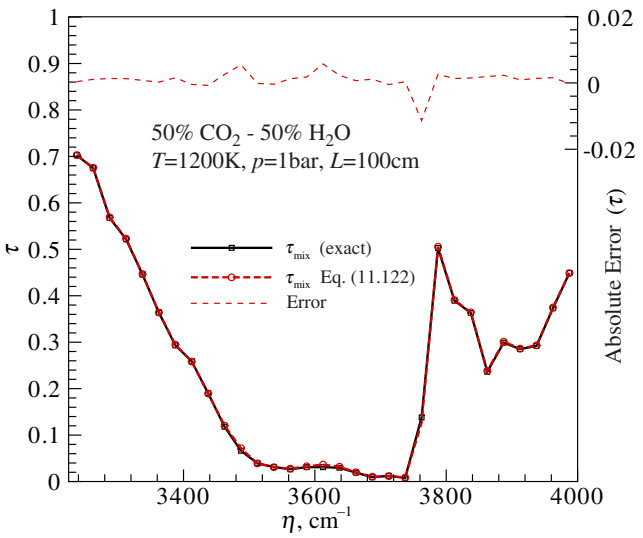

FIGURE 11-18
Narrow band transmissivity of a CO_2–H_2O mixture from individual species k-distributions, equation (11.126).

predetermined and chosen such that they cover the entire range of values of all component species. Carrying out mixing with this model consistently outperforms the models of Solovjov and Webb [123] (by a factor of 10 or more). Its accuracy is demonstrated in Fig. 11-18 for a mixture of water vapor and carbon dioxide in the 2.7 μm region (where both gases heavily overlap), with absolute errors mostly below 0.005 (roughly the same as obtained by direct multiplication of transmissivities). The mixing scheme described here is incorporated into the NBKDIR database in Appendix F, i.e., NBKDIR allows for the retrieval of mixture k-distributions.

Example 11.5. Consider a mixture of two diatomic gases, both having absorption coefficients, $\kappa_{1\eta}$ and $\kappa_{2\eta}$, that obey Elsasser's model across a narrow band of width $\Delta\eta = 10\,\mathrm{cm}^{-1}$. The following is known for the two gases:

$$\text{Gas 1}: \quad d_1 = 0.2500\,\mathrm{cm}^{-1},\ \gamma_1 = 0.0250\,\mathrm{cm}^{-1},\ \frac{S_1}{d_1} = 1\,\mathrm{cm}^{-1};\quad \beta_1 = \pi\frac{\gamma_1}{d_1} = \frac{\pi}{10} = 0.314;$$

$$\text{Gas 2}: \quad d_2 = 0.1429\,\mathrm{cm}^{-1},\ \gamma_2 = 0.0050\,\mathrm{cm}^{-1},\ \frac{S_2}{d_2} = 2\,\mathrm{cm}^{-1};\ \beta_2 = \pi\frac{\gamma_2}{d_2} = \frac{7\pi}{200} = 0.110.$$

Determine the narrow band k-distribution for this mixture.

Solution
The individual k-distributions for the two component gases are given from the previous example as

$$k_i = \left(\frac{S}{d}\right)_i \frac{\sinh 2\beta_i}{\cosh 2\beta_i - \cos\pi(1-g_i)};\quad i = 1, 2. \tag{11.127}$$

The k-distribution of the mixture is immediately found from the rightmost expression in equation (11.125) as

$$g_{\mathrm{mix}}(k_{\mathrm{mix}}) = \int_{g_1=0}^{1} g_2(k_{\mathrm{mix}} - k_1)\,dg_1, \quad k_{\min} = k_{1\min} + k_{2\min} \le k_{\mathrm{mix}} \le k_{\max} = k_{1\max} + k_{2\max}, \tag{11.128}$$

where k_1 is obtained from equation (11.127), while g_2 is found from its inverse, or

$$g_2(k) = \begin{cases} 0, & k < k_{2\min}, \\ 1 - \dfrac{1}{\pi}\cos^{-1}\left[\cosh 2\beta_2 - \left(\dfrac{S}{d}\right)_2 \dfrac{\sinh 2\beta_2}{k}\right], & k_{2\min} < k < k_{2\max}, \\ 1, & k > k_{2\max}. \end{cases}$$

The integration in equation (11.128) is best carried out numerically. Here care must be taken that the argument of $\cos^{-1}$ does not fall outside its allowable range (between −1 and +1). The same holds true

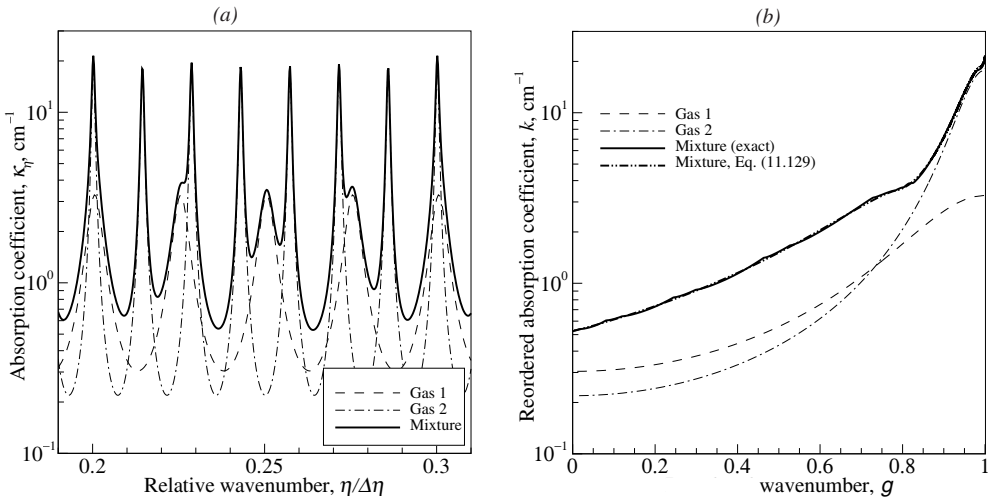

FIGURE 11-19
Narrow band *k*-distribution for a two-component mixture (Example 11.5): *(a)* absorption coefficients, *(b)* *k*-distributions.

for the mixing of any two *k*-distributions, i.e., $g_2 \equiv 0$ for $k_{\text{mix}} - k_1 \le k_{2\,\text{min}}$, and $g_2 \equiv 1$ for $k_{\text{mix}} - k_1 \ge k_{2\,\text{max}}$. The result of a simple trapezoidal rule integration is shown in Fig. 11-19. Frame *(a)* shows the absorption coefficients for the mixture and the two component gases, and Frame *(b)* the corresponding *k*-distributions. The mixture *k*-distribution is calculated in two ways: "exactly," using the absorption coefficient in Fig. 11-19*a*, or equation (11.109) (with random and different η_1 for each gas), and with equation (11.128). Semilog plots are employed to better separate the various absorption coefficients and *k*-distributions. It is apparent that both mixture *k*-distributions virtually coincide (in fact, transmissivities calculated with both *k*-distributions coincide to within 5 digits).

Nonhomogeneous Gases

Correlated-*k* Like the statistical models the *k*-distribution is not straightforward to apply to nonhomogeneous paths. However, it was found that for many important situations the *k*-distributions are essentially "correlated," i.e., if *k*-distributions $k(g)$ are known at two locations in a nonhomogeneous medium, then the absorption coefficient can essentially be mapped from one location to the other (documented to some extent by Lacis and Oinas [105]). This implies that all the values of η that correspond to one value of κ and g at one location, more or less map to the same value of g (but a different κ) at another location [105, 117]: pressure changes affect all lines equally (causing more or less broadening by higher/lower total pressure p, increasing line strengths uniformly by changes in partial pressure of the absorbing gas, p_a). We may then write, with good accuracy,

$$\overline{\tau}_\eta(0 \to X) = \frac{1}{\Delta\eta} \int_{\Delta\eta} \exp\left(-\int_0^X \kappa_\eta \, dX\right) d\eta \simeq \int_0^1 \exp\left(-\int_0^X k(X, g) \, dX\right) dg. \tag{11.129}$$

This assumption of a correlated *k*-distribution has proven very successful in the atmospheric sciences, where temperatures change only from about 200 K to 320 K, but pressure changes can be very substantial [105, 116, 117].

Scaled-*k* A more restrictive, but mathematically precise condition for correlation of *k*-distributions is to assume the dependence on wavenumber and location in the absorption coefficient to be separable, i.e.,

$$\kappa_\eta(\eta, T, p, p_a) = k_\eta(\eta) u(T, p, p_a), \tag{11.130}$$

where $k_\eta(\eta)$ is the absorption coefficient at some reference condition, and $u(T,p,p_a)$ is a non-dimensional function depending on local conditions of the gas, but not on wavenumber. This is commonly known as the *scaling approximation*. Substituting this into equation (11.129) gives

$$\overline{\tau}_\eta(0\to X)=\frac{1}{\Delta\eta}\int_{\Delta\eta}\exp\left(-k_\eta(\eta)\int_0^X u\,dX\right)d\eta=\frac{1}{\Delta\eta}\int_{\Delta\eta}\exp\left(-k_\eta\overline{X}\right)d\eta\,, \tag{11.131}$$

where $\overline{X}$ is now a path-integrated value for X. Comparing with equation (11.96), we find that in this case there is only a single k-distribution, based on the reference absorption coefficient k_η, and

$$\overline{\tau}_\eta(0\to X)=\int_0^1 e^{-k(g)\overline{X}}dg;\qquad \overline{X}=\int_0^X u\,dX. \tag{11.132}$$

As for homogeneous media equations (11.129) and (11.132) provide reordered absorption coefficients, which can be used in arbitrary radiation solvers without restrictions. At first glance, equation (11.129) looks superior to equation (11.132), since the assumption of a scaled absorption coefficient is more restrictive. However, in practice one needs to approximate an actual absorption coefficient, which is neither scaled nor correlated: if the scaling method is employed, the scaling function $u(T,p,p_a)$ and its reference state for k_η can be freely chosen and, thus, optimized for a problem at hand. On the other hand, if the correlated-k method is used, the absorption coefficient is simply *assumed* to be correlated (even though it is not), and the inherent error cannot be minimized. Following Modest and Zhang [126] and assuming constant total pressure, reference state temperature T_0 and partial pressure p_{a0} may be chosen from

$$p_{a0}=\frac{1}{V}\int_V p_a\,dV, \tag{11.133}$$

$$\overline{\kappa}_\eta(T_0,x_0)I_{b\eta}(T_0)=\frac{1}{V}\int_V\overline{\kappa}_\eta(T,x)I_{b\eta}(T)\,dV, \tag{11.134}$$

where $\overline{\kappa}_\eta=\int_{\Delta\eta}\kappa_\eta\,d\eta/\Delta\eta$ is the average absorption coefficient, i.e., volume-averaged partial pressure and a mean temperature based on average emission from the volume. For the scaling function Modest and Zhang suggest equating exact and approximate radiation leaving from a homogeneous slab of the length under consideration, or

$$\int_0^1\exp\left[-k(T,p_a,g)L\right]dg=\int_0^1\exp\left[-k(T_0,p_{a0},g)u(T,p,p_a)L\right]dg. \tag{11.135}$$

Correlated-k and scaled-k are about equally efficient numerically: both require evaluation of the local k-distribution $k(T,p_a,g)$ everywhere along the path. As an illustration a simple (yet severe) example is shown in Fig. 11-20, showing transmissivity through, and emissivity from, a slab of hot gas at 1000 K adjacent to a cold slab at 300 K. Both layers are at the same total and partial pressures, and are of equal width [127]. The transmissivity for a blackbody beam $I_{b\eta}(T_h=1000\,\mathrm{K})$, through such a double layer is, from Chapter 10,

$$\overline{\tau}_\eta=\frac{I_\eta(L)_{\mathrm{tr}}}{I_{b\eta}(T_h)}=\frac{1}{\Delta\eta}\int_{\Delta\eta}\exp[-\kappa_\eta(T_h,x)L_h-\kappa_\eta(T_c,x)L_c]\,d\eta, \tag{11.136}$$

while the emissivity is defined here as the intensity of emitted radiation exiting the cold layer, as compared to the Planck function of the hot layer. Employing equation (10.29) this is readily evaluated as

$$\overline{\epsilon}_\eta=\frac{I_\eta(L)_{\mathrm{em}}}{I_{b\eta}(T_h)}=\frac{1}{\Delta\eta}\int_{\Delta\eta}\left[e^{-\kappa_\eta(T_c,x)L_c}-e^{-\kappa_\eta(T_c,x)L_c-\kappa_\eta(T_h,x)L_h}+\frac{I_{b\eta}(T_c)}{I_{b\eta}(T_h)}\left(1-e^{-\kappa_\eta(T_c,x)L_c}\right)\right]d\eta. \tag{11.137}$$

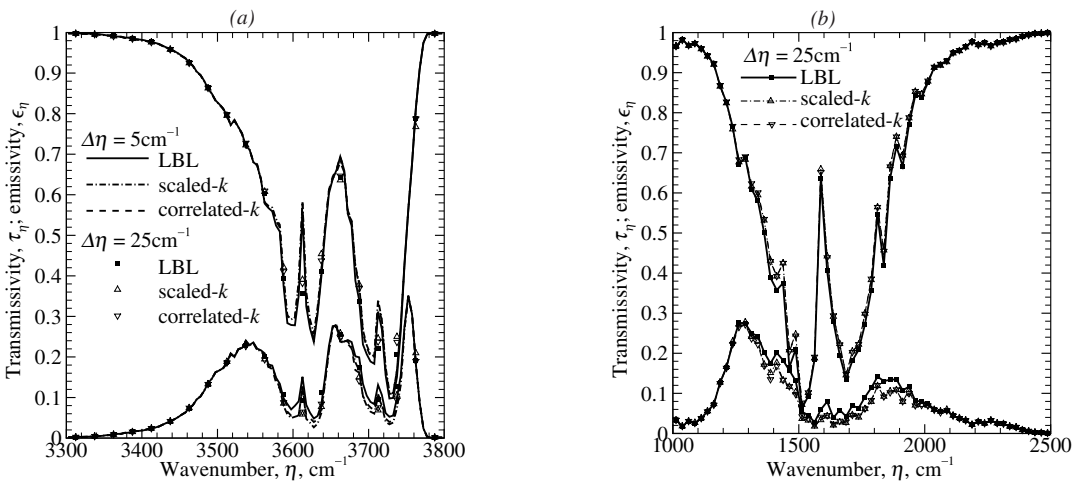

FIGURE 11-20
Narrow band transmissivities and emissivities for two-temperature slab, as calculated by the LBL, scaled-*k*, and correlated-*k* methods: *(a)* 2.7 μm band of CO_2 with $p_{CO_2} = 0.1$ bar, *(b)* 6.3 μm band of H_2O with $p_{H_2O} = 0.2$ bar.

Note that, while transmissivities are more regularly shown in the narrow band literature, the emissivity is generally more descriptive of heat transfer problems. Figure 11-20*a* shows these narrow band transmissivities and emissivities for the 2.7 μm band of CO_2 for a partial pressure of $p_{CO_2} = 0.1$ bar, as calculated by the LBL, scaled-*k*, and correlated-*k* methods, using the original HITEMP 1995 database [62], and all for a resolution of $\Delta\eta = 5\,\text{cm}^{-1}$ (lines) and $25\,\text{cm}^{-1}$ (symbols). Both correlated and scaled *k*-distributions predict transmissivity very accurately with the exception of small discrepancies near the minima at $3600\,\text{cm}^{-1}$ and $3700\,\text{cm}^{-1}$. Similar errors also show up in the emissivity, but are somewhat amplified. This amplification was observed for all bands studied (i.e., the effect is not limited to regions of small emissivities, as in this figure). For both, transmissivity and emissivity, results from the two *k*-distributions are virtually identical, although correlated-*k* performs slightly better for the 2.7 μm band (in the case of the 4.3 μm band, not shown, roles are reversed and scaled-*k* slightly outperforms correlated-*k*). Figure 11-20*b* shows transmissivities and emissivities for the wide 6.3 μm water vapor band. Conditions are the same as for Fig. 11-20*a*, except that $p_{H_2O} = 0.2$ bar and only a $\Delta\eta = 25\,\text{cm}^{-1}$ resolution is shown (a resolution of $5\,\text{cm}^{-1}$ results in a very irregular shape which, while the *k*-distributions follow this behavior accurately, makes them difficult to compare). Again, both *k*-distributions predict transmissivities rather accurately, and the slight errors are somewhat amplified in the emissivities. And, again, both *k*-distributions give virtually the same results, with scaled-*k* being a little more accurate for this band. In summary, one may say that both models perform about equally well; this implies that—for narrow bands and for temperatures not exceeding 1000 K—the absorption coefficients for water vapor and carbon dioxide are relatively well correlated. Note also that the present case, with a sharp step in temperature, is rather extreme; accuracy can be expected to be significantly better in more realistic combustion systems.

Unfortunately, for nonhomogeneous media with even more extreme temperature gradients the correlation between *k*-distributions at different temperatures breaks down. The reason for this is that different lines can have vastly different temperature dependence through the exponential term in equations (11.32): at low temperatures lines near the band center are strongest (with largest κ_η), while at high temperatures lines away from the band center exhibit the largest κ_η. Since the correlated *k*-distribution pairs values of equal absorption coefficients, this results in pairing wrong spectral values in hot and cold regions. This is not only true for wide spectral ranges, but also on a narrow band level, since a vibration–rotation band consists of

many slightly displaced subbands, generated by different levels of vibrational energies (different B_v), some of which undergo transitions only at elevated temperatures [large values for E_l in equation (11.32)], known as "hot lines." For more detail the reader may want to consult the monograph by Taine and Soufiani [4]. The lack of correlation in nonisothermal media was first recognized by Rivière and coworkers [118–120], who devised the so-called "fictitious gas technique": starting with a high-resolution database, they grouped lines according to the values of their lower energy levels, $E_j = hcB_v j(j+1)$ (i.e., according to their temperature dependence), found the k-distribution for each of the fictitious gases and, in a further approximation, estimated the gas transmissivity as the product of the transmissivities of the fictitious gases,

$$\overline{\tau}_\eta = \prod_{i=1}^{n_g} \int_0^1 \exp\left[-\int_0^X k_i(g,X)\,dX\right] dg, \tag{11.138}$$

where n_g is the number of fictitious gases. A very similar approach was taken by Bharadwaj and Modest [109], employing the fictitious gas approach applied to k-distributions obtained from the Malkmus model. Unfortunately, these methods can only supply the mean transmissivity for a gas layer, i.e., they lose all the advantages of the k-distributions, and are limited in their application in the same way as the statistical narrow band models.

Comparison of k-Distributions and Statistical Models

The k-distribution method has a number of important advantages over the statistical narrow band models, although the statistical models, in particular the Malkmus model combined with the Curtis–Godson scaling approximation, outperform k-distributions in a couple of respects:

1. Perhaps the greatest advantage that k-distributions have is that they formulate radiative properties in terms of a (reordered) absorption coefficient. This implies that radiative heat transfer rates may be calculated using any desired solution method for the radiative transfer equation. If based on exact line-by-line property data, the method is essentially exact (for a homogeneous medium). Statistical narrow band models, on the other hand, calculate gas column transmissivity, and heat transfer rates can only be determined in terms of these transmissivities.
2. Statistical narrow band models are, due to the transmissivity approach, limited to application in black enclosures without scattering. No such restriction is necessary for k-distributions (as long as wall reflectance and scattering properties remain constant across the narrow band).
3. The k-distribution method is valid for spectral lines of any shape; statistical narrow band models, on the other hand, are generally limited to Lorentz lines (although some formulations for Doppler and Voigt profiles exist). This is not unimportant, since in combustion applications the lines often have Voigt profiles as seen from Fig. 11-9.
4. Statistical narrow band models return an explicit expression for averaged transmissivity, while the k-distribution requires integration (quadrature) over the (reordered) narrow spectrum. On the other hand, the narrow band is limited to several tens of wavenumbers for statistical models (to avoid significant changes in statistical parameters, such as $\overline{S}$ and d), but can span several hundreds of wavenumbers for k-distributions (only limited by changes in Planck function and, if present, spectral variations of wall emittances and scattering properties).
5. Neither method treats nonhomogeneous paths to complete satisfaction. In fields with moderate temperature gradients and moderate-to-strong pressure variations the correlated-

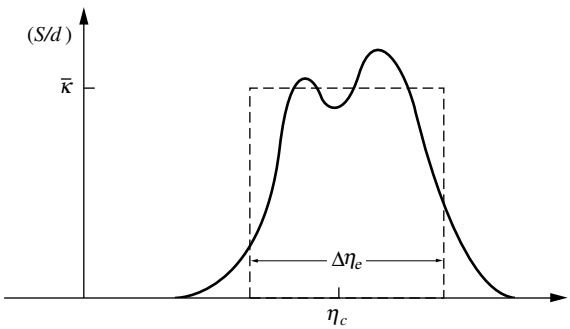

FIGURE 11-21
The box model for the approximation of total band absorptance.

k approach performs extremely well, while the Curtis–Godson approximation loses accuracy in the presence of strong pressure variations. On the other hand, in fields with extreme temperature fields all methods have some problems; under such conditions only the correlated-k, fictitious-gas approach performs well. However, the fictitious-gas approach calculates gas layer transmissivities only, i.e., it is under the same limitations as the statistical methods.

11.10 WIDE BAND MODELS

The heat transfer engineer is usually only interested in obtaining heat fluxes or divergences of heat fluxes integrated over the entire spectrum. Therefore, it is desirable to have models that can more readily predict the total absorption or emission from an entire band as was done in Example 11.3. These models are known as *wide band models* since they treat the spectral range of the entire band.

It is theoretically possible to use quantum mechanical relations, such as equations (11.33), to accurately predict the radiative behavior of entire bands. This has been attempted by Greif and coworkers [128, 129] in a series of papers. While such calculations are more accurate, they tend to be too involved, so simpler methods are sought for practical applications.

The Box Model

In this very simple model the band is approximated by a rectangular box of width $\Delta\eta_e$ (the effective band width) and height $\overline{\kappa}$ as shown in Fig. 11-21. With these assumptions we can calculate the total band absorptance for a homogeneous gas layer as

$$A \equiv \int_{\text{band}} \epsilon_\eta \, d\eta = \int_0^\infty \left(1 - e^{-\kappa_\eta X}\right) d\eta = \Delta\eta_e \left(1 - e^{-\overline{\kappa} X}\right), \tag{11.139}$$

where both $\Delta\eta_e$ and $\overline{\kappa}$ may be functions of temperature and pressure. The box model was developed by Penner [20] and successfully applied to diatomic gases. However, the determination of the effective band width is something of a "black art." Once $\Delta\eta_e$ has been found (by using the somewhat arbitrary criterion given by Penner [20] or some other means), $\overline{\kappa}$ may be related to the *band intensity* α, defined as

$$\alpha \equiv \int_0^\infty \kappa_\eta \, d\eta = \int_0^\infty \left(\frac{S}{d}\right)_\eta d\eta, \tag{11.140}$$

leading to

$$\overline{\kappa} = \alpha / \Delta\eta_e. \tag{11.141}$$

If the molecular gas layer forms a radiation barrier between two surfaces of unequal temperature, then a suitable choice for the effective band width can give quite reasonable results. However,

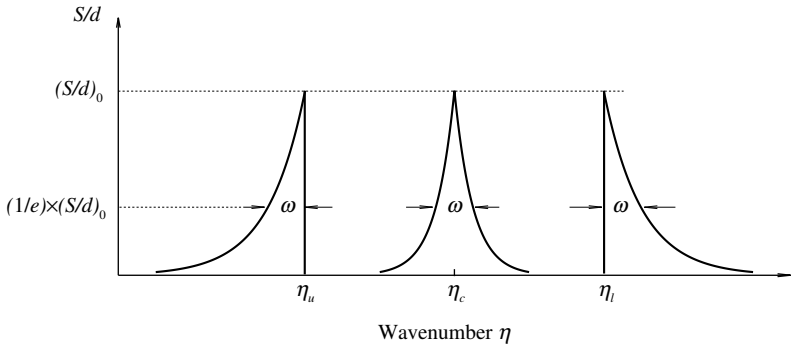

FIGURE 11-22
Band shapes for exponential wide band model.

if emission from a hot gas is considered, then the results become very sensitive to the correct choice of $\Delta\eta_e$. Nevertheless, the box model—because of its great simplicity—enjoys considerable popularity for use in heat transfer models (see Chapter 20).

Example 11.6. Calculate the effective band width $\Delta\eta_e$ for which the box model predicts the correct total band absorptance for Example 11.3.

Solution
Integrating equation (11.83) over the entire band gives $\alpha = (S/d)_0 \times \omega = 500\,\text{cm}^{-2}$ and $\overline{\kappa}X = \alpha X/\Delta\eta_e = 10{,}000\,\text{cm}^{-1}/\Delta\eta_e$. Equation (11.139) then, with $A = 264.7\,\text{cm}^{-1}$, results in $\Delta\eta_e = 264.7\,\text{cm}^{-1}$ by trial and error. $\Delta\eta_e$ is seen to be substantially larger than ω and essentially equal to A, because the band in this example is optically very thick. Even in the band wings far away from the band center the band is optically opaque ($\tau \gg 1$). This result must be accounted for in the choice of $\Delta\eta_e$. For optically thick gases finding the correct $\Delta\eta_e$ is equivalent to finding A itself. Drawing a box seemingly best approximating the actual band shape can lead to large errors!

The Exponential Wide Band Model

The exponential wide band model, first developed by Edwards and Menard [130], is by far the most successful of the wide band models. The original model has been further developed in a series of papers by Edwards and coworkers [131–134]. The word "successful" here implies that the model is able to correlate experimental data for band absorptances with an average error of approximately ±20% (but with maximum errors as high as 50% to 80%). We present here the latest version of Edwards, together with its terminology (based on Goody's narrow band model), followed by a short discussion of newer models by Felske and Tien [135] (Goody's model) and Wang [136] (Malkmus' model). For a more exhaustive discussion on Edwards' model the reader may want to consult Edwards' monograph on gas radiation [1].

Since it is known from quantum mechanics that the line strength decreases exponentially in the band wings far away from the band center,[8] Edwards assumed that the smoothed absorption coefficient S/d has one of the following three shapes, as shown in Fig. 11-22:

with upper limit head

$$\frac{S}{d} = \frac{\alpha}{\omega}\, e^{-(\eta_u - \eta)/\omega}, \tag{11.142a}$$

symmetric band

$$\frac{S}{d} = \frac{\alpha}{\omega}\, e^{-2|\eta_c - \eta|/\omega}, \tag{11.142b}$$

with lower limit head

[8]This fact is easily seen by letting $j \gg 1$ in equations (11.28*a*) and (11.33*a*) for the *P*-branch, and in equations (11.28*c*) and (11.33*b*) for the *R*-branch.

TABLE 11.2
Exponential wide band correlation for an isothermal gas.

$\beta \le 1$	$0 \le \tau_0 \le \beta$	$A^* = \tau_0$	Linear regime
	$\beta \le \tau_0 \le 1/\beta$	$A^* = 2\sqrt{\tau_0 \beta} - \beta$	Square root regime
	$1/\beta \le \tau_0 < \infty$	$A^* = \ln(\tau_0 \beta) + 2 - \beta$	Logarithmic regime
$\beta \ge 1$	$0 \le \tau_0 \le 1$	$A^* = \tau_0$	Linear regime
	$1 \le \tau_0 < \infty$	$A^* = \ln \tau_0 + 1$	Logarithmic regime

α, β, and ω from Table 11.3 and equations (11.144) through (11.147), $\tau_0 = \alpha X/\omega$.

$$\frac{S}{d} = \frac{\alpha}{\omega} e^{-(\eta - \eta_l)/\omega}, \tag{11.142c}$$

where α is the integrated absorption coefficient or the *band strength parameter* (or area under the curves in Fig. 11-22), which was defined in equation (11.140), and ω is the *band width parameter*,[9] giving the width of the band at $1/e$ of maximum intensity. The band can be expected to be fairly symmetric if, during rotational energy changes, the B does not change too much [recall equations (11.28*a*) through (11.28*c*)]. η_c is then the wavenumber connected with the vibrational transition. On the other hand, if the change in B is substantial, then either the R- or the P-branch may fold back, leading to bands with upper or lower head. Thus, the wavenumbers η_u and η_l are the wavenumbers where this folding back occurs, and not the band center. The sharp exponential apex is, of course, not very realistic. The rationale is that, if the band center is optically thick, then it is opaque no matter what the shape, while if it is thin, then only the total α is of importance. Edwards and Menard [130] proceeded to evaluate the band absorptance using the general statistical model by substituting expressions (11.142) into equation (11.78) and carrying out the integration in an approximate fashion. Since equation (11.78) contains the line overlap parameter β and the optical thickness τ, the authors were able to describe the total band absorptance as a function of three parameters, namely,

$$A^* = A/\omega = A^*(\alpha, \beta, \tau_0), \tag{11.143}$$

where τ_0 is the optical thickness at the band center (symmetric band) or the band head. Their results are summarized in Table 11.2.[10]

Example 11.7. Determine the total band absorptance of the previous two examples by the exponential wide band model.

Solution
From Example 11.3 we have $\tau_0 = 200$ and $\beta = \pi/10$. Thus, since $\tau_0 > 1/\beta$, we find from Table 11.2 $A^* = \ln(\tau_0 \beta) + 2 - \beta = \ln(200 \times \pi/10) + 2 - \pi/10 = 5.826$ and $A = A^* \omega = 5.826 \times 50 = 291.3\,\text{cm}^{-1}$. The difference between the two results is primarily due to the fact that in Example 11.3 we treated the optically thin band wings as optically thick.

The parameters α, β, and ω are functions of temperature and must be determined experimentally. Values for the most important combustion gases—H_2O, CO_2, CO, CH_4, NO, and

[9]The band width parameter ω, as used here, applies only to the wide band correlation. If equations (11.142) are used for spectral (i.e., narrow band) calculations, Edwards [1] suggests increasing the value of ω by 20% for better agreement between wide band model and band-integrated narrow band model calculations.

[10]In the original version the parameters $C_1 = \alpha$, $C_3 = \omega$, and $C_2 = \sqrt{4 C_1 C_3 \beta^*}$ were used, where β^* is the value of β for a gas mixture at a total pressure of 1 atm with zero partial pressure of the absorbing gas. Also, limits between regimes were slightly different, using A itself rather than τ_0.

SO_2—for a reference temperature of $T_0 = 100\,\mathrm{K}$ are given in Table 11.3. Most of these correlation data are based on work by Edwards and coworkers and are summarized in [1]. Data for the purely rotational band of H_2O have been taken from the more modern work of Modak [137]. Values for other bands and other gases may be found in the literature, e.g., for H_2O, CO_2, and CH_4 [1, 131, 134, 138–142], for CO [1, 131, 134, 143–145], for SO_2 [1, 134, 146], for NH_3 [147], for NO [148], for N_2O [149], and for C_2H_2 [150] (in the older of these references the parameters for the slightly different original model are given; in a number of papers a pressure path length has been used instead of a density path length). The temperature dependence of the band correlation parameters for vibration–rotation bands is given by Edwards [1] as

$$\alpha(T) = \alpha_0 \frac{\Psi(T)}{\Psi(T_0)}, \tag{11.144}$$

$$\beta(T) = \beta^* P_e = \beta_0^* \sqrt{\frac{T_0}{T}} \frac{\Phi(T)}{\Phi(T_0)} P_e, \tag{11.145}$$

$$\omega(T) = \omega_0 \sqrt{\frac{T}{T_0}}, \tag{11.146}$$

and

$$P_e = \left[\frac{p}{p_0}\left(1 + (b-1)\frac{p_a}{p}\right)\right]^n, \quad (p_0 = 1\,\mathrm{atm},\ T_0 = 100\,\mathrm{K}), \tag{11.147}$$

where

$$\Psi(T) = \left\{1 - \exp\left(-\sum_{k=1}^{m} u_k(T)\delta_k\right)\right\} \frac{\displaystyle\prod_{k=1}^{m} \sum_{v_k=v_{0,k}}^{\infty} \frac{(v_k + g_k + |\delta_k| - 1)!}{(g_k - 1)!\, v_k!}\, e^{-u_k(T)v_k}}{\displaystyle\prod_{k=1}^{m} \sum_{v_k=0}^{\infty} \frac{(v_k + g_k - 1)!}{(g_k - 1)!\, v_k!}\, e^{-u_k(T)v_k}}, \tag{11.148}$$

$$\Phi(T) = \frac{\left\{\displaystyle\prod_{k=1}^{m} \sum_{v_k=v_{0,k}}^{\infty} \sqrt{\frac{(v_k + g_k + |\delta_k| - 1)!}{(g_k - 1)!\, v_k!}\, e^{-u_k(T)v_k}}\right\}^2}{\displaystyle\prod_{k=1}^{m} \sum_{v_k=v_{0,k}}^{\infty} \frac{(v_k + g_k + |\delta_k| - 1)!}{(g_k - 1)!\, v_k!}\, e^{-u_k(T)v_k}}, \tag{11.149}$$

and

$$u_k(T) = hc\eta_k/kT, \quad v_{0,k} = \begin{cases} 0 & \text{for} \quad \delta_k \geq 0, \\ |\delta_k| & \text{for} \quad \delta_k \leq 0. \end{cases} \tag{11.150}$$

In these rather complicated expressions the v_k are vibrational quantum numbers, δ_k is the change in vibrational quantum number during transition (±1 for a fundamental band, etc.), and the g_k are statistical weights for the transition (degeneracy = number of ways the transition can take place). Values for the η_k, δ_k, and g_k are given in Table 11.3. The effective pressure P_e gives the pressure dependence of line broadening due to collisions of absorbing molecules with other absorbing molecules and with nonabsorbing molecules that may be present (for example, nitrogen and other inert gases contained in a mixture). Note that the definition for P_e is slightly different here from equation (11.39) (this was done for empirical reasons, to achieve better agreement with experimental data). For the case of nonnegative δ_k or $v_{0,k} = 0$ (the majority of gas bands listed in Table 11.3), the series in the expression for Ψ and the denominator of Φ may be simplified [98] to

$$\sum_{v_k=0}^{\infty} \frac{(v_k + g_k + \delta_k - 1)!}{(g_k - 1)! v_k!}\, e^{-u_k v_k} = \frac{(g_k + \delta_k - 1)!}{(g_k - 1)!} \left(1 - e^{-u_k}\right)^{-g_k - \delta_k}. \tag{11.151}$$

TABLE 11.3
Wide band model correlation parameters for various gases.

Band Location		Vibr. Quantum Step	Pressure Parameters		Correlation Parameters		
λ [μm]	η_c [cm^{-1}]	(δ_k)	n	b	α_0 [cm^{-1}/(g/m^2)]	β_0^*	ω_0 [cm^{-1}]
H_2O $m = 3$, $\eta_1 = 3652\,\text{cm}^{-1}$, $\eta_2 = 1595\,\text{cm}^{-1}$, $\eta_3 = 3756\,\text{cm}^{-1}$, $g_k = (1,1,1)$							
71 μm[a]	$\eta_c = 140\,\text{cm}^{-1}$	(0, 0, 0)	1	$8.6\sqrt{\frac{T_0}{T}} + 0.5$	5.455	0.143	69.3
6.3 μm	$\eta_c = 1600\,\text{cm}^{-1}$	(0, 1, 0)	1	$8.6\sqrt{\frac{T_0}{T}} + 0.5$	41.2	0.094	56.4
2.7 μm	$\eta_c = 3760\,\text{cm}^{-1}$	(0, 2, 0) (1, 0, 0) (0, 0, 1)	1	$8.6\sqrt{\frac{T_0}{T}} + 0.5$	0.2 2.3 23.4	0.132[b,c]	60.0[b]
1.87 μm	$\eta_c = 5350\,\text{cm}^{-1}$	(0, 1, 1)	1	$8.6\sqrt{\frac{T_0}{T}} + 0.5$	3.0	0.082	43.1
1.38 μm	$\eta_c = 7250\,\text{cm}^{-1}$	(1, 0, 1)	1	$8.6\sqrt{\frac{T_0}{T}} + 0.5$	2.5	0.116	32.0
CO_2 $m = 3$, $\eta_1 = 1351\,\text{cm}^{-1}$, $\eta_2 = 666\,\text{cm}^{-1}$, $\eta_3 = 2396\,\text{cm}^{-1}$, $g_k = (1,2,1)$							
15 μm	$\eta_c = 667\,\text{cm}^{-1}$	(0, 1, 0)	0.7	1.3	19.0	0.062	12.7
10.4 μm[d]	$\eta_c = 960\,\text{cm}^{-1}$	(−1, 0, 1)	0.8	1.3	2.47×10^{-9}	0.040	13.4
9.4 μm[d]	$\eta_c = 1060\,\text{cm}^{-1}$	(0, −2, 1)	0.8	1.3	2.48×10^{-9}	0.119	10.1
4.3 μm	$\eta_u = 2410\,\text{cm}^{-1}$	(0, 0, 1)	0.8	1.3	110.0	0.247	11.2
2.7 μm	$\eta_c = 3660\,\text{cm}^{-1}$	(1, 0, 1)	0.65	1.3	4.0	0.133	23.5
2.0 μm	$\eta_c = 5200\,\text{cm}^{-1}$	(2, 0, 1)	0.65	1.3	0.060	0.393	34.5
CO $m = 1$, $\eta_1 = 2143\,\text{cm}^{-1}$, $g_1 = 1$							
4.7 μm	$\eta_c = 2143\,\text{cm}^{-1}$	(1)	0.8	1.1	20.9	0.075	25.5
2.35 μm	$\eta_c = 4260\,\text{cm}^{-1}$	(2)	0.8	1.0	0.14	0.168	20.0
CH_4 $m = 4$, $\eta_1 = 2914\,\text{cm}^{-1}$, $\eta_2 = 1526\,\text{cm}^{-1}$, $\eta_3 = 3020\,\text{cm}^{-1}$, $g_k = (1,2,3,3)$							
7.7 μm	$\eta_c = 1310\,\text{cm}^{-1}$	(0, 0, 0, 1)	0.8	1.3	28.0	0.087	21.0
3.3 μm	$\eta_c = 3020\,\text{cm}^{-1}$	(0, 0, 1, 0)	0.8	1.3	46.0	0.070	56.0
2.4 μm	$\eta_c = 4220\,\text{cm}^{-1}$	(1, 0, 0, 1)	0.8	1.3	2.9	0.354	60.0
1.7 μm	$\eta_c = 5861\,\text{cm}^{-1}$	(1, 1, 0, 1)	0.8	1.3	0.42	0.686	45.0
NO $m = 1$, $\eta_1 = 1876\,\text{cm}^{-1}$, $g_1 = 1$							
5.3 μm	$\eta_c = 1876\,\text{cm}^{-1}$	(1)	0.65	1.0	9.0	0.181	20.0
SO_2 $m = 3$, $\eta_1 = 1151\,\text{cm}^{-1}$, $\eta_2 = 519\,\text{cm}^{-1}$, $\eta_3 = 1361\,\text{cm}^{-1}$, $g_k = (1,1,1)$							
19.3 μm	$\eta_c = 519\,\text{cm}^{-1}$	(0, 1, 0)	0.7	1.28	4.22	0.053	33.1
8.7 μm	$\eta_c = 1151\,\text{cm}^{-1}$	(1, 0, 0)	0.7	1.28	3.67	0.060	24.8
7.3 μm	$\eta_c = 1361\,\text{cm}^{-1}$	(0, 0, 1)	0.65	1.28	29.97	0.493	8.8
4.3 μm	$\eta_c = 2350\,\text{cm}^{-1}$	(2, 0, 0)	0.6	1.28	0.423	0.475	16.5
4.0 μm	$\eta_c = 2512\,\text{cm}^{-1}$	(1, 0, 1)	0.6	1.28	0.346	0.589	10.9

[a] For the rotational band $\alpha = \alpha_0 \exp\left(-9(\sqrt{T_0/T} - 1)\right)$, $\beta^* = \beta_0^*\sqrt{T_0/T}$.
[b] Combination of three bands, all but weak (0, 2, 0) band are fundamental bands, $\alpha_0 = 25.9\,\text{cm}^{-1}/(\text{g/m}^2)$.
[c] Line overlap for overlapping bands from equation (11.154).
[d] "Hot bands," very weak at room temperature, exponential growth in strength at high temperatures.

$$\alpha = \alpha_0 \frac{\Psi}{\Psi_0}, \quad \omega = \omega_0\sqrt{\frac{T}{T_0}}, \quad \beta = \beta^* P_e = \beta_0^*\sqrt{\frac{T_0}{T}}\frac{\Phi}{\Phi_0}P_e, \quad P_e = \left[\frac{p}{p_0}\left(1 + (b-1)\frac{p_a}{p}\right)\right]^n.$$

Ψ from equations (11.144) and (11.148), Φ from equation (11.149), $T_0 = 100\,\text{K}$, $p_0 = 1\,\text{atm}$.

If $v_{0,k} \neq 0$, then $v_{0,k}$ terms need to be subtracted from the above result.

Because of the low reference temperature of $T_0 = 100\,\text{K}$, the values for $u_{0,k}$ are relatively large, so both Φ_0 and Ψ_0 are very simple to evaluate and, for $v_{0,k} = 0$,

$$\Psi_0 \approx \prod_{k=1}^{m} \frac{(g_k + \delta_k - 1)!}{(g_k - 1)!}, \quad \Phi_0 \approx 1. \tag{11.152}$$

If only one of the vibrational modes undergoes a transition (only one $\delta_k \neq 0$), then all other modes cancel out of the expression for Ψ; and if the transition results in a fundamental band (single transition with $\delta_k = 1$), then $\Psi \equiv 1$. This implies that, for a fundamental band, $\alpha(T) = \alpha_0 = \text{const}$. Unfortunately, the temperature dependence of the broadening mechanism is always more complicated, and Φ must generally be evaluated from equation (11.149).

If several bands overlap each other (e.g., the three H_2O bands situated around 2.7 μm), then also the individual lines overlap lines from other bands, resulting in an effective overlap parameter β that is larger than for any of the individual bands. The band strength and overlap parameter for overlapping bands are calculated [1] from

$$\alpha = \sum_{j=1}^{J} \alpha_j, \tag{11.153}$$

$$\beta = \frac{1}{\alpha}\left[\sum_{j=1}^{J} \sqrt{\alpha_j \beta_j}\right]^2, \tag{11.154}$$

where J is the number of overlapping bands.

When the exponential wide band model was first presented by Edwards and Menard, the temperature dependence for the broadening parameter was not calculated by quantum statistics but was rather correlated from experimental data that, because of their scatter, generally resulted in fairly simple formulae; but extrapolation to higher temperatures tended to be very inaccurate. Most of the bands listed in Table 11.3 are fundamental bands, not because calculations for these bands are simpler, but because fundamental bands tend to be much stronger than overtones or combined-mode bands, often making them the only important ones for heat transfer calculations.

To facilitate hand calculations, the temperature dependence of band strength parameters α (for nonfundamental bands) and overlap parameters β^* are shown in graphical form in Fig. 11-23 for water vapor. A similar plot is given in Fig. 11-24 for the important bands of carbon dioxide, and Fig. 11-25 shows the temperature dependence of the line overlap parameter for the fundamental bands of methane and carbon monoxide (with $\alpha = \alpha_0 = \text{const}$). For more accurate computer calculations the subroutines `wbmh2o`, `wbmco2`, `wbmch4`, `wbmco`, `wbmno`, and `wbmso2` are given in Appendix F. Alternatively, very accurate polynomial fits for these functions have been given by Lallemant and Weber [151].

Example 11.8. Consider a water vapor–air mixture at 3 atm and 600 K, with 5% water vapor by volume. What is the most important H_2O band and what is its total band absorptance for a path of 10 cm?

Solution

At 600 K the Planck function has its maximum around 5 μm. Since total emission will depend on the blackbody intensity [see equation (11.58)], we seek a band with large α in the vicinity of 5 μm. Inspection of Table 11.3 shows that the strongest vibration–rotation band for water vapor lies at 6.3 μm and is, therefore, the band we are interested in. From the table we find $\alpha = \alpha_0 = 41.2\,\text{cm}^{-1}/(\text{g/m}^2)$, $\beta = \beta_0^*\sqrt{T_0/T}(\Phi/\Phi_0)P_e$ with $\beta_0^* = 0.094$, and $\omega = \omega_0\sqrt{T/T_0} = 56.4\sqrt{600/100} = 138.15\,\text{cm}^{-1}$. To evaluate the effective broadening pressure we find $n = 1$ and $b = 8.6\sqrt{100/600} + 0.5 = 4.01$ and with a volume fraction $x = p_a/p$ the effective pressure becomes $P_e = \{(p/1\,\text{atm})[1+(b-1)x]\}^n = 3[1+3.01\times0.05] = 3.452$. Estimating the temperature dependence of the line overlap parameter from Fig. 11-23 leads to $\beta^*/\beta_0^* \simeq 0.65$ and

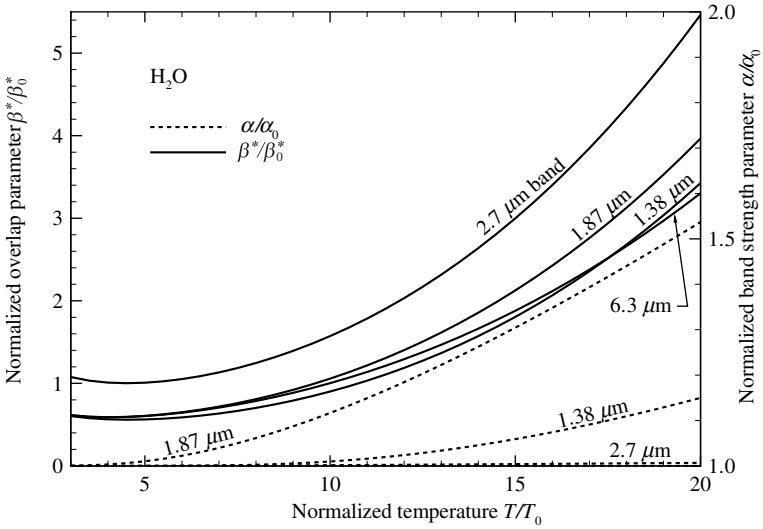

FIGURE 11-23
Temperature dependence of the line overlap parameter, β^*, and band strength parameter, α, for water vapor.

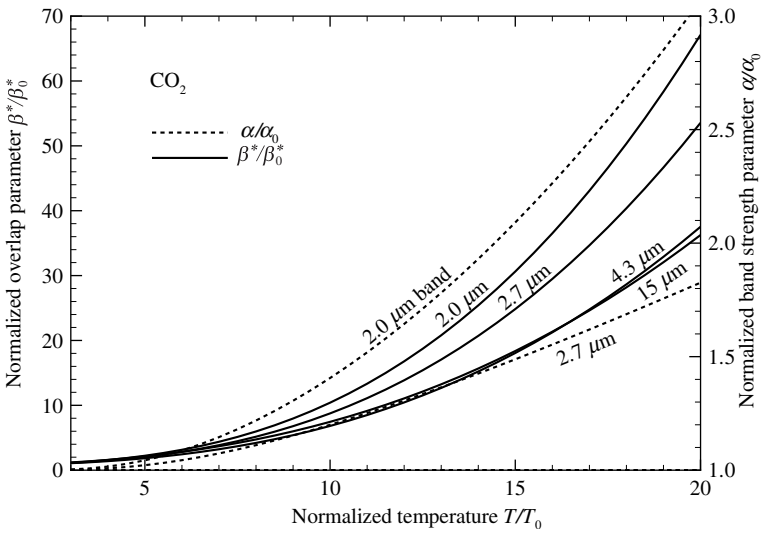

FIGURE 11-24
Temperature dependence of line overlap parameter, β^*, and band strength parameter, α, for carbon dioxide.

$\beta = 0.094 \times 0.65 \times 3.452 = 0.211$. Since all values for α in Table 11.3 are based on a mass absorption coefficient, we must calculate X as $X = \rho_a s$, where ρ_a is the partial density of the absorbing gas (**not** the density of the gas mixture). For our water vapor with a partial pressure of $p_a = 0.05 \times 3 = 0.15$ atm and a molecular weight of $\mathscr{M} = 18$ g/mol, we get from the ideal gas law

$$\rho_a = \frac{\mathscr{M} p_a}{R_u T} = \frac{18\,\text{g/mol} \times 0.15\,\text{atm}}{8.3145\,\text{J/mol K} \times 600\,\text{K}} \frac{1.0132 \times 10^5\,\text{J/m}^3}{1\,\text{atm}} = 54.84\,\text{g/m}^3$$

and $X = 54.84 \times 0.1 = 5.48\,\text{g/m}^2$. Finally, from $\tau_0 = \alpha X/\omega$ we get $\tau_0 = 41.2 \times 5.48/138.15 = 1.634$. Since the value of τ_0 lies between the values of β and $1/\beta$ we are in the square-root regime and

$$A^* = 2\sqrt{\tau_0 \beta} - \beta = 2\sqrt{1.634 \times 0.211} - 0.211 = 0.964$$

or $A = 0.964 \times 138.15 = 133\,\text{cm}^{-1}$.

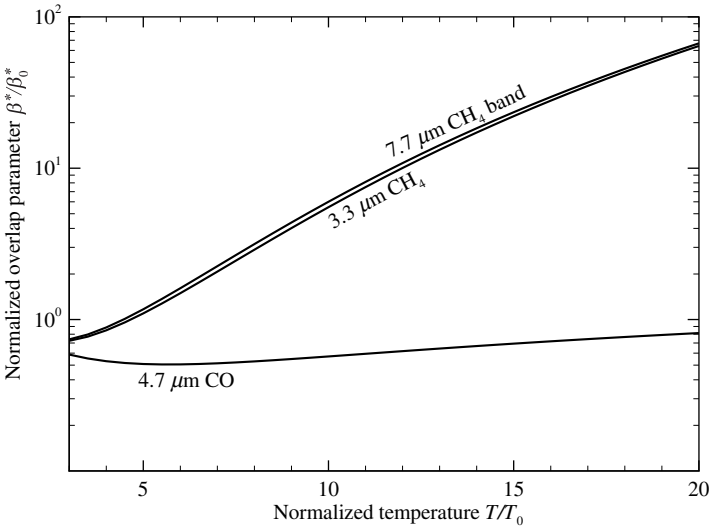

FIGURE 11-25
Temperature dependence of the line overlap parameter, β^*, for the fundamental bands of methane and carbon monoxide.

The calculation of exact values for Φ and Ψ for nonfundamental bands is rather tedious and is best left to computer calculations with the subroutines given in Appendix F.

While the correlation in Table 11.2 is simple and straightforward (aside from the temperature dependence of α and β), it is often preferable to have a single continuous correlation formula. A simple analytical expression can be obtained for the high-pressure limit, i.e., when the lines become very wide from broadening resulting in very strong overlap, or $\beta \to \infty$, leading to $\kappa_\eta = (\overline{S}/d)_\eta$ and

$$A^* = E_1(\tau_0) + \ln \tau_0 + \gamma_E = \mathrm{Ein}(\tau_0), \qquad \beta \to \infty, \tag{11.155}$$

where $E_1(\tau)$ is known as an *exponential integral function*, which is discussed in some detail in Appendix E. Felske and Tien [135] have given a formula for all ranges of β, based on results from the numerical quadrature of equation (11.78):

$$A^* = 2E_1\left(\sqrt{\frac{\tau_0\beta}{1+\beta/\tau_0}}\right) + E_1\left(\frac{1}{2}\sqrt{\frac{\tau_0/\beta}{1+\beta/\tau_0}}\right) - E_1\left(\frac{1+2\beta}{2}\sqrt{\frac{\tau_0/\beta}{1+\beta/\tau_0}}\right) + \ln\left(\frac{\tau_0\beta}{(1+\beta/\tau_0)(1+2\beta)}\right) + 2\gamma_E, \tag{11.156}$$

or, more compactly,

$$A^* = 2\,\mathrm{Ein}(w) + \mathrm{Ein}\left(\frac{w}{2\beta}\right) - \mathrm{Ein}\left(\left[\frac{1}{2\beta}+1\right]w\right), \qquad w = \left(\frac{\overline{W}}{d}\right)_{0,\mathrm{Goody}} = \frac{\tau_0}{\sqrt{1+\tau_0/\beta}}. \tag{11.157}$$

A previous, somewhat simpler expression by Tien and Lowder [152] is known today to be seriously in error for small values of β [135, 153], and is not recommended.

Edwards' wide band model, given in Table 11.2, as well as the continuous correlation by Felske and Tien, are based on equation (11.70) together with Goody's statistical model, equation (11.78), the best narrow band model available at the time of Edwards and Menard's [130] original paper. Since then it has been found that the Malkmus model introduced in 1967, equation (11.79), describes the radiative behavior of most gases better than Goody's model [104]. It was shown by Wang [136] that an exact closed-form solution for the band absorptance can be

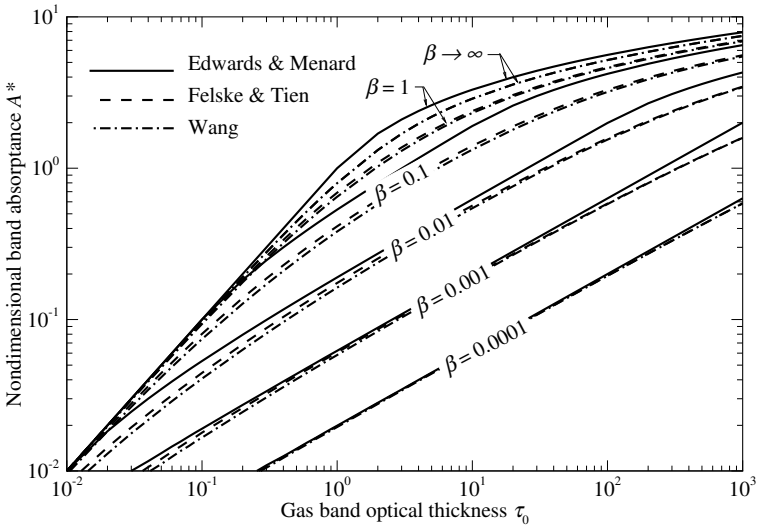

FIGURE 11-26
Comparison of various band absorptance correlations.

found, if equation (11.142) is combined with Malkmus' narrow band model, leading to

$$A^* = e^{\beta}\left[E_1(\beta + w) - E_1(\beta)\right] + \ln(1 + w/\beta) + \mathrm{Ein}(w), \qquad w = \left(\frac{\overline{W}}{d}\right)_{0,\mathrm{Malkmus}} = \frac{\beta}{2}\left[\sqrt{1 + 4\tau_0/\beta} - 1\right]. \tag{11.158}$$

Results from Wang's model, equation (11.158), are compared in Fig. 11-26 with those of Edwards and Menard, Table 11.2, and Felske and Tien, equation (11.156). The agreement between all three models is good. However, the band absorptance based on Malkmus' model, equation (11.158), is always slightly below that predicted by Goody's model, equation (11.156). Both the Felske and Tien and the Wang models go to the correct strong-overlap limit ($\beta \to \infty$), equation (11.155), while the older Edwards and Menard model shows its more approximate character, substantially overpredicting band absorptances for large β, particularly for intermediate values of τ_0.

A considerable number of other band correlations are available in the literature, based on numerous variations of the Elsasser and statistical models. An exhaustive discussion of the older (up to 1978) correlations and their accuracies (as compared with numerical quadrature results based on the plain Elsasser and the general statistical models) has been given by Tiwari [154].

Example 11.9. Repeat Example 11.8, using the Felske and Tien and the Wang models.

Solution
All relations developed for Edwards and Menard's model, equations (11.144) through (11.147), are equally valid for these two models, as are the data in Table 11.3. Thus, we have again $\tau_0 = 1.634$ and $\beta = 0.211$. Sticking these numbers into equations (11.156) and (11.158) (or, rather, using the Fortran functions `ftwbm` and `wangwbm`, or the stand-alone program `wbmodels`, all supplied in Appendix F) gives

$$A^*_{\mathrm{FT}} = 0.6916, \qquad A^*_{\mathrm{Wang}} = 0.6427.$$

As expected, the results are fairly close to each other, with the Malkmus-based Wang correlation predicting an about 7% lower band absorptance. Both values are significantly lower than those predicted by Edwards and Menard's model, which—as inspection of Fig. 11-26 shows—considerably overpredicts band absorptances for strong line overlap (large β) at intermediate optical thicknesses τ_0.

Wide Band Model for Nonhomogeneous Gases

As indicated in the previous section on narrow band models, the spectral emissivity for a nonhomogeneous path (with varying temperature and/or gas pressures) [cf. equation (11.61)] is

$$\epsilon_\eta = 1 - \exp\left(-\int_0^X \kappa_\eta \, dX\right), \tag{11.159}$$

from which we may calculate the total band absorptance as

$$A = \int_0^\infty \epsilon_\eta \, d\eta = \int_0^\infty \left[1 - \exp\left(-\int_0^X \kappa_\eta \, dX\right)\right] d\eta. \tag{11.160}$$

Here we have replaced the geometric path s by X in case a linear absorption coefficient is not used, but rather one based on density (as was done for the correlation parameters in Table 11.3) or pressure. Since we would still like to use the simple wide band model, appropriate path-averaged values for the correlation parameters α, β, and ω must be found. Attempts at such scaling were made by Chan and Tien [155], Cess and Wang [156], and Edwards and Morizumi [157], and are summarized by Edwards [1]. The average value for α follows readily from the weak line limit (linear regime in Table 11.2) as

$$\widetilde{\alpha} \equiv \frac{1}{X}\int_0^X \int_0^\infty \kappa_\eta \, d\eta \, dX = \frac{1}{X}\int_0^X \int_0^\infty \left(\frac{S}{d}\right)_\eta d\eta \, dX = \frac{1}{X}\int_0^X \alpha \, dX. \tag{11.161}$$

The definition of an average value for ω is

$$\widetilde{\omega} \equiv \frac{1}{\widetilde{\alpha} X}\int_0^X \omega\alpha \, dX, \tag{11.162}$$

while the averaged value for β is found by comparison with the square root regime in Table 11.2 as

$$\widetilde{\beta} \equiv \frac{1}{\widetilde{\omega\alpha} X}\int_0^X \beta\omega\alpha \, dX. \tag{11.163}$$

There is little theoretical justification for the choice of $\widetilde{\omega}$ and $\widetilde{\beta}$,[11] but comparison with spectral calculations using equations (11.90), (11.94), and (11.78) showed that they give excellent results [157].

Example 11.10. Reconsider Example 11.8, but assume that the water vapor–air mixture temperature varies linearly between 400 K and 800 K over its path of 10 cm. How does this affect the total band absorptance for the 6.3 μm band?

Solution

We may express the temperature variation as $T = 400\,\text{K}(1 + s'/s)$, where s' is distance along path s, and the density variation as

$$\rho_a = \rho_{600}\frac{600\,\text{K}}{T} = 6\rho_{600}\frac{T_0}{T} = \frac{\frac{3}{2}\rho_{600}}{1 + s'/s}.$$

Thus,

$$X = \int_0^s \rho_a \, ds' = 6\rho_{600}\int_0^s \left(\frac{T_0}{T}\right) ds' = \frac{3}{2}\rho_{600} s \int_0^1 \frac{d\xi}{1+\xi} = \tfrac{3}{2} X_{600} \ln 2 = 1.040\, X_{600} = 5.702\,\text{g/m}^2.$$

The path-averaged band strength becomes

$$\widetilde{\alpha} = \frac{1}{X}\int_0^s \alpha\rho_a \, ds = \frac{1}{X}\alpha_0 X = \alpha_0 = 41.2\,\text{cm}^{-1}/(\text{g/m}^2),$$

[11] Note that there are two different definitions for $\widetilde{\beta}$, one for narrow band calculations and the present one for the wide band model.

since the 6.3 μm band is a fundamental band and α is independent of temperature. For the averaged $\widetilde{\omega}$ we get, from $\omega = \omega_0\sqrt{T/T_0} = \omega_0\sqrt{4}\sqrt{1+s'/s}$,

$$\begin{aligned}\widetilde{\omega} &= \frac{1}{\widetilde{\alpha}X}\int_0^s \omega\alpha\rho_a\, ds' = \frac{6\omega_0\rho_{600}}{X}\int_0^s \sqrt{\frac{T}{T_0}}\,\frac{T_0}{T}\, ds' = \frac{3\omega_0\rho_{600}s}{X}\int_0^1 \frac{d\xi}{\sqrt{1+\xi}} \\ &= \frac{3\omega_0 X_{600}}{X}\times 2\sqrt{1+\xi}\Big|_0^1 = 6\left(\sqrt{2}-1\right)\frac{X_{600}}{X}\,\omega_0 = \frac{6\left(\sqrt{2}-1\right)}{\frac{3}{2}\ln 2}\times 56.4\,\mathrm{cm}^{-1} \\ &= 134.8\,\mathrm{cm}^{-1}.\end{aligned}$$

And, finally, the overlap parameter is obtained from

$$\begin{aligned}\widetilde{\beta} &= \frac{1}{\widetilde{\omega}\widetilde{\alpha}X}\int_0^s \beta\omega\alpha\rho_a\, ds' = \frac{6\rho_{600}}{\widetilde{\omega}X}\int_0^s \left(\beta_0^* P_e\frac{\beta^*}{\beta_0^*}\right)\left(\omega_0\sqrt{\frac{T}{T_0}}\right)\left(\frac{T_0}{T}\right) ds' \\ &= 6\,\beta_0^* P_e\frac{\omega_0}{\widetilde{\omega}}\frac{X_{600}}{X}\int_0^1 \frac{\beta^*}{\beta_0^*}\sqrt{\frac{T_0}{T}}\, d\xi'.\end{aligned}$$

Inspection of Fig. 11-23 reveals that the integrand varies between $0.59/\sqrt{4} \simeq 0.30$ (at 400 K), to $0.66/\sqrt{6} \simeq 0.27$ (at 600 K), back to $0.80/\sqrt{8} \simeq 0.29$ (at 800 K); i.e., the integrand is relatively constant. Keeping in mind the inherent inaccuracies of the wide band model, the integral may be approximated by using an average value of 0.28. Then

$$\widetilde{\beta} \simeq 0.28\times 6\beta_0^* P_e\frac{\omega_0}{\widetilde{\omega}}\frac{X_{600}}{X} = \frac{0.28\times 6\beta_0^* P_e}{6\left(\sqrt{2}-1\right)} = \frac{0.28\times 0.09427\times 3.4515}{\sqrt{2}-1} = 0.220.$$

The effective optical thickness at the band center is now

$$\tau_0 = \widetilde{\alpha}X/\widetilde{\omega} = 41.2\times 5.702/134.8 = 1.743.$$

Again we are in the square root regime and

$$A^* = 2\sqrt{\tau_0\widetilde{\beta}} - \widetilde{\beta} = 2\sqrt{1.743\times 0.220} - 0.220 = 1.018 \text{ and } A = 137\,\mathrm{cm}^{-1}.$$

Thus, although the temperature varied considerably over the path (by a factor of two) values for α, β, and ω changed only slightly, and the final value for the band absorptance changed by less than 3%. In view of the accuracy of the wide band correlation, the assumption of an isothermal gas can often lead to satisfactory results. This has been corroborated by Felske and Tien [158], who suggested a linear average for temperature, and a second independent linear average for density (as opposed to density evaluated at average temperature). They found negligible discrepancy for a large number of nonisothermal examples.

Wide Band *k*-Distributions

Wide band models allow us to determine the radiative emission (or the absorption of incoming radiation) from a volume of gas over an entire vibration–rotation band with a single calculation; but they are inherently less accurate than narrow band models, and they have the same limitations, i.e., they are difficult to apply to nonhomogeneous gases, and they cannot be used at all in enclosures that have nonblack walls and/or in the presence of scattering particles.

The *k*-distribution method, on the other hand, smoothes the spectrum by simply reordering it, rather than supplying an effective transmissivity, and, therefore, it can readily be applied to nonblack walls as well as to scattering media. For a homogeneous medium the method is essentially exact, even for an entire vibration–rotation band, except for the assumption that the Planck function, $I_{b\eta}$, is invariable across the band. This has prompted a number of researchers to generate wide band *k*-distributions based on exponential wide band correlation data. The first such *k*-distribution was generated by Wang and Shi [159], using the Malkmus narrow band

model together with exponentially decaying average line strength. In order to obtain a finite-range reordered wavenumber, $0 \le g \le 1$, as was done for narrow band k-distributions, they truncated the exponentially decaying band wings [see Fig. 11-22 and equation (11.142*b*)]. This resulted in an analytical expression for the wide band k-distribution, $F(k)$. However, evaluation of the reordered wavenumber, $g(k) = \int F\,dk$, and its inversion to $k(g)$ required numerical integration. Marin and Buckius [160] took a very similar approach but used the exponential wide band model together with both the Malkmus model and also the Goody model; they also provided approximate, explicit expressions for water vapor and carbon dioxide [161–163]. Lee *et al.* [164,165] were able to find the k-distribution directly from wide band correlations, using a rather obscure version of Edwards' model. This approach was further refined by Parthasarathy *et al.* [166], using Wang's wide band model [136]. Denison and Fiveland [167] also provided closed-form approximations for the cumulative k-distribution, based on Edwards' original wide band model given in Table 11.2. Comparison with narrow band calculations has shown that results from this model have very respectable accuracy [168].

The band absorptance for a vibration–rotation band is given by equation (11.139). Assuming a symmetric band, such as given by equation (11.142*b*), and reordering according to Section 11.9 leads to

$$A = 2\int_0^\infty \left(1 - e^{-\kappa_\eta X}\right) d|\eta - \eta_c| = 2\int_0^\infty \left(1 - e^{-\kappa X}\right) F(\kappa)\,d\kappa = 2\int_0^\infty \left(1 - e^{-\kappa(g)X}\right) dg, \tag{11.164}$$

where the k-distribution

$$F(\kappa) = \int_0^\infty \delta(\kappa - \kappa_\eta)\,d\eta, \tag{11.165}$$

is defined over an unbounded (wide band) spectral range $\Delta\eta \to \infty$ and, thus, g is also unbounded [cf. equations (11.98) and (11.101)] and equivalent to $|\eta - \eta_c|$. The reordered band can also be regarded as symmetrical, if desired (with g going into both directions away from η_c). Nondimensionalizing equation (11.164) gives

$$A^* = \frac{A}{\omega} = 2\int_0^\infty \left(1 - e^{-\kappa^*\tau_0}\right) F^*(\kappa^*)\,d\kappa^* = \int_0^\infty \left(1 - e^{-\kappa^*(g^*)\tau_0}\right) dg^*,$$
$$\tau_0 = \frac{\alpha}{\omega}X, \quad \kappa^* = \frac{\kappa\omega}{\alpha}, \quad F^* = \frac{\alpha F}{\omega^2}, \quad g^* = 2\frac{g}{\omega}. \tag{11.166}$$

Differentiating equation (11.166) with respect to τ_0, and using Wang's expression for band absorptance, equation (11.158), yields

$$\frac{dA^*}{d\tau_0} = \frac{1}{\tau_0}\left\{1 - \exp\left[\frac{\beta}{2}\left(1 - \sqrt{1 + \frac{4\tau_0}{\beta}}\right)\right]\right\} = 2\int_0^\infty e^{-\kappa^*\tau_0}\kappa^* F^*(\kappa^*)\,d\kappa^*. \tag{11.167}$$

Comparing both sides of this equation it is apparent that $F^*(\kappa^*)$ is related to the inverse Laplace transform of $dA^*/d\tau_0$,

$$2\kappa^* F^*(\kappa^*) = \mathscr{L}^{-1}\left(\frac{dA^*}{d\tau_0}\right). \tag{11.168}$$

Using Wang's model an analytical expression can be obtained for the inverse [166]:

$$F^*(\kappa^*) = \frac{1}{4\kappa^*}\left\{\operatorname{erfc}\left[\frac{\sqrt{\beta}}{2}\left(\sqrt{\kappa^*} - \frac{1}{\sqrt{\kappa^*}}\right)\right] - e^{\beta}\operatorname{erfc}\left[\frac{\sqrt{\beta}}{2}\left(\sqrt{\kappa^*} + \frac{1}{\sqrt{\kappa^*}}\right)\right]\right\}. \tag{11.169}$$

The cumulative k-distribution g^*, or reordered wavenumber, must be found and inverted numerically from

$$\int_{\kappa^*}^\infty F^*(\kappa^*)\,d\kappa^* = \frac{1}{2}g^* = \frac{g}{\omega}. \tag{11.170}$$

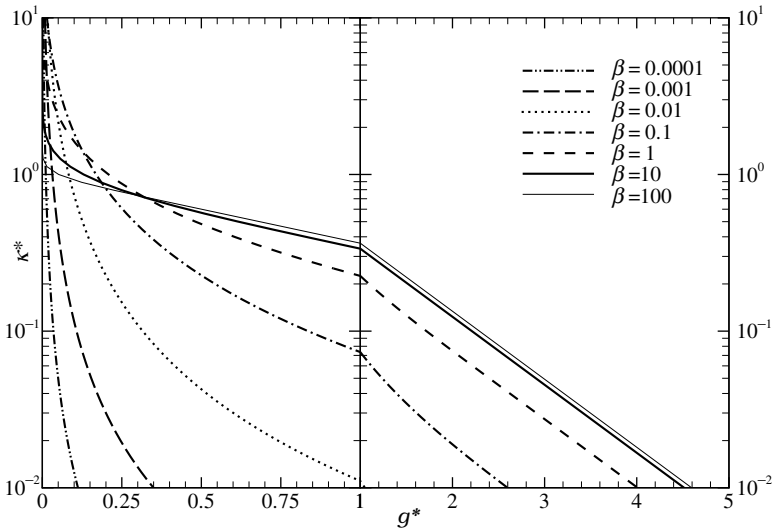

FIGURE 11-27
Nondimensional reordered absorption coefficient κ^* for an exponential wide band *vs.* nondimensional cumulative k-distribution g^*.

Figure 11-27 shows the resulting reordered, nondimensional absorption coefficient κ^* *vs.* artificial, normalized wavenumber g^*. For large values of β there is strong line overlap and $\kappa_\eta \simeq (S/d)_\eta$, and essentially no reordering is necessary. For that case F^* approaches $F^* \to 1/2\kappa^*$ for $\kappa^* < 1$ and $F^* \to 0$ for $\kappa^* > 1$, leading to $\kappa^* \to e^{-g^*}$, $g^* \gtrsim 0.1$.[12] For smaller values of β, or less line overlap, but with identical average absorption coefficient the maximum value of the spectral absorption coefficient increases, and fewer spectral positions will have intermediate values, making the distribution more and more compressed toward small g^*, with larger values near $g^* = 0$.

Example 11.11. The water vapor–air mixture of Example 11.8 is contained in a nonblack furnace of varied dimensions mixed with soot and scattering particles. In order to make accurate predictions of the radiative heat flux possible across the 6.3 μm water vapor band, determine a reordered correlated k-distribution for this mixture.

Solution
For the water vapor–air mixture of Example 11.8 we have for the 6.3 μm band $\alpha = 41.2\,\mathrm{cm}^{-1}/(\mathrm{g/m}^2)$, $\omega = 138.15\,\mathrm{cm}^{-1}$, $\beta = 0.211$, and $\rho_a = 54.84\ \mathrm{g/m}^3$. Obtaining a reordered, nondimensional absorption coefficient $\kappa^* = \kappa^*(g^*)$ from equation (11.170) [by utilizing the Fortran subroutine `wbmkvsg` given in Appendix F], we get from equation (11.166)

$$\kappa(g) = \kappa(|\eta - \eta_c|) = \frac{\rho_a \alpha}{\omega}\kappa^*\left(\frac{2g}{\omega}\right) = \frac{\rho_a \alpha}{\omega}\kappa^*\left(\frac{2|\eta - \eta_c|}{\omega}\right),$$

where we have replaced the α in equation (11.166) by $\rho_a\alpha$ in order to obtain a linear, rather than density-based, absorption coefficient [see equation (11.18)], which is generally preferred for spectral calculations. This equivalent spectral absorption coefficient for the 6.3 μm water vapor band, centered at $\eta_c = 1600\,\mathrm{cm}^{-1}$, is shown in Fig. 11-28, and is compared with the spectral narrow band average absorption coefficient, $(S/d)_\eta$ for the same conditions. Since, for $\beta = 0.211$, there is relatively little line overlap, average values $(S/d)_\eta$ must come from strongly varying κ_η with values much larger and much smaller than the average; thus the abundance of large κ (near $\eta = \eta_c$) with a quick drop-off away from the band center.

Figure 11-28 makes the band appear less wide than indicated by the band width parameter ω. This was done for mathematical convenience: as Fig. 11-11 shows, a band with small β

[12] By convention $\mathrm{erfc}(x) = 0$ for $x \to +\infty$, and $\mathrm{erfc}(x) = 2$ for $x \to -\infty$ [98].

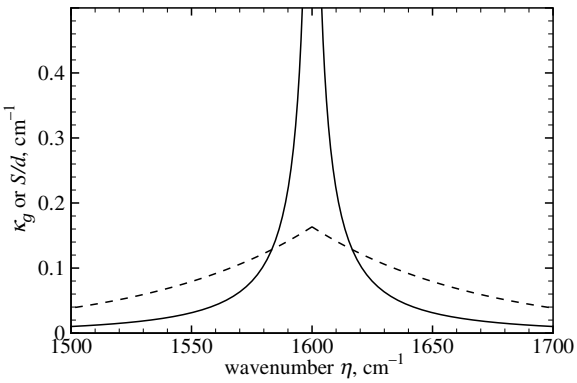

FIGURE 11-28
Reordered absorption coefficient for Example 11.11.

contains many strong lines separated by small κ; we have simply chosen to collect all the large values of κ near the band center.

The wide band k-distribution presented here requires numerical integration of equation (11.170) and its inversion to obtain the reordered absorption coefficient $k(g)$; the reordered absorption coefficient recovers the total band absorptance as defined by exponential wide band model parameters. On the other hand, in the work of Marin and Buckius [161–163] explicit (albeit cumbersome) expressions are given for $k(g)$, which approximate the wide band k-distributions obtained from the HITEMP 1995 database [62]. While probably more accurate below 1000 K (the limit of applicability of HITEMP), the Marin and Buckius formulation depends strongly on the arbitrary and nonphysical choice for the cutoff wavenumber (chosen to find a best fit with HITEMP-generated k-distributions).

11.11 TOTAL EMISSIVITY AND MEAN ABSORPTION COEFFICIENT

Total Emissivity

In less sophisticated, more practical engineering treatment it is usually sufficient to evaluate the emission from a hot gas (usually considered isothermal) that reaches a wall. The total emissivity is defined as the portion of total emitted radiation over a path X that is not attenuated by self-absorption, divided by the maximum possible emission or, from equation (11.48) and considering only emission within the gas,

$$\epsilon \equiv \frac{\int_0^\infty I_{b\eta}\epsilon_\eta\, d\eta}{\int_0^\infty I_{b\eta}\, d\eta} = \frac{\int_0^\infty I_{b\eta}\left(1-e^{-\kappa_\eta X}\right) d\eta}{\int_0^\infty I_{b\eta}\, d\eta} = \sum_{i=1}^{N}\left(\frac{\pi I_{b\eta 0}}{\sigma T^4}\right)_i \int_{\Delta\eta_{\text{band}}}\left(1-e^{-\kappa_\eta X}\right) d\eta = \sum_{i=1}^{N}\left(\frac{\pi I_{b\eta 0}}{\sigma T^4}\right)_i A_i, \tag{11.171}$$

where two simplifying assumptions have been made: (*i*) The spectral width of each of the N bands is so narrow that the Planck function varies only negligibly over this range, and (*ii*) the bands do not overlap. While the first assumption is generally very good (with the exception of pure rotational bands such as the one for water vapor listed in Table 11.3), bands do sometimes overlap (for example, the 2.7 μm bands in a water vapor–CO_2 mixture).

If two or more bands of the species contained in a gas mixture overlap, the emission from the mixture will be smaller than the sum of the individual contributions (because of increased self-absorption). This problem has been dealt with, in an approximate fashion, by Hottel and Sarofim [11]. They argued that the transmissivities of species a and b over the overlapping region $\Delta\eta$ are independent from one another, that is,

$$\overline{\tau}_{a+b} = \frac{1}{\Delta\eta}\int_{\Delta\eta} e^{-\kappa_{\eta a}X}\, e^{-\kappa_{\eta b}X}\, d\eta \approx \frac{1}{\Delta\eta}\int_{\Delta\eta} e^{-\kappa_{\eta a}X}\, d\eta\ \frac{1}{\Delta\eta}\int_{\Delta\eta} e^{-\kappa_{\eta b}X}\, d\eta = \overline{\tau}_a\,\overline{\tau}_b. \tag{11.172}$$

If we define the total emissivity for a single band as

$$\epsilon_i \equiv \left(\frac{\pi I_{b\eta 0}}{\sigma T^4}\right)_i A_i, \tag{11.173}$$

then this expression leads to the total emissivity of two overlapping bands, or

$$\epsilon_{a+b} = \epsilon_a + \epsilon_b - \epsilon_a \epsilon_b. \tag{11.174}$$

This equation is only accurate if both bands fully overlap. If the overlap is only partial, then the correction term, $\epsilon_a \epsilon_b$, should be calculated based on the fractions of band emissivity that pertain to the overlap region (i.e., a quantity that is not available from wide band correlations). An approximate way of dealing with this problem has been suggested by Felske and Tien [158].

A total absorptivity for the gas may be defined in the same way as equation (11.171). However, as for surfaces, in the absorptivity the absorption coefficient must be evaluated at the temperature of the gas, while the Planck function is based on the blackbody temperature of the radiation source.

It is clear from equation (11.171) that the total emissivity is equal to the sum of band absorptances multiplied by the weight factor $(\pi I_{b\eta 0}/\sigma T^4)$. Since the band absorptance is roughly proportional to the band strength parameter α (exactly proportional for small values of optical path X), comparison of the factors $[\alpha(\pi I_{b\eta 0}/\sigma T^4)]_i$ gives an idea of which bands need to be considered for the calculation of the total emissivity.

Example 11.12. What is the total emissivity of a 20 cm thick layer of pure CO at 800 K and 1 atm?

Solution

For these conditions CO has a single important absorption band in the infrared. Comparing $\alpha I_{b\eta 0}$ for the 4.7 μm and 2.35 μm bands (see Table 11.3) we find with $(\eta_0/T)_{4.3} = 2143\,\mathrm{cm^{-1}}/800\,\mathrm{K} = 2.679\,\mathrm{cm^{-1}/K}$ and $(\eta_0/T)_{2.35} = 4260\,\mathrm{cm^{-1}}/800\,\mathrm{K} = 5.325\,\mathrm{cm^{-1}/K}$,

$$\left(\frac{\alpha E_{b\eta 0}}{T^3}\right)_{4.7} \Bigg/ \left(\frac{\alpha E_{b\eta 0}}{T^3}\right)_{2.35} = \frac{20.9 \times 1.5563}{0.14 \times 0.2659} = 874.$$

Therefore, since the 4.7 μm band is much stronger ($\alpha_{4.7}/\alpha_{2.35} \simeq 150$) and located in a more important part of the spectrum $\left(E_{b\eta 4.7}/E_{b\eta 2.35} \simeq 6\right)$, the influence of the 2.35 μm band can be neglected. We first need to calculate the band absorptance for the 4.7 μm band. Since values in Table 11.3 are based on the mass absorption coefficient, we need to calculate the density of the CO from the ideal gas law, as we did in Example 11.8:

$$\rho_a = \frac{\mathscr{M} p_a}{R_u T} = \frac{28\,\mathrm{g/mol} \times 1\,\mathrm{atm}}{8.3145\,\mathrm{J/mol\,K} \times 800\,\mathrm{K}} \frac{1.0132 \times 10^5\,\mathrm{J/m^3}}{1\,\mathrm{atm}} = 426.6\,\mathrm{g/m^3}$$

and $X = \rho_a s = 85.32\,\mathrm{g/m^2}$. We also find from Table 11.3 that $n = 0.8$ and $b = 1.1$, so that $P_e = 1.1^{0.8} = 1.079$ and $\beta_0^* P_e = 0.075 \times 1.079 = 0.081$. Further we find $\alpha = 20.9\,\mathrm{cm^{-1}/(g/m^2)}$, $\omega = 25.5\sqrt{800/100} = 72.125\,\mathrm{cm^{-1}}$, and $\tau_0 = \alpha X/\omega = 20.9 \times 85.32/72.125 = 24.72$. From Fig. 11-25 or subroutine `wbmco` we obtain $\beta^*/\beta_0^* = 0.529$ and $\beta = (\beta^*/\beta_0^*)\beta_0^* P_e = 0.529 \times 0.081 = 0.043$. Thus, $\tau_0 > 1/\beta$ and we are in the logarithmic regime, and

$$A^* = \ln(\tau_0 \beta) + 2 - \beta = 2.018 \text{ and } A = 145.6\,\mathrm{cm^{-1}}.$$

Sticking this into equation (11.171),

$$\begin{aligned}
\epsilon_{\mathrm{CO}}(800\,\mathrm{K}, 1\,\mathrm{atm}) &= \left(\frac{\pi I_{b\eta 0}}{\sigma T^4}\right)_{\eta_0 = 2143\,\mathrm{cm^{-1}}} \times A = \left(\frac{E_{b\eta 0}}{T^3}\right)_{\eta_0 = 2143\,\mathrm{cm^{-1}}} \times \frac{A}{\sigma T} \\
&= 1.5563 \times 10^{-8}\,\frac{\mathrm{W}}{\mathrm{m^2\,cm^{-1}\,K^3}} \times \frac{145.6\,\mathrm{cm^{-1}}}{5.670 \times 10^{-8} \times 800\,\mathrm{W/m^2\,K^3}} \\
&= 0.0500.
\end{aligned}$$

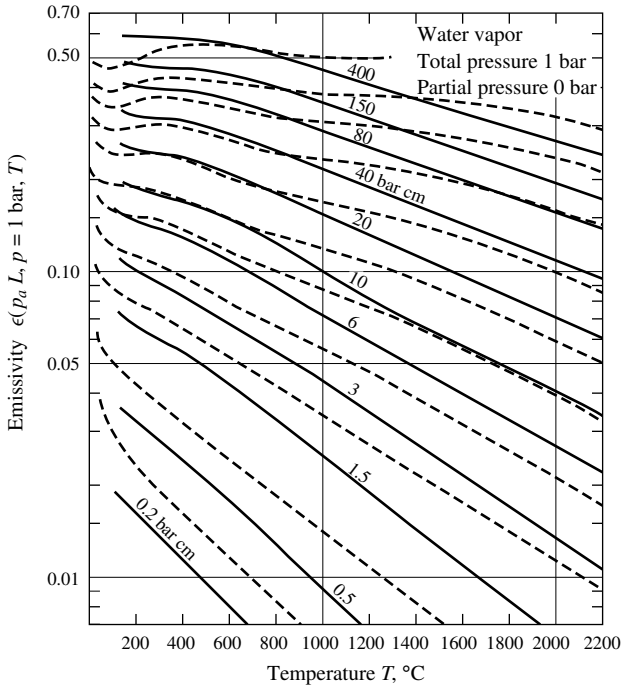

FIGURE 11-29
Total emissivity of water vapor at a total gas pressure of 1 bar and zero partial pressure, from Hottel [18] (solid lines) and Leckner [169] (dashed lines).

If only total emissivities are desired, it would be very convenient to have correlations, tables, or charts from which the total emissivity can be read directly, rather than having to go through the algebra of the wide band correlations plus equation (11.171). A number of investigators have included total emissivity charts with their wide band correlation data; for example, Brosmer and Tien [141,150] compiled data on CH_4 and C_2H_2, and Tien and coworkers [149] did the same for N_2O. However, by far the most monumental work has been collected by Hottel [18] and Hottel and Sarofim [11]. They considered primarily combustion gases, but they also presented charts for a number of other gases. Their data for total emissivity and absorptivity are presented in the form

$$\epsilon = \epsilon(p_a L, p, T_g), \tag{11.175}$$

$$\alpha = \alpha(p_a L, p, T_g, T_s) \approx \left(\frac{T_g}{T_s}\right)^{1/2} \epsilon\left(p_a L \frac{T_s}{T_g}, p, T_s\right), \tag{11.176}$$

where T_g is the gas temperature and T_s is the temperature of an external blackbody (or gray) source such as a hot surface. Originally, the power for T_g/T_s recommended by Hottel was 0.65 for CO_2 and 0.45 for water vapor, but with greater theoretical understanding the single value of 0.5 has become accepted [11]. In equation (11.176) p_a is the partial pressure of the absorbing gas and p is the total pressure. (Hottel and Sarofim preferred a pressure path length over the density path length used by Edwards.) The emissivities were given in chart form *vs.* temperature, with pressure path length as parameter, and for an overall pressure of 1 atm. Later work by Leckner [169], Ludwig and coworkers [170,171], Sarofim and coworkers [172] and others has shown that the original charts by Hottel [11,18], while accurate for many conditions (in particular, over the ranges covered by experimental data of the times), are seriously in error for some conditions (primarily those based on extrapolation of experimental data). New charts, based on the integration of spectral data, have been prepared by Leckner [169] and Ludwig and coworkers [170, 171], and show good agreement among each other. Emissivity charts, comparing the newly calculated data by Leckner [169] with Hottel's [18], are shown in Fig. 11-29 for water vapor and in Fig. 11-30 for carbon dioxide. These charts give the emissivities for the limiting case of vanishing partial pressure of the absorbing gas ($p_a \to 0$).

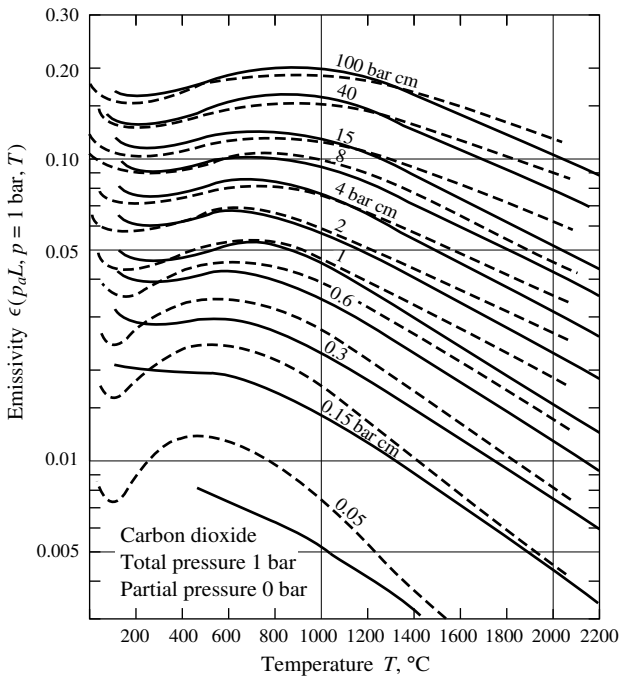

FIGURE 11-30
Total emissivity of carbon dioxide at a total gas pressure of 1 bar and zero partial pressure, from Hottel [18] (solid lines) and Leckner [169] (dashed lines).

The original charts by Hottel also included pressure correction charts for the evaluation of cases with $p_a \neq 0$ and $p \neq 1\,\text{bar}$, as well as charts for the overlap parameter $\Delta\epsilon$. Again, these factors were found to be somewhat inaccurate under extreme conditions and have been improved upon in later work. Particularly useful for calculations are the correlations given by Leckner [169], which (for temperatures above 400 K) have a maximum error of 5% for water vapor and 10% for CO_2, respectively, compared to his spectrally integrated emissivities (i.e., the dashed lines in Figs. 11-29 and 11-30). In his correlation the zero-partial-pressure emissivity is given by

$$\epsilon_0(p_aL, p{=}1\,\text{bar}, T_g) = \exp\left[\sum_{i=0}^{M}\sum_{j=0}^{N} c_{ji}\left(\frac{T_g}{T_0}\right)^j\left(\log_{10}\frac{p_aL}{(p_aL)_0}\right)^i\right], \quad T_0 = 1000\,\text{K},\ (p_aL)_0 = 1\,\text{bar cm}, \tag{11.177}$$

and the c_{ji} are correlation constants given in Table 11.4 for water vapor and carbon dioxide. The emissivity for different pressure conditions is then found from

$$\frac{\epsilon(p_aL, p, T_g)}{\epsilon_0(p_aL, 1\,\text{bar}, T_g)} = 1 - \frac{(a-1)(1-P_E)}{a+b-1+P_E}\exp\left(-c\left[\log_{10}\frac{(p_aL)_m}{p_aL}\right]^2\right), \tag{11.178}$$

where P_E is an effective pressure, and a, b, c, and $(p_aL)_m$ are correlation parameters, also given in Table 11.4.

As noted before, in a mixture that contains both carbon dioxide and water vapor, the bands partially overlap and another correction factor must be introduced, which is found from

$$\Delta\epsilon = \left[\frac{\zeta}{10.7 + 101\zeta} - 0.0089\zeta^{10.4}\right]\left(\log_{10}\frac{(p_{H_2O} + p_{CO_2})L}{(p_aL)_0}\right)^{2.76}, \tag{11.179}$$

with

$$\zeta = \frac{p_{H_2O}}{p_{H_2O} + p_{CO_2}}. \tag{11.180}$$

TABLE 11.4
Correlation constants for the determination of the total emissivity for water vapor and carbon dioxide [169].

Gas	Water Vapor	Carbon Dioxide
M, N	2, 2	2, 3
$\begin{matrix} c_{00} & \dots & c_{N0} \\ \vdots & \ddots & \vdots \\ c_{0M} & \dots & c_{NM} \end{matrix}$	$\begin{matrix} -2.2118 & -1.1987 & 0.035596 \\ 0.85667 & 0.93048 & -0.14391 \\ -0.10838 & -0.17156 & 0.045915 \end{matrix}$	$\begin{matrix} -3.9893 & 2.7669 & -2.1081 & 0.39163 \\ 1.2710 & -1.1090 & 1.0195 & -0.21897 \\ -0.23678 & 0.19731 & -0.19544 & 0.044644 \end{matrix}$
P_E	$(p + 2.56p_a/\sqrt{t})/p_0$	$(p + 0.28p_a)/p_0$
$(p_aL)_m/(p_aL)_0$	$13.2t^2$	$0.054/t^2, \quad t < 0.7$ $0.225t^2, \quad t > 0.7$
a	$2.144, \quad t < 0.75$ $1.888 - 2.053 \log_{10} t, \quad t > 0.75$	$1 + 0.1/t^{1.45}$
b	$1.10/t^{1.4}$	0.23
c	0.5	1.47
$T_0 = 1000\,\text{K},\ p_0 = 1\,\text{bar},\ t = T/T_0,\ (p_aL)_0 = 1\,\text{bar cm}$		

This factor is directly applicable to emissivity and absorptivity.

To summarize, the total emissivity and absorptivity of gases containing CO_2, water vapor, or both, may be calculated from:

$$\epsilon_i(p_iL, p, T_g) = \epsilon_{0i}(p_iL, 1\,\text{bar}, T_g)\left(\frac{\epsilon}{\epsilon_0}\right)_i(p_iL, p, T_g), \qquad i = \text{CO}_2 \text{ or } \text{H}_2\text{O}, \tag{11.181a}$$

$$\alpha_i(p_iL, p, T_g, T_s) = \left(\frac{T_g}{T_s}\right)^{1/2}\epsilon_i\left(p_iL\frac{T_s}{T_g}, p, T_s\right), \qquad i = \text{CO}_2 \text{ or } \text{H}_2\text{O}, \tag{11.181b}$$

$$\epsilon_{\text{CO}_2+\text{H}_2\text{O}} = \epsilon_{\text{CO}_2} + \epsilon_{\text{H}_2\text{O}} - \Delta\epsilon\left(p_{\text{H}_2\text{O}}L, p_{\text{CO}_2}L\right), \tag{11.181c}$$

$$\alpha_{\text{CO}_2+\text{H}_2\text{O}} = \alpha_{\text{CO}_2} + \alpha_{\text{H}_2\text{O}} - \Delta\epsilon\left(p_{\text{H}_2\text{O}}L\frac{T_s}{T_g}, p_{\text{CO}_2}L\frac{T_s}{T_g}\right). \tag{11.181d}$$

For the convenience of the reader Appendix F contains the Fortran routines `totemiss` and `totabsor`, which calculate the total emissivity or absorptivity of a CO_2–water vapor mixture from Leckner's correlation, and which can also be called from the stand-alone program `Leckner` through user prompts.

Example 11.13. Consider a 1 m thick layer of a gas mixture at 1000 K and 5 bar that consists of 10% carbon dioxide, 20% water vapor, and 70% nitrogen. What is the total normal intensity escaping from this layer?

Solution
From equations (11.48) and (11.171) we see that the exiting total intensity is

$$I = \int_0^\infty I_{b\eta}\left(1 - e^{-\kappa_\eta X}\right)d\eta = \int_0^\infty I_{b\eta}\epsilon_\eta\, d\eta = \frac{\epsilon\sigma T^4}{\pi},$$

where ϵ is the total emissivity of the water vapor–carbon dioxide mixture. First we calculate the emissivity of CO_2 at a total pressure of 1 bar from Table 11.4: With $p_{\text{CO}_2}L = 0.1 \times 5\,\text{m bar} = 50\,\text{bar cm}$ and $T_g = 1000\,\text{K}$ we find $\epsilon_{\text{CO}_2,0}(1\,\text{bar}) = 0.157$ (which may also be estimated from Fig. 11-30); for a total pressure of 5 bar we find from Table 11.4 the effective pressure is $P_E = 5.14$, $a = 1.1$, $b = 0.23$, $c = 1.47$,

and $(p_aL)_m = 0.225\,\text{bar cm}$. Thus, from equation (11.178)

$$\left(\frac{\epsilon}{\epsilon_0}\right)_{CO_2} = 1 - \frac{0.1\times(-4.14)}{0.33+5.14}\exp\left[-1.47\times\left(\log_{10}\frac{0.225}{50}\right)^2\right] \approx 1.00,$$

and

$$\epsilon_{CO_2} \approx 0.157.$$

Similarly, for water vapor with $p_{H_2O}L = 0.2\times 5\,\text{m bar} = 100\,\text{bar cm}$ we find $\epsilon_{H_2O,0}(1\,\text{bar}) \approx 0.359$ and the pressure correction factor becomes, with $P_E = 7.56$, $a = 1.88$, $b = 1.1$, $c = 0.5$, and $(p_aL)_m = 13.2\,\text{bar cm}$,

$$\left(\frac{\epsilon}{\epsilon_0}\right)_{H_2O} = 1 - \frac{0.888\times(-6.56)}{1.988+7.56}\exp\left[-0.5\times\left(\log_{10}\frac{13.2}{100}\right)^2\right] = 1.414,$$

and

$$\epsilon_{H_2O} \approx 0.359\times 1.414 = 0.508.$$

Finally, since we have a mixture of carbon dioxide and water vapor, we need to deduct for the band overlaps: From equation (11.179), with $\zeta = \frac{2}{3}$, $\Delta\epsilon = 0.072$. Thus, the total emissivity is $\epsilon = 0.157 + 0.508 - 0.072 = 0.593$. Alternatively, and more easily, using subroutine `totemiss` with `ph2o` = 1., `pco2` = .5, `ptot` = 5, `L` = 100, and `Tg` = 1000 returns the same numbers.

The total normal intensity is then

$$I = 0.593\times 5.670\times10^{-8}\,\text{W/(m}^2\,\text{K}^4)\times(1000\,\text{K})^4/\pi\,\text{sr} = 10.70\,\text{kW/m}^2\,\text{sr}.$$

It is apparent from this example that the calculation of total emissivities is far from an exact science and carries a good deal of uncertainty. Carrying along three digits in the above calculations is optimistic at best. The reader should understand that accurate emissivity values are difficult to measure, and that too many parameters are involved to make simple and accurate correlations possible.

Mean Absorption Coefficients

We noted in the previous chapter that the emission term in the equation of transfer, equation (10.21), and in the divergence of the radiative heat flux, equation (10.59), is proportional to $\kappa_\eta I_{b\eta}$. Thus, for the evaluation of total intensity or heat flux divergence it is convenient to define the following total absorption coefficient, known as the *Planck-mean absorption coefficient*:

$$\kappa_P \equiv \frac{\int_0^\infty I_{b\eta}\kappa_\eta\,d\eta}{\int_0^\infty I_{b\eta}\,d\eta} = \frac{\pi}{\sigma T^4}\int_0^\infty I_{b\eta}\kappa_\eta\,d\eta. \tag{11.182}$$

Using narrow band averaged values for the absorption coefficient, and making again the assumption that the Planck function varies little across each vibration–rotation band, equation (11.182) may be restated as

$$\kappa_P = \sum_{i=1}^{N}\left(\frac{\pi I_{b\eta 0}}{\sigma T^4}\right)_i\int_{\Delta\eta_{\text{band}}}\left(\frac{S}{d}\right)d\eta = \sum_{i=1}^{N}\left(\frac{\pi I_{b\eta 0}}{\sigma T^4}\right)_i\alpha_i, \tag{11.183}$$

where the sum is over all N bands, and the $I_{b\eta 0}$ are evaluated at the center of each band. It is interesting to note that the Planck-mean absorption coefficient depends only on the band strength parameter α and, therefore, on temperature (but not on pressure). Values for α have been measured and tabulated by a number of investigators for various gases and, using them, Planck-mean absorption coefficients have been presented by Tien [3], but these values are today known to be seriously in error. Alternatively, the Planck-mean absorption coefficient can be

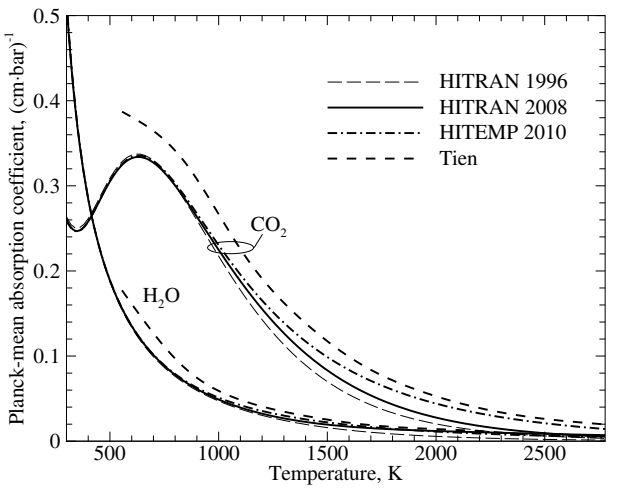

FIGURE 11-31
Planck-mean absorption coefficients for carbon dioxide, and water vapor.

calculated directly from high-resolution databases such as HITRAN [32] and HITEMP [74] as [173]

$$\kappa_P = \frac{\pi}{\sigma T^4} \int_0^\infty I_{b\eta} \sum_j \kappa_{\eta j}\, d\eta = \sum_j \left(\frac{\pi I_{b\eta 0}}{\sigma T^4} \right)_j \int_0^\infty \kappa_{\eta j}\, d\eta = \sum_j \left(\frac{\pi I_{b\eta 0}}{\sigma T^4} \right)_j S_j, \tag{11.184}$$

where the summation is now over all the spectral lines of the gas, and the $I_{b\eta 0}$ are evaluated at the center of each line. Figures 11-31 through 11-33 show Planck-mean absorption coefficients calculated from the HITEMP 2010 (CO_2, H_2O, and CO) and HITRAN 2008 databases (all gases). For some gases, which saw major updates in the most recent HITRAN 2008 version, the values obtained from HITRAN 1996 [57] are also shown for comparison. At higher temperatures the Planck-mean absorption coefficients from HITRAN 2008 are generally larger than those from HITRAN 1996, due to the inclusion of many more lines from higher vibrational energy levels. Accordingly, today's HITRAN 2008 can be used with confidence up to about 1000 K. The latest version of HITEMP [74] includes many more "hot lines," and strives to be accurate for temperatures up to 3000 K.

Sometimes the Planck-mean absorption coefficient is required for absorption (rather than emission), for example, when gas and radiation source are at different temperatures. This expression is known as the *modified Planck-mean absorption coefficient*, and is defined as

$$\kappa_m(T, T_s) \equiv \frac{\int_0^\infty I_{b\eta}(T_s)\kappa_\eta(T)\, d\eta}{\int_0^\infty I_{b\eta}(T_s)\, d\eta}. \tag{11.185}$$

An approximate expression relating κ_m to κ_P has been given by Cess and Mighdoll [174] as

$$\kappa_m(T, T_s) = \kappa_P(T_s)\left(\frac{T_s}{T}\right). \tag{11.186}$$

In later chapters we shall see that in optically thick situations the radiative heat flux becomes proportional to

$$\frac{1}{\kappa_\eta} \nabla I_{b\eta} = \frac{1}{\kappa_\eta} \frac{dI_{b\eta}}{dT} \nabla T. \tag{11.187}$$

This has led to the definition of an optically thick or *Rosseland-mean absorption coefficient* as

$$\frac{1}{\kappa_R} \equiv \int_0^\infty \frac{1}{\kappa_\eta} \frac{dI_{b\eta}}{dT}\, d\eta \Bigg/ \int_0^\infty \frac{dI_{b\eta}}{dT}\, d\eta = \frac{\pi}{4\sigma T^3} \int_0^\infty \frac{1}{\kappa_\eta} \frac{dI_{b\eta}}{dT}\, d\eta. \tag{11.188}$$

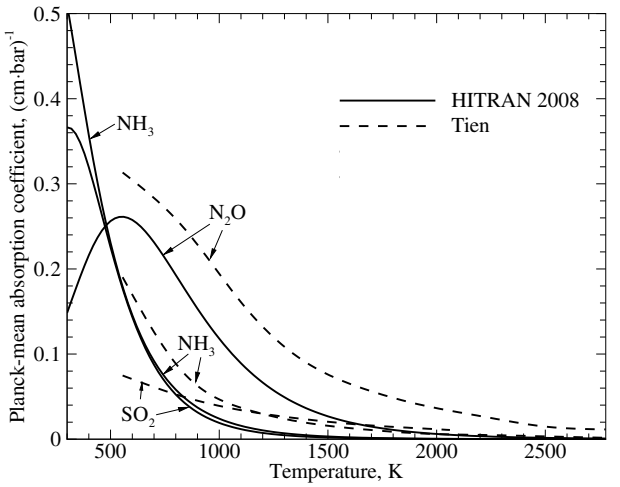

FIGURE 11-32
Planck-mean absorption coefficients for ammonia, nitrous oxide, and sulfur dioxide.

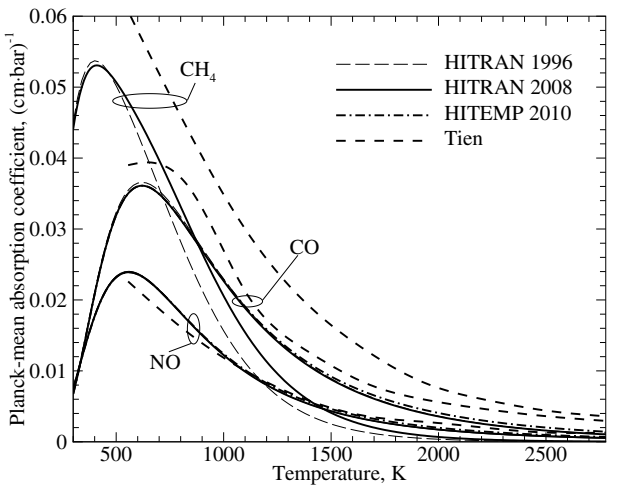

FIGURE 11-33
Planck-mean absorption coefficients for carbon monoxide, nitric oxide, and methane.

Even though they noted the difficulty of integrating equation (11.188) over the entire spectrum (with zero absorption coefficient between bands), Abu-Romia and Tien [145] and Tien [3] attempted to evaluate the Rosseland-mean absorption coefficient for pure gases. Since the results are, at least by this author, regarded as very dubious they will not be reproduced here. We shall return to the Rosseland absorption coefficient when its use is warranted, i.e., when a medium is optically thick over the entire spectrum (for example, an optically thick particle background with or without molecular gases).

11.12 EXPERIMENTAL METHODS

Before going on to employ the above concepts of radiation properties of molecular gases in the solution of the radiative equation of transfer and the calculation of radiative heat fluxes, we want to briefly look at some of the more common experimental methods of determining these properties. While light sources, monochromators, detectors, and optical components are similar to the ones used for surface property measurements, as discussed in Section 3.10, gas property measurements result in transmission studies (as opposed to reflection measurements for surfaces).

All transmission measurements resemble one another to a certain extent: They consist of a

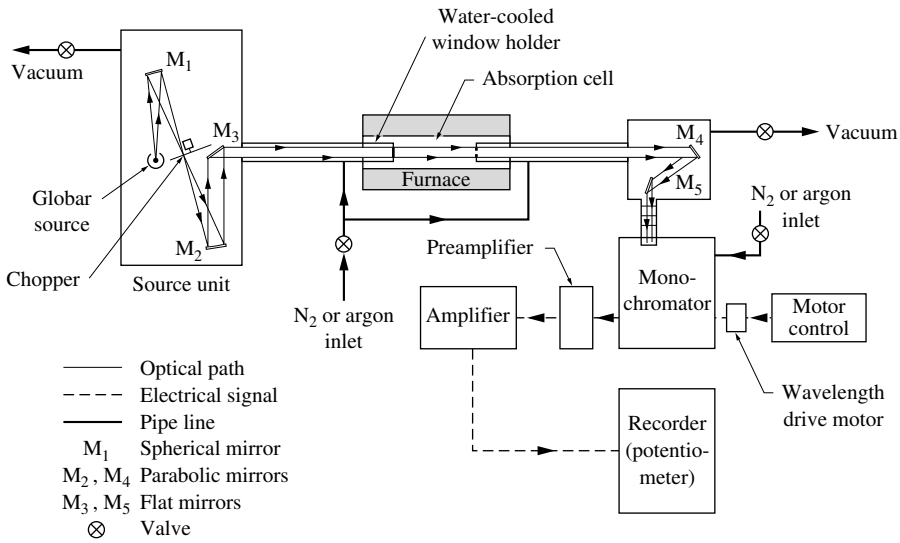

FIGURE 11-34
General setup of gas radiation measurement apparatus [175].

light source, a monochromator or FTIR spectrometer (unless, for measurements over a narrow spectral range, a tunable laser is used as source), a chopper, a test cell with the (approximately isothermal) gas whose properties are to be measured, a detector, associated optics, and an amplifier–recorder device. The chopper often serves two purposes: (*i*) A pyroelectric detector cannot measure radiative intensity, rather, it measures *changes* in intensity; and (*ii*) if the beam is chopped before going through the sample gas then, by measuring the difference in intensity between chopper open and closed conditions, indeed only transmission of the incident light beam is measured. That is, any emission from the (possibly very hot) test gas and/or stray radiation will not be part of the signal. A typical setup is shown in Fig. 11-34, depicting an apparatus used by Tien and Giedt [175]. A chopper is not required if an FTIR spectrometer is used, since the light is modulated inside the unit. However, for high test gas temperatures care must be taken to eliminate sample emission from the signal [176,177]. Usually, gas temperatures are measured independently, and knowledge of gas absorption coefficients is acquired. But it is also possible to radiatively determine the gas temperature, if accurate knowledge of the absorption coefficient is given, such as detailed line structure of diatomic molecules together with FTIR spectrometry [178–180].

Measurements of radiative properties of gases may be characterized by the nature of the test gas containment and by the spectral width of the measurements. As indicated by Edwards [1], we distinguish among (1) hot window cell, (2) cold window cell, (3) nozzle seal cell, and (4) free jet devices; these may be used to make (*a*) narrow band measurements, (*b*) total band absorptance measurements, or (*c*) total emissivity/absorptivity measurements.

The hot window cell uses an isothermal gas within a container that is closed off at both ends by windows that are kept at the same temperature as the gas. While this setup is the most nearly ideal situation for measurements, it is generally very difficult to find window material that (*i*) can withstand the high temperatures at which gas properties are often measured, (*ii*) are transparent in the spectral regions where measurements are desired (usually near-infrared to infrared) and do not experience "thermal runaway" (strong increase in absorptivity at a certain temperature level), and (*iii*) do not succumb to chemical attack from the test gas and other gases. Such cells have been used, for example, by Penner [20], Goldstein [181], and Oppenheim and Goldman [182].

The cold window cell, as the name implies, lets the probing beam enter and exit the test

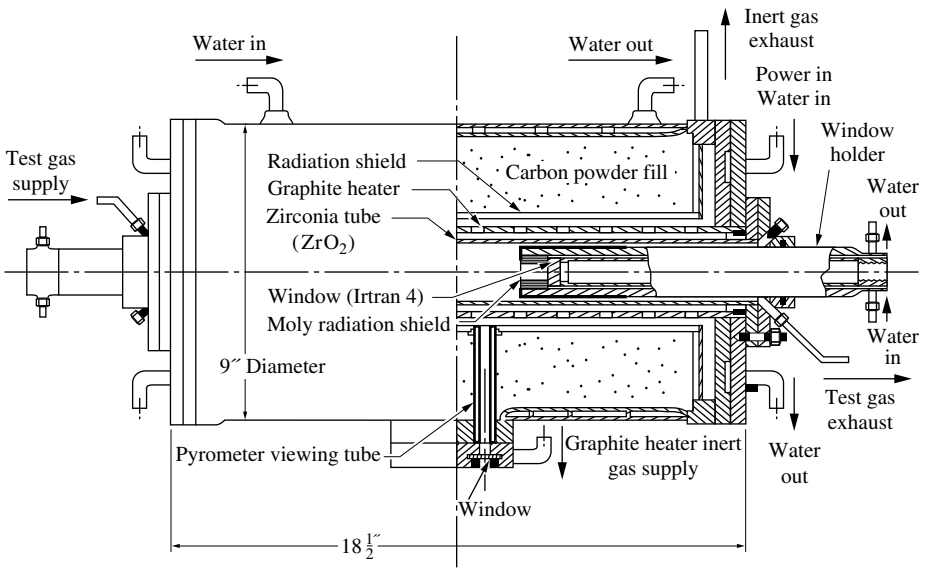

FIGURE 11-35
Schematic of the high-temperature gas furnace used by Tien and Giedt [175].

cell through water-cooled windows. This method has the advantage that the problems in a hot window cell are nearly nonexistent. However, if the geometric path of the gas is relatively short, this method introduces serious temperature and density variations along the path. Tien and Giedt [175] designed a high-temperature furnace, consisting of a zirconia tube surrounded by a graphite heater, that allowed temperatures up to 2000 K. The furnace was fitted with water-cooled, movable zinc selenide windows, which are transmissive between 0.5 μm and 20 μm and stay inert to reactions with water vapor and carbon oxides for temperatures below 550 K. A schematic of their furnace is shown in Fig. 11-35. While allowing high temperatures, it is impossible to obtain truly isothermal gas columns with such a device. For example, for a nominal cell at 1750 K of 30 cm length, they found that the temperature gradually varied by a rather substantial 350 K over the central 2/3 of the cell, and then rapidly dropped to 330 K over the outer 1/3. This apparatus was used by Tien and coworkers to measure the properties of various gases [144, 146–149, 183].

Nozzle seal cells are open flow cells in which the absorbing gas is contained within the cell by layers on each end of inert gases such as argon or nitrogen. This system eliminates some of the problems with windows, but may also cause density and temperature gradients near the seal; in addition, some scattering may be introduced by the turbulent eddies of the mixing flows [184]. This type of apparatus has been used by Hottel and Mangelsdorf [13] and Eckert [185] for total emissivity measurements of water vapor and carbon dioxide. Most of the measurements made by Edwards and coworkers also used nozzle seal cells [131, 132, 134, 143, 184, 186, 187]. A schematic of the apparatus used by Bevans and coworkers [186] is shown in Fig. 11-36. Using a burner and jet for gas radiation measurements eliminates the window problems, and is in many ways similar to the nozzle seal cell. Free jet devices can be used for extremely high temperatures, but they also introduce considerable uncertainty with respect to gas temperature and density distribution and to path length. Ferriso and Ludwig [188] used such a device for spectral measurements of the 2.7 μm water vapor band.

More recently, Modest has constructed a high-temperature gas transmissometer, shown schematically in Fig. 11-37 and used by Bharadwaj et al. [63, 65, 66] to measure transmissivities of carbon dioxide and water vapor. The device is based on the infrared emissometer [189–191] shown in Fig. 3-44 and combines the advantages of hot-window and cold-window absorption

cells. In essence, the apparatus consists of a hermetically sealed high-temperature furnace, a motorized tube fitted with an optical window, a sealed optical path, and an FTIR spectrometer with internal infrared light source and an external detector, which can only detect the modulated light from the FTIR. Light from the FTIR is imaged onto a platinum mirror inside the furnace; the reflected light, in turn, is imaged onto the external detector. The cold drop-tube with an optical window is placed into position and retracted by a high-speed motor. The gas column between platinum mirror and optical window forms an isothermal absorption cell and, since the optical window resides within the furnace's hot zone for only a few seconds at a time, this device is able to measure transmissivities of truly isothermal high-temperature gas columns.

All multispectral diagnostic techniques discussed so far have employed single-detector monochromator or FTIR spectroscopy. Such devices can provide spectral scans in a wide range of resolutions and of great accuracy, but to obtain a spectrally resolved measurement with good signal-to-noise ratio takes tens of seconds for low-resolution narrow-band scans to hours for high-resolution full-spectrum measurements. Very few attempts have been made to date to obtain time-resolved multispectral signals from turbulent systems, because—to obtain snapshots of a turbulent flowfield—exposure times must be of order of 0.1 ms or less. Richardson et al. [192, 193] were perhaps the first to attempt such measurements, using a 32-element InSb linear array detector fitted with a grating monochromator. The apparatus was quite similar to the one shown in Fig. 11-34, except that there is no need to rotate the monochromator's prism or grating, with the spectrally separated light hitting different elements of the array detector simultaneously. Their device was able to collect a 32-spectrum signal over 160 μs, storing 250 samples for each detector element. This resulted in an equivalent FTIR resolution of 32 cm^{-1} when collecting a spectrum of 250 cm^{-1}, with a signal-to-noise ratio of about 50. Their improved second device was able to hold 2048 full spectra collected every 16 μs. A similar apparatus was built by Keltner et al. [194], using a 256×256 MCT array detector. They argued that the use of (dual) prisms is preferable to grating monochromators in connection with array detectors. This dual prism arrangement was also used by Ji et al. [195], together with a 160-element PbSe linear array detector. The resulting high-speed spectrometer, is capable of taking near-instantaneous snapshots at a rate of 390 Hz. The device was calibrated against a blackbody, and spectra from a laminar premixed flame were compared with measurements using a grating spectrometer–InSb detector combination. Later measurements have been carried out with this high-speed infrared array spectrometer, to provide radiation data for the otherwise well-documented Sandia Workshop flames [196–198], and for a sooty ethylene air diffusion flame [199].

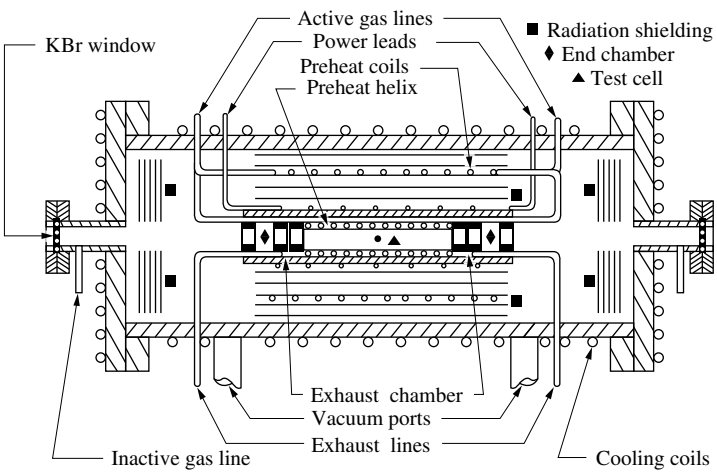

FIGURE 11-36
Schematic of nozzle seal gas containment system by Bevans and coworkers [186].

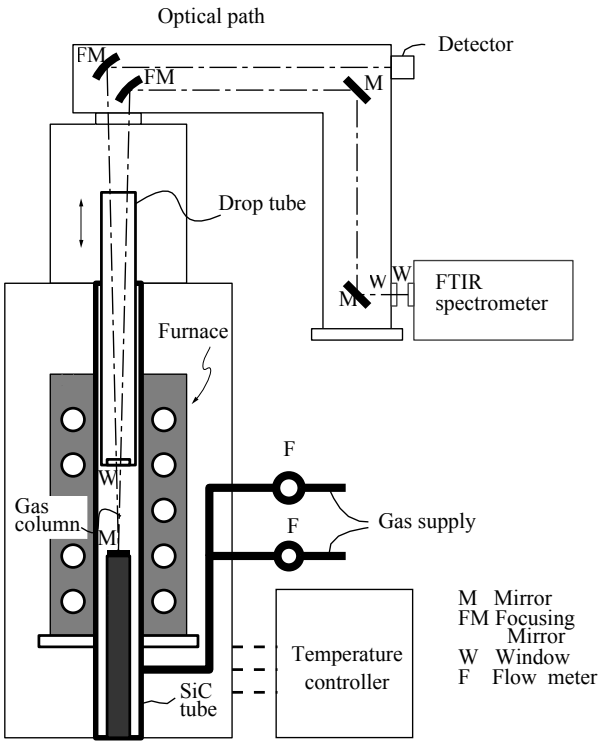

FIGURE 11-37
Schematic of a drop-tube transmissometer [63].

Data Correlation

The half-width of a typical spectral line in the infrared is on the order of $0.1\,\mathrm{cm}^{-1}$. To get a strong enough signal with a monochromator, any spectral measurement is by experimental necessity an average over several wavenumbers and, therefore, dozens or even hundreds of lines, unless an extremely monochromatic laser beam is employed. Thus, the measured transmissivity or (after subtracting from unity) absorptivity/emissivity is of the narrow band average type. Most FTIR measurements also fall into this category, although they generally have much better resolution than monochromators; resolutions better than $0.1\,\mathrm{cm}^{-1}$ are possible with high-end spectrometers. A correlation for the average absorption coefficient may be found by inverting equation (11.68) or equation (11.70), depending on whether the Elsasser or one of the statistical models is to be used, in either case yielding

$$\frac{S}{d} = \frac{S}{d}(\overline{\epsilon}_\eta, X, \gamma/d), \tag{11.189}$$

where the $\overline{\epsilon}_\eta$ and X (density or pressure path length) are measured quantities, and the width-to-spacing ratio must be determined independently. Most early measurements have assumed a constant γ/d for the entire band, in which case the width-to-spacing ratio can be obtained in a number of ways: (*i*) direct prediction of γ and d, (*ii*) using an independently determined band intensity, α, as the closing parameter, or (*iii*) finding a best fit for β (which is directly related to γ/d) in the exponential wide band model. With the recent advent of high-resolution databases it has been recognized that line spacing can vary dramatically across a band. The first narrow band correlation with variable β was done by Brosmer and Tien [200] for propylene, using Goody's model and least-mean-square-error fits.

In medium-resolution measurements of CO_2 Modest and Bharadwaj [63] correlated their experimental transmissivities to the Malkmus model through a least-mean-square-error fit. As an example the 2.7 μm bands of CO_2 at 300 and 1000 K are shown in Fig. 11-38 and compared with

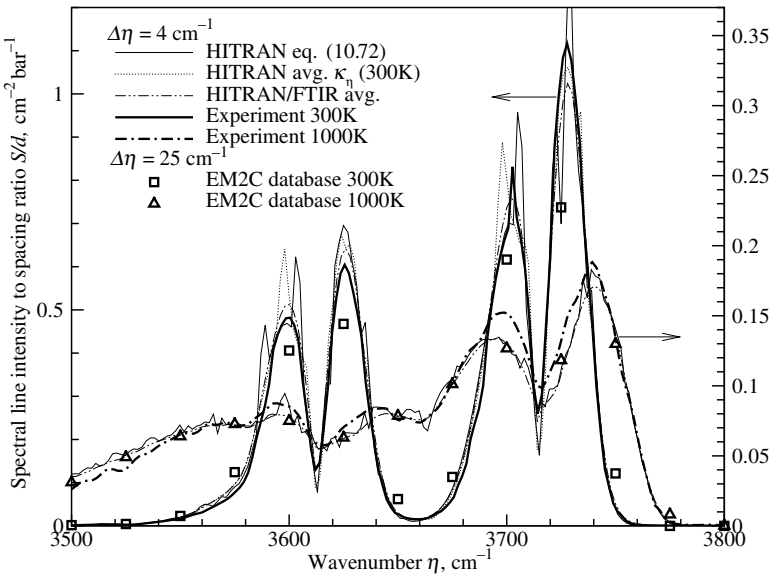

FIGURE 11-38
Narrow band correlation for the 2.7 μm band of carbon dioxide; experimental data from [63].

data obtained from the most accurate databases of the time, HITRAN 1996 [57] and EM2C [106]. CO_2 is seen to have two bands around 2.7 μm, one centered at 3615 cm^{-1}, the other at 3715 cm^{-1}. Agreement between experiment-based correlation and HITRAN 1996 is seen to be excellent except near the four S/d peaks, where the absorption coefficient is dominated by a few widely-spaced strong lines (about 1.8 cm^{-1} apart). This leads to a jagged appearance if the statistical definition for S/d is used, equation (11.82), and even if straight averaging over 4 cm^{-1} (equal to the experimental resolution) is carried out. The line labeled "HITRAN/FTIR avg." was obtained by averaging the absorption coefficient with the FTIR's instrument response function [201] as weight factor, which comes close to simulating the actual experiment. Results from the EM2C database are also shown for comparison. Because of its relatively low resolution of 25 cm^{-1} this database cannot capture the dual peaks, but agreement with experiment is excellent if the lower resolution is accounted for.

Measured spectral absorptivities may be integrated to determine total band absorptances. Plotting those band absorptances that fall into the logarithmic regime *vs.* XP_e on semilog paper gives a straight line whose slope is the band width parameter (cf. Table 11.2). Preparing a linear plot of A/P_e *vs.* $\sqrt{X/P_e}$ for data in the square root regime gives again a straight line, this time with $\sqrt{\alpha\omega\beta^*}$ as the slope (where $\beta^* = \beta/P_e = \pi\gamma/d$ is the width-to-spacing ratio for a dilute mixture, cf. Tables 11.2 and 11.3). Finally, total emissivity values may be calculated by substituting the measured total band absorptances into equation (11.171).

Experimental Errors

Most of the earlier gas property measurements were subject to considerable experimental errors, as listed by Edwards [184]: (1) inhomogeneity and uncertainty in the values of temperature, pressure, and composition, (2) scattering by mixing zones in nozzle seals and free jets, (3) reflection and scattering by optical windows, and/or (4) deterioration of the window material due to adsorption or "thermal runaway." In addition, essentially all data until the 1980s were poorly correlated, using fixed values for γ/d (across an entire vibration–rotation band), with a resulting correlational accuracy of ±20% at best. Only the more modern measurements by Phillips [107,108] and Bharadwaj et al. [63,65,66] apparently have experimental accuracies better than 5% and have been accurately correlated.

References

1. Edwards, D. K.: "Molecular gas band radiation," in *Advances in Heat Transfer*, vol. 12, Academic Press, New York, pp. 115–193, 1976.
2. Goody, R. M., and Y. L. Yung: *Atmospheric Radiation – Theoretical Basis*, 2nd ed., Oxford University Press, New York, 1989.
3. Tien, C. L.: "Thermal radiation properties of gases," in *Advances in Heat Transfer*, vol. 5, Academic Press, New York, pp. 253–324, 1968.
4. Taine, J., and A. Soufiani: "Gas IR radiative properties: From spectroscopic data to approximate models," in *Advances in Heat Transfer*, vol. 33, Academic Press, New York, pp. 295–414, 1999.
5. Rayleigh, L.: "On the light from the sky, its polarization and colour," *Philos. Mag.*, vol. 41, pp. 107–120, 274–279, 1871, (reprinted in *Scientific Papers by Lord Rayleigh*, vol. I: 1869–1881, No. 8, Dover, New York, 1964).
6. Langley, S. P.: "Experimental determination of wave-lengths in the invisible prismatic spectrum," *Mem. Natl. Acad. Sci.*, vol. 2, pp. 147–162, 1883.
7. Eddington, A. S.: *The Internal Constitution of the Stars*, Cambridge University Press, England, 1926, (also Dover Publications, New York, 1959).
8. Chandrasekhar, S.: *An Introduction to the Study of Stellar Structure*, University of Chicago Press, 1939.
9. Chandrasekhar, S.: *Radiative Transfer*, Dover Publications, New York, 1960, (originally published by Oxford University Press, London, 1950).
10. Paschen, F.: *Annalen der Physik und Chemie*, vol. 53, p. 334, 1894.
11. Hottel, H. C., and A. F. Sarofim: *Radiative Transfer*, McGraw-Hill, New York, 1967.
12. Hottel, H. C.: "Heat transmission by radiation from non-luminous gases," *Transactions of AIChE*, vol. 19, pp. 173–205, 1927.
13. Hottel, H. C., and H. G. Mangelsdorf: "Heat transmission by radiation from non-luminous gases II. Experimental study of carbon dioxide and water vapor," *Transactions of AIChE*, vol. 31, pp. 517–549, 1935.
14. Hottel, H. C., and V. C. Smith: "Radiation from non-lumunious flames," *Transactions of ASME, Journal of Heat Transfer*, vol. 57, pp. 463–470, 1935.
15. Hottel, H. C., and I. M. Stewart: "Space requirement for the combustion of pulverized coal," *Industrial Engineering Chemistry*, vol. 32, pp. 719–730, 1940.
16. Hottel, H. C., and R. B. Egbert: "The radiation of furnace gases," *Transactions of ASME, Journal of Heat Transfer*, vol. 63, pp. 297–307, 1941.
17. Hottel, H. C., and R. B. Egbert: "Radiant heat transmission from water vapor," *Transactions of AIChE*, vol. 38, pp. 531–565, 1942.
18. Hottel, H. C.: "Radiant heat transmission," in *Heat Transmission*, ed. W. H. McAdams, 3rd ed., ch. 4, McGraw-Hill, New York, 1954.
19. Hottel, H. C., and E. S. Cohen: "Radiant heat exchange in a gas-filled enclosure: Allowance for nonuniformity of gas temperature," *AIChE Journal*, vol. 4, pp. 3–14, 1958.
20. Penner, S. S.: *Quantitative Molecular Spectroscopy and Gas Emissivities*, Addison Wesley, Reading, MA, 1960.
21. Plass, G. N.: "Models for spectral band absorption," *Journal of the Optical Society of America*, vol. 48, no. 10, pp. 690–703, 1958.
22. Plass, G. N.: "Spectral emissivity of carbon dioxide from 1800–2500 cm^{-1}," *Journal of the Optical Society of America*, vol. 49, pp. 821–828, 1959.
23. Tien, C. L., and J. H. Lienhard: *Statistical Thermodynamics*, rev. ed., McGraw–Hill Inc., New York, 1978.
24. Davidson, N.: *Statistical Mechanics*, McGraw-Hill, New York, 1962, also Dover Publications 2003.
25. Heitler, W.: *The Quantum Theory of Radiation*, 3rd ed., Dover Publications, New York, 2010.
26. Griem, H. R.: *Spectral Line Broadening by Plasmas (Pure & Applied Physics)*, Academic Press, New York, 1974.
27. Salzmann, D.: *Atomic physics in hot plasmas*, Oxford University Press, New York, 1998.
28. Bethe, H. A., and E. E. Salpeter: *Quantum Mechanics of One- and Two-Electron Systems*, Academic Press, New York, 1957, also Dover Publications 2008.
29. Herzberg, G.: *Atomic Spectra and Atomic Structure*, 2nd ed., Van Nostrand, New York, 1944, also Dover Publications 2010.
30. Herzberg, G.: *Molecular Spectra and Molecular Structure, Vol. II: Infrared and Raman Spectra of Polyatomic Molecules*, Van Nostrand, Princeton, NJ, 1945.
31. Herzberg, G.: *Molecular Spectra and Molecular Structure, Vol. I: Spectra of Diatomic Molecules*, 2nd ed., Van Nostrand, Princeton, NJ, 1950, also Reitell Press 2007.
32. Rothman, L. S., I. E. Gordon, A. Barbe, D. C. Benner, P. F. Bernath, M. Birk, V. Boudon, L. R. Brown, A. Campargue, J.-P. Champion, K. Chance, L. H. Coudert, V. Dana, V. M. Devi, S. Fally, J.-M. Flaud, R. R. Gamache, A. Goldman, D. Jacquemart, I. Kleiner, N. Lacome, W. J. Lafferty, J.-Y. Mandin, S. T. Massie, S. N. Mikhailenko, C. E. Miller, N. Moazzen-Ahmadi, O. V. Naumenko, A. V. Nikitin, J. Orphal, V. I. Perevalov, A. Perrin, A. Predoi-Cross, C. P. Rinsland, M. Rotger, M. Simeckova, M. A. H. Smith, K. Sung, S. A. Tashkun, J. Tennyson, R. A. Toth, A. C. Vandaele, and J. V. Auwera: "The HITRAN 2008 molecular spectroscopic database," *Journal of Quantitative Spectroscopy and Radiative Transfer*, vol. 110, pp. 533–572, 2009.
33. Park, C.: "Stagnation-point radiation for Apollo 4," *Journal of Thermophysics and Heat Transfer*, vol. 18, no. 1, pp. 349–357, 2004.

34. Feldick, A. M., M. F. Modest, and D. A. Levin: "Closely coupled flowfield–radiation interactions during hypersonic reentry," *Journal of Thermophysics and Heat Transfer*, vol. 25, no. 4, pp. 481–492, 2011.
35. Niro, F., N. F. Boulet, and J.-M. Hartmann: "Spectra calculations in central and wing regions of CO_2 IR bands between 10 and 20 μm. I: model and laboratory measurements," *Journal of Quantitative Spectroscopy and Radiative Transfer*, vol. 88, pp. 483–498, 2004.
36. Farooq, A., J. B. Jeffries, and R. K. Hanson: "High-pressure measurements of CO_2 absorption near 2.7μm: Line mixing and finite duration collision effects," *Journal of Quantitative Spectroscopy and Radiative Transfer*, vol. 111, no. 7-8, pp. 949–960, 2010.
37. Breene, R. G.: *Theories of Spectral Line Shape*, John Wiley & Sons, New York, 1981.
38. Rosenmann, L., J.-M. Hartmann, M.-Y. Perrin, and J. Taine: "Accurate tabulation of IR and Raman CO_2 line broadening by CO_2, H_2O, N_2, O_2 in the 300–2400 K temperature range," *Applied Optics*, vol. 27, pp. 3902–3907, 1988.
39. Delaye, C., J.-M. Hartmann, and J. Taine: "Calculated tabulations of H_2O line broadening by H_2O, N_2, O_2 and CO_2 at high temperature," *Applied Optics*, vol. 28, pp. 5080–5087, 1989.
40. Hartmann, J.-M., L. Rosenmann, M.-Y. Perrin, and J. Taine: "Accurate calculated tabulations of CO line broadening by H_2O, N_2, O_2 and CO_2 in the 200–3000 K temperature range," *Applied Optics*, vol. 27, pp. 3063–3065, 1988.
41. Hartung-Chambers, L.: "Predicting radiative heat transfer in thermochemical nonequilibrium flow fields," *NASA Technical Memorandum 4564*, 1994.
42. Wang, A., and M. F. Modest: "Importance of combined Lorentz–Doppler broadening in high-temperature radiative heat transfer applications," *ASME Journal of Heat Transfer*, vol. 126, no. 5, pp. 858–861, 2004.
43. Drayson, S. R.: "Rapid computation of the Voigt profile," *Journal of Quantitative Spectroscopy and Radiative Transfer*, vol. 16, pp. 611–614, 1976.
44. Pierluissi, J. H., P. C. Vanderwood, and R. B. Gomez: "Fast calculational algorithm for the Voigt profile," *Journal of Quantitative Spectroscopy and Radiative Transfer*, vol. 18, pp. 555–558, 1977.
45. Hui, A. K., B. H. Armstrong, and A. A. Wray: "Rapid computation of the Voigt and complex error functions," *Journal of Quantitative Spectroscopy and Radiative Transfer*, vol. 19, p. 509, 1978.
46. Humlíček, J.: "Optimized computation of the Voigt and complex probability functions," *Journal of Quantitative Spectroscopy and Radiative Transfer*, vol. 27, p. 437, 1982.
47. Ladenburg, R., and F. Reiche: "Über selektive Absorption," *Annalen der Physik*, vol. 42, p. 181, 1913.
48. Lamet, J.-M., P. Rivière, M.-Y. Perrin, and A. Soufiani: "Narrow-band model for nonequilibrium air plasma radiation," *Journal of Quantitative Spectroscopy and Radiative Transfer*, vol. 111, no. 1, pp. 87–104, 2010.
49. Park, C.: *Nonequilibrium Hypersonic Aerothermodynamics*, Wiley, New York, 1990.
50. Johnston, C. O., B. R. Hollis, and K. A. Sutton: "Non-Boltzmann modeling for air shock-layer radiation at lunar-return conditions," *Journal of Spacecraft and Rockets*, vol. 45, no. 5, pp. 879–890, 2008.
51. Panesi, M., T. Magin, A. Bourdon, A. Biltel, and O. Chazot: "Fire II flight experiment analysis by means of a collisional-radiative model," *Journal of Thermophysics and Heat Transfer*, vol. 23, no. 2, pp. 236–248, 2009.
52. Bansal, A., and M. F. Modest: "Spectral modeling of radiative heat transfer in carbonaceous atmospheres using new k-distribution models," *49th AIAA Aerospace Sciences Conference, AIAA Paper 2011-0247*, 2011.
53. Capitelli, M.: *Nonequilibrium Vibrational Kinetics*, Topics in Current Physics, Springer Verlag, New York, 1986.
54. McClatchey, R. A., W. S. Benedict, S. A. Clough, D. E. Burch, K. Fox, L. S. Rothman, and J. S. Garing: "AFCRL atmospheric absorption line parameters compilation," Technical Report AFCRL-TR-0096, 1973.
55. Rothman, L. S., R. R. Gamache, A. Goldman, L. R. Brown, R. A. Toth, H. M. Pickett, R. L. Poynter, J.-M. Flaud, C. Camy-Peyret, A. Barbe, N. Husson, C. P. Rinsland, and M. A. H. Smith: "The HITRAN database: 1986 edition," *Applied Optics*, vol. 26, no. 19, pp. 4058–4097, 1987.
56. Rothman, L. S., R. R. Gamache, R. H. Tipping, C. P. Rinsland, M. A. H. Smith, D. C. Benner, V. M. Devi, J.-M. Flaud, C. Camy-Peyret, A. Perrin, A. Goldman, S. T. Massie, L. R. Brown, and R. A. Toth: "The HITRAN molecular database: Editions of 1991 and 1992," *Journal of Quantitative Spectroscopy and Radiative Transfer*, vol. 48, no. 5/6, pp. 469–507, 1992.
57. Rothman, L. S., C. P. Rinsland, A. Goldman, S. T. Massie, D. P. Edwards, J.-M. Flaud, A. Perrin, C. Camy-Peyret, V. Dana, J.-Y. Mandin, J. Schroeder, A. McCann, R. R. Gamache, R. B. Wattson, K. Yoshino, K. V. Chance, K. W. Jucks, L. R. Brown, V. Nemtchinov, and P. Varanasi: "The HITRAN molecular spectroscopic database and HAWKS (HITRAN atmospheric workstation): 1996 edition," *Journal of Quantitative Spectroscopy and Radiative Transfer*, vol. 60, pp. 665–710, 1998.
58. Rothman, L. S., A. Barbe, D. C. Benner, L. R. Brown, C. Camy-Peyret, M. R. Carleer, K. Chance, C. Clerbaux, V. Dana, V. M. Devi, A. Fayt, J.-M. Flaud, R. R. Gamache, A. Goldman, D. Jacquemart, K. W. Jucks, W. J. Lafferty, J.-Y. Mandin, S. Massie, V. Nemtchinov, D. Newnham, A. Perrin, C. P. Rinsland, J. Schroeder, K. M. Smith, M. A. H. Smith, K. Tang, R. A. Toth, J. V. Auwera, P. Varanasi, and K. Yoshino: "The HITRAN spectroscopic molecular database: Edition of 2000 including updates through 2001," *Journal of Quantitative Spectroscopy and Radiative Transfer*, vol. 82, no. 1–4, pp. 5–44, 2003.
59. Rothman, L. S., D. Jacquemart, A. Barbe, D. C. Benner, M. Birk, L. R. Brown, M. R. Carleer, C. Chackerian, Jr., K. Chance, L. H. Coudert, V. Dana, V. M. Devi, J.-M. Flaud, R. R. Gamache, A. Goldman, J.-M. Hartmann, K. W. Jucks, A. G. Maki, J.-Y. Mandin, S. T. Massie, J. Orphal, A. Perrin, C. P. Rinsland, M. A. H. Smith, J. Tennyson, R. N. Tolchenov, R. A. Toth, J. V. Auwera, P. Varanasi, and G. Wagner: "The HITRAN 2004 molecular spectroscopic database," *Journal of Quantitative Spectroscopy and Radiative Transfer*, vol. 96, pp. 139–204, 2005.

60. Scutaru, D., L. Rosenmann, and J. Taine: "Approximate band intensities of CO_2 hot bands at 2.7, 4.3 and 12 μm for high temperature and medium resolution applications," *Journal of Quantitative Spectroscopy and Radiative Transfer*, vol. 52, pp. 765–781, 1994.
61. Rivière, P., S. Langlois, A. Soufiani, and J. Taine: "An approximate data base of H_2O infrared lines for high temperature applications at low resolution. statistical narrow-band model parameters," *Journal of Quantitative Spectroscopy and Radiative Transfer*, vol. 53, pp. 221–234, 1995.
62. Rothman, L. S., R. B. Wattson, R. R. Gamache, J. Schroeder, and A. McCann: "HITRAN, HAWKS and HITEMP high temperature databases," *Proceedings of SPIE*, vol. 2471, pp. 105–111, 1995.
63. Modest, M. F., and S. P. Bharadwaj: "High-resolution, high-temperature transmissivity measurements and correlations for carbon dioxide–nitrogen mixtures," *Journal of Quantitative Spectroscopy and Radiative Transfer*, vol. 73, no. 2–5, pp. 329–338, 2002.
64. Fleckl, T., H. Jäger, and I. Obernberger: "Experimental verification of gas spectra calculated for high temperatures using the HITRAN/HITEMP database," *Journal of Physics D: Applied Physics*, vol. 35, no. 23, pp. 3138–3144, 2002.
65. Bharadwaj, S. P., M. F. Modest, and R. J. Riazzi: "Medium resolution transmission measurements of water vapor at high temperature," *ASME Journal of Heat Transfer*, vol. 128, pp. 374–381, 2006.
66. Bharadwaj, S. P., and M. F. Modest: "Medium resolution transmission measurements of CO_2 at high temperature – an update," *Journal of Quantitative Spectroscopy and Radiative Transfer*, vol. 103, pp. 146–155, 2007.
67. Tashkun, S. A., V. I. Perevalov, A. D. Bykov, N. N. Lavrentieva, and J.-L. Teffo: *Carbon Dioxide Spectroscopic databank (CDSD)*: available from ftp://ftp.iao.ru/pub/CDSD-1000, 2002.
68. Tashkun, S. A., and V. I. Perevalov: "Carbon dioxide spectroscopic databank (CDSD): updated and enlarged version for atmospheric applications," in *Tenth HITRAN conference, Cambridge, MA; Paper T2.3*, 2008, available from ftp://ftp.iao.ru/pub/CDSD-2008.
69. Tashkun, S. A., and V. I. Perevalov: "CDSD-4000: High-resolution, high-temperature carbon dioxide spectroscopic databank," *Journal of Quantitative Spectroscopy and Radiative Transfer*, vol. 112, no. 9, pp. 1403–1410, 2011, available from ftp://ftp.iao.ru/pub/CDSD-4000.
70. Partridge, H., and D. W. Schwenke: "The determination of an accurate isotope dependent potential energy surface for water from extensive *ab initio* calculations and experimental data," *J. Chem. Phys.*, vol. 106, no. 11, pp. 4618–4639, 1997.
71. Jørgensen, U. G., P. Jensen, G. O. Sørensen, and B. Aringer: "H_2O in stellar atmospheres," *Astron. Astrophys.*, vol. 372, pp. 249–259, 2001.
72. Barber, R. J., J. Tennyson, G. J. Harris, and R. N. Tolchenov: "A high-accuracy computed water line list," *Mon. Not. R. Astron. Soc.*, vol. 368, pp. 1087–1094, 2006.
73. Perez, P., A. Boischot, L. Ibgui, and A. Roblin: "A spectroscopic database for water vapor adapted to spectral properties at high temperature, and moderate resolution," *Journal of Quantitative Spectroscopy and Radiative Transfer*, vol. 103, no. 2, pp. 231–244, 2007.
74. Rothman, L. S., I. E. Gordon, R. J. Barber, H. Dothe, R. R. Gamache, A. Goldman, V. I. Perevalov, S. A. Tashkun, and J. Tennyson: "HITEMP, the high-temperature molecular spectroscopic database," *Journal of Quantitative Spectroscopy and Radiative Transfer*, vol. 111, no. 15, pp. 2139–2150, 2010.
75. Perrin, M.-Y., and A. Soufiani: "Approximate radiative properties of methane at high temperature," *Journal of Quantitative Spectroscopy and Radiative Transfer*, vol. 103, pp. 3–13, 2007.
76. Nicolet, W. E.: "User's manual for RAD/EQUIL/1973, a general purpose radiation transport program," *NASA CR-132470*, 1973.
77. Whiting, E., and C. Park: "Radiative heating at the stagnation point of the AFE vehicle," *NASA Technical Memorandum 102829*, pp. 395–418, 1990.
78. Whiting, E., C. Park, Y. Liu, J. Arnold, and J. Paterson: "NEQAIR96, nonequilibrium and equilibrium radiative transport and spectra program: User's manual," NASA reference publication 1389, NASA/Ames Research Center, Moffett Field, CA 94035-1000, December 1996.
79. Laux, C. O.: "Optical diagnostics and radiative emission of air plasmas," Ph.D. thesis, Stanford University, Stanford, CA, 1993.
80. Laux, C. O.: "Radiation and nonequilibrium collisional-radiative models," in *Physico-Chemical Modeling of High Enthalpy and Plasma Flows*, eds. D. Fletcher, J.-M. Charbonnier, G. S. R. Sarma, and T. Magin, von Karman Institute Lecture Series 2002-07, Rhode-Saint-Genèse, Belgium, 2002, available from http://specair-radiation.net/.
81. Fujita, K., and T. Abe: "SPRADIAN, structured package for radiation analysis: Theory and application," Technical Report Report No. 669, Japanese Aerospace Exploration Agency (JAXA), 1997.
82. Hyun, S. Y., C. Park, K. S. Chang, H. Katsurayama, K. Fujita, and T. Abe: "User's manual: Program SPRADIAN07 (structured package for radiation analysis 2007)," Technical report, 2007.
83. Johnston, C. O., B. R. Hollis, and K. A. Sutton: "Spectrum modeling for air shock-layer radiation at lunar-return conditions," *Journal of Spacecraft and Rockets*, vol. 45, no. 5, pp. 865–878, 2008.
84. Ralchenko, Y., A. E. Kramida, and J. Reader: "NIST atomic spectra database, version 4," National Institute of Standards and Technology (NIST), Physics Lab, 2010, available from http://www.nist.gov/pml/data/asd.cfm.
85. The Opacity Project Team: "The opacity project, vol. 1," Technical report, Bristol and Philadelphia: Intitute of Physics Publishing, 1995.
86. Cunto, W., C. Mendoza, F. Ochsenbein, and C. J. Zeippen: "TOPbase at the CDS," *Astronomy and Astrophysics*, vol. 275, pp. L5–L8, 1993.

87. Sohn, I., A. Bansal, D. A. Levin, and M. F. Modest: "Advanced radiation calculations of hypersonic reentry flows using efficient databasing schemes," *Journal of Thermophysics and Heat Transfer*, vol. 24, no. 3, pp. 623–637, 2010.
88. Bansal, A., A. M. Feldick, and M. F. Modest: "Simulation of hypersonic flow and radiation over a Mars reentry vehicle using OpenFOAM," *50th AIAA Aerospace Sciences Conference, Paper No. AIAA-2012-0650*, 2012.
89. Schenker, G. N., and B. Keller: "Line-by-line calculations of the absorption of infrared radiation by water vapor in a box-shaped enclosure filled with humid air," *International Journal of Heat and Mass Transfer*, vol. 38, pp. 3127–3134, 1995.
90. Chauveau, S., C. Deron, M.-Y. Perrin, P. Rivière, and A. Soufiani: "Radiative transfer in LTE air plasmas for temperatures up to 15,000 K," *Journal of Quantitative Spectroscopy and Radiative Transfer*, vol. 77, pp. 113–130, 2003.
91. Beier, K., and E. Lindermeir: "Comparison of line-by-line and molecular band IR modeling of high altitude missile plume," *Journal of Quantitative Spectroscopy and Radiative Transfer*, vol. 105, pp. 111–127, 2007.
92. Taine, J.: "A line-by-line calculation of low-resolution radiative properties of CO_2–CO–transparent nonisothermal gases mixtures up to 3000 K," *Journal of Quantitative Spectroscopy and Radiative Transfer*, vol. 30, no. 4, pp. 371–379, 1983.
93. Hartmann, J.-M., R. Levi Di Leon, and J. Taine: "Line-by-line and narrow-band statistical model calculations for H_2O," *Journal of Quantitative Spectroscopy and Radiative Transfer*, vol. 32, no. 2, pp. 119–127, 1984.
94. Zhang, H., and M. F. Modest: "Multi-group full-spectrum *k*-distribution database for water vapor mixtures in radiative transfer calculations," *International Journal of Heat and Mass Transfer*, vol. 46, no. 19, pp. 3593–3603, 2003.
95. Solovjov, V. P., and B. W. Webb: "The cumulative wavenumber method for modeling radiative transfer in gas mixtures with soot," *Journal of Quantitative Spectroscopy and Radiative Transfer*, vol. 93(1-3), pp. 273–287, 2005.
96. André, F., and R. Vaillon: "The k-moment method for modeling the blackbody weighted transmission function for narrow and wide band radiative properties of gases," *Journal of Quantitative Spectroscopy and Radiative Transfer*, vol. 108, no. 1, pp. 1–16, 2007.
97. Elsasser, W. M.: *Heat transfer by infrared radiation in the atmosphere*, Harvard University Press, Cambridge, MA, 1943.
98. Abramowitz, M., and I. A. Stegun (eds.): *Handbook of Mathematical Functions*, Dover Publications, New York, 1965.
99. Goody, R. M.: "A statistical model for water-vapour absorption," *Quart. J. R. Meteorol. Soc.*, vol. 78, p. 165, 1952.
100. Godson, W. L.: "The computation of infrared transmission by atmospheric water vapour: I and II," *Journal of Meteorology*, vol. 12, p. 272 and 533, 1955.
101. Malkmus, W.: "Random Lorentz band model with exponential-tailed S^{-1} line-intensity distribution function," *Journal of the Optical Society of America*, vol. 57, no. 3, pp. 323–329, 1967.
102. Grosshandler, W. L.: "Radiative transfer in nonhomogeneous gases: A simplified approach," *International Journal of Heat and Mass Transfer*, vol. 23, pp. 1447–1457, 1980.
103. Grosshandler, W. L.: "RADCAL: a narrow-band model for radiation calculations in a combustion environment," Technical Report NIST Technical Note 1402, National Institute of Standards and Technology, 1993.
104. Soufiani, A., J.-M. Hartmann, and J. Taine: "Validity of band-model calculations for CO_2 and H_2O applied to radiative properties and conductive–radiative transfer," *Journal of Quantitative Spectroscopy and Radiative Transfer*, vol. 33, pp. 243–257, 1985.
105. Lacis, A. A., and V. Oinas: "A description of the correlated-*k* distribution method for modeling nongray gaseous absorption, thermal emission, and multiple scattering in vertically inhomogeneous atmospheres," *Journal of Geophysical Research*, vol. 96, no. D5, pp. 9027–9063, 1991.
106. Soufiani, A., and J. Taine: "High temperature gas radiative property parameters of statistical narrow-band model for H_2O, CO_2 and CO, and correlated-*k* model for H_2O and CO_2," *International Journal of Heat and Mass Transfer*, vol. 40, no. 4, pp. 987–991, 1997.
107. Phillips, W. J.: "Band model parameters of the 2.7 μm band of H_2O," *Journal of Quantitative Spectroscopy and Radiative Transfer*, vol. 43, 1990.
108. Phillips, W. J.: "Band model parameters of the 4.3 μm CO_2 band in the 300–1000 K temperature range," *Journal of Quantitative Spectroscopy and Radiative Transfer*, vol. 48, 1992.
109. Bharadwaj, S. P., and M. F. Modest: "A multiscale Malkmus model for treatment of inhomogeneous gas paths," *International Journal of Thermal Sciences*, vol. 46, pp. 479–490, 2007.
110. Rivière, P., and A. Soufiani: "Generalized Malkmus line intensity distribution for CO_2 infrared radiation in Doppler broadening regime," *Journal of Quantitative Spectroscopy and Radiative Transfer*, vol. 112, no. 3, pp. 475–485, 2011.
111. Liu, F., G. J. Smallwood, and O. L. Gülder: "Application of the statistical narrow-band correlated-*k* method to non-grey gas radiation in CO_2 mixtures: approximate treatments of overlapping bands," *Journal of Quantitative Spectroscopy and Radiative Transfer*, vol. 68, pp. 401–417, 2001.
112. Young, S. J.: "Nonisothermal band model theory," *Journal of Quantitative Spectroscopy and Radiative Transfer*, vol. 18, pp. 1–28, 1977.
113. Lindquist, G. H., and F. S. Simmons: "A band model formulation for very non uniform paths," *Journal of Quantitative Spectroscopy and Radiative Transfer*, vol. 12, pp. 807–820, 1972.

114. Arking, A., and K. Grossman: "The influence of line shape and band structure on temperatures in planetary atmospheres," *Journal of the Atmospheric Sciences*, vol. 29, pp. 937–949, 1972.
115. Kondratyev, K. Y.: *Radiation in the Atmosphere*, Academic Press, New York, 1969.
116. Goody, R. M., R. West, L. Chen, and D. Crisp: "The correlated *k* method for radiation calculations in nonhomogeneous atmospheres," *Journal of Quantitative Spectroscopy and Radiative Transfer*, vol. 42, pp. 539–550, 1989.
117. Fu, Q., and K. N. Liou: "On the correlated *k*-distribution method for radiative transfer in nonhomogeneous atmospheres," *Journal of the Atmospheric Sciences*, vol. 49, no. 22, pp. 2139–2156, 1992.
118. Rivière, P., A. Soufiani, and J. Taine: "Correlated-*k* and fictitious gas methods for H_2O near 2.7 μm," *Journal of Quantitative Spectroscopy and Radiative Transfer*, vol. 48, pp. 187–203, 1992.
119. Rivière, P., D. Scutaru, A. Soufiani, and J. Taine: "A new ck data base suitable from 300 to 2500 K for spectrally correlated radiative transfer in CO_2–H_2O transparent gas mixtures," in *Tenth International Heat Transfer Conference*, Taylor & Francis, pp. 129–134, 1994.
120. Rivière, P., A. Soufiani, and J. Taine: "Correlated-*k* and fictitious gas model for H_2O infrared radiation in the Voigt regime," *Journal of Quantitative Spectroscopy and Radiative Transfer*, vol. 53, pp. 335–346, 1995.
121. Domoto, G. A.: "Frequency integration for radiative transfer problems involving homogeneous non-gray gases: The inverse transmission function," *Journal of Quantitative Spectroscopy and Radiative Transfer*, vol. 14, pp. 935–942, 1974.
122. Wang, A., and M. F. Modest: "High-accuracy, compact database of narrow-band *k*-distributions for water vapor and carbon dioxide," *Journal of Quantitative Spectroscopy and Radiative Transfer*, vol. 93, pp. 245–261, 2005.
123. Solovjov, V. P., and B. W. Webb: "SLW modeling of radiative transfer in multicomponent gas mixtures," *Journal of Quantitative Spectroscopy and Radiative Transfer*, vol. 65, pp. 655–672, 2000.
124. Modest, M. F., and R. J. Riazzi: "Assembly of full-spectrum *k*-distributions from a narrow-band database; effects of mixing gases, gases and nongray absorbing particles, and mixtures with nongray scatterers in nongray enclosures," *Journal of Quantitative Spectroscopy and Radiative Transfer*, vol. 90, no. 2, pp. 169–189, 2005.
125. Pal, G., and M. F. Modest: "*k*-distribution methods for radiation calculations in high pressure combustion," *50th Aerospace Sciences Meeting, Paper No. AIAA-2012-0529*, 2012.
126. Modest, M. F., and H. Zhang: "The full-spectrum correlated-*k* distribution for thermal radiation from molecular gas–particulate mixtures," *ASME Journal of Heat Transfer*, vol. 124, no. 1, pp. 30–38, 2002.
127. Modest, M. F.: "Narrow-band and full-spectrum *k*-distributions for radiative heat transfer—correlated-*k* vs. scaling approximation," *Journal of Quantitative Spectroscopy and Radiative Transfer*, vol. 76, no. 1, pp. 69–83, 2003.
128. Hsieh, T. C., and R. Greif: "Theoretical determination of the absorption coefficient and the total band absorptance including a specific application to carbon monoxide," *International Journal of Heat and Mass Transfer*, vol. 15, pp. 1477–1487, 1972.
129. Chu, K. H., and R. Greif: "Theoretical determination of band absorption for nonrigid rotation with applications to CO, NO, N_2O, and CO_2," *ASME Journal of Heat Transfer*, vol. 100, pp. 230–234, 1978.
130. Edwards, D. K., and W. A. Menard: "Comparison of models for correlation of total band absorption," *Applied Optics*, vol. 3, pp. 621–625, 1964.
131. Edwards, D. K., L. K. Glassen, W. C. Hauser, and J. S. Tuchscher: "Radiation heat transfer in nonisothermal nongray gases," *ASME Journal of Heat Transfer*, vol. 89, pp. 219–229, 1967.
132. Weiner, M. M., and D. K. Edwards: "Non-isothermal gas radiation in superposed vibration–rotation bands," *Journal of Quantitative Spectroscopy and Radiative Transfer*, vol. 8, pp. 1171–1183, 1968.
133. Edwards, D. K.: "Radiative transfer characteristics of materials," *ASME Journal of Heat Transfer*, vol. 91, pp. 1–15, 1969.
134. Edwards, D. K., and A. Balakrishnan: "Thermal radiation by combustion gases," *International Journal of Heat and Mass Transfer*, vol. 16, pp. 25–40, 1973.
135. Felske, J. D., and C. L. Tien: "A theoretical closed form expression for the total band absorptance of infrared-radiating gases," *ASME Journal of Heat Transfer*, vol. 96, pp. 155–158, 1974.
136. Wang, W. C.: "An analytical expression for the total band absorptance of infrared-radiating gases," *Journal of Quantitative Spectroscopy and Radiative Transfer*, vol. 29, pp. 279–281, 1983.
137. Modak, A. T.: "Exponential wide band parameters for the pure rotational band of water vapor," *Journal of Quantitative Spectroscopy and Radiative Transfer*, vol. 21, pp. 131–142, 1979.
138. Edwards, D. K., and W. A. Menard: "Correlations for absorption by methane and carbon dioxide gases," *Applied Optics*, vol. 3, pp. 847–852, 1964.
139. Edwards, D. K., and W. A. Menard: "Correlation of absorption by water vapor at temperatures from 300 K to 1100 K," *Applied Optics*, vol. 4, pp. 715–721, 1965.
140. Edwards, D. K., B. J. Flornes, L. K. Glassen, and W. Sun: "Comparison of models for correlation of total band absorption," *Applied Optics*, vol. 3, pp. 621–625, 1964.
141. Brosmer, M. A., and C. L. Tien: "Infrared radiation properties of methane at elevated temperatures," *Journal of Quantitative Spectroscopy and Radiative Transfer*, vol. 33, no. 5, pp. 521–532, 1985.
142. Fuss, S. P., O. A. Ezekoye, and M. J. Hall: "The absorptance of infrared radiation by methane at elevated temperatures," *ASME Journal of Heat Transfer*, pp. 918–923, 1996.
143. Edwards, D. K.: "Absorption of radiation by carbon monoxide gas according to the exponential wide-band model," *Applied Optics*, vol. 4, no. 10, pp. 1352–1353, 1965.

144. Abu-Romia, M. M., and C. L. Tien: "Measurements and correlations of infrared radiation of carbon monoxide at elevated temperatures," *Journal of Quantitative Spectroscopy and Radiative Transfer*, vol. 6, pp. 143–167, 1966.
145. Abu-Romia, M. M., and C. L. Tien: "Appropriate mean absorption coefficients for infrared radiation of gases," *ASME Journal of Heat Transfer*, vol. 89C, pp. 321–327, 1967.
146. Chan, S. H., and C. L. Tien: "Infrared radiation properties of sulfur dioxide," *ASME Journal of Heat Transfer*, vol. 93, pp. 172–177, 1971.
147. Tien, C. L.: "Band and total emissivity of ammonia," *International Journal of Heat and Mass Transfer*, vol. 16, pp. 856–857, 1973.
148. Green, R. M., and C. L. Tien: "Infrared radiation properties of nitric oxide at elevated temperatures," *Journal of Quantitative Spectroscopy and Radiative Transfer*, vol. 10, pp. 805–817, 1970.
149. Tien, C. L., M. F. Modest, and C. R. McCreight: "Infrared radiation properties of nitrous oxide," *Journal of Quantitative Spectroscopy and Radiative Transfer*, vol. 12, pp. 267–277, 1972.
150. Brosmer, M. A., and C. L. Tien: "Thermal radiation properties of acetylene," *ASME Journal of Heat Transfer*, vol. 107, pp. 943–948, 1985.
151. Lallemant, N., and R. Weber: "A computationally efficient procedure for calculating gas radiative properties using the exponential wide band model," *International Journal of Heat and Mass Transfer*, vol. 39, pp. 3273–3286, 1996.
152. Tien, C. L., and J. E. Lowder: "A correlation for total band absorption of radiating gases," *International Journal of Heat and Mass Transfer*, vol. 9, pp. 698–701, 1966.
153. Cess, R. D., and S. N. Tiwari: "Infrared radiative energy transfer in gases," in *Advances in Heat Transfer*, vol. 8, Academic Press, New York, pp. 229–283, 1972.
154. Tiwari, S. N.: "Models for infrared atmospheric radiation," in *Advances in Geophysics*, vol. 20, Academic Press, New York, 1978.
155. Chan, S. H., and C. L. Tien: "Total band absorptance of non-isothermal infrared-radiating gases," *Journal of Quantitative Spectroscopy and Radiative Transfer*, vol. 9, pp. 1261–1271, 1969.
156. Cess, R. D., and L. S. Wang: "A band absorptance formulation for non-isothermal gaseous radiation," *International Journal of Heat and Mass Transfer*, vol. 13, pp. 547–555, 1970.
157. Edwards, D. K., and S. J. Morizumi: "Scaling vibration–rotation band parameters for nonhomogeneous gas radiation," *Journal of Quantitative Spectroscopy and Radiative Transfer*, vol. 10, pp. 175–188, 1970.
158. Felske, J. D., and C. L. Tien: "Infrared radiation from non-homogeneous gas mixtures having overlapping bands," *Journal of Quantitative Spectroscopy and Radiative Transfer*, vol. 14, pp. 35–48, 1974.
159. Wang, W. C., and G. Y. Shi: "Total band absorptance and *k*-distribution function for atmospheric gases," *Journal of Quantitative Spectroscopy and Radiative Transfer*, vol. 39, pp. 387–398, 1988.
160. Marin, O., and R. O. Buckius: "Wide band correlated-*k* method applied to absorbing, emitting and scattering media," *Journal of Thermophysics and Heat Transfer*, vol. 10, pp. 364–371, 1996.
161. Marin, O., and R. O. Buckius: "A model of the cumulative distribution function for wide band radiative properties," *Journal of Quantitative Spectroscopy and Radiative Transfer*, vol. 59, pp. 671–685, 1998.
162. Marin, O., and R. O. Buckius: "A simplified wide band model of the cumulative distribution function for water vapor," *International Journal of Heat and Mass Transfer*, vol. 41, pp. 2877–2892, 1998.
163. Marin, O., and R. O. Buckius: "A simplified wide band model of the cumulative distribution function for carbon dioxide," *International Journal of Heat and Mass Transfer*, vol. 41, pp. 3881–3897, 1998.
164. Lee, P. Y. C., G. D. Raithby, and K. G. T. Hollands: "The "reordering" concept of the absorption coefficient for modelling nongray gases," in *Radiative Heat Transfer: Current Research*, vol. HTD-276, ASME, pp. 21–30, 1994.
165. Lee, P. Y. C., K. G. T. Hollands, and G. D. Raithby: "Reordering the absorption coefficient within the wide band for predicting gaseous radiant exchange," *ASME Journal of Heat Transfer*, vol. 118, no. 2, pp. 394–400, 1996.
166. Parthasarathy, G., J. C. Chai, and S. V. Patankar: "A simple approach to nongray gas modeling," *Numerical Heat Transfer*, vol. 29, pp. 394–400, 1996.
167. Denison, M. K., and W. A. Fiveland: "A correlation for the reordered wave number of the wideband absorptance of radiating gases," *ASME Journal of Heat Transfer*, vol. 119, pp. 853–856, 1997.
168. Ströhle, J., and P. J. Coelho: "On the application of the exponential wide band model to the calculation of radiative heat transfer in one- and two-dimensional enclosures," *International Journal of Heat and Mass Transfer*, vol. 45, pp. 2129–2139, 2002.
169. Leckner, B.: "Spectral and total emissivity of water vapor and carbon dioxide," *Combustion and Flame*, vol. 19, pp. 33–48, 1972.
170. Boynton, F. P., and C. B. Ludwig: "Total emissivity of hot water vapor – II, semi-empirical charts deduced from long-path spectral data," *International Journal of Heat and Mass Transfer*, vol. 14, pp. 963–973, 1971.
171. Ludwig, C. B., W. Malkmus, J. E. Reardon, and J. A. L. Thomson: "Handbook of infrared radiation from combustion gases," Technical Report SP-3080, NASA, 1973.
172. Sarofim, A. F., I. H. Farag, and H. C. Hottel: "Radiative heat transmission from nonluminous gases. Computational study of the emissivities of carbon dioxide," ASME paper no. 78-HT-55, 1978.
173. Zhang, H., and M. F. Modest: "Evaluation of the Planck-mean absorption coefficients from HITRAN and HITEMP databases," *Journal of Quantitative Spectroscopy and Radiative Transfer*, vol. 73, no. 6, pp. 649–653, 2002.
174. Cess, R. D., and P. Mighdoll: "Modified Planck mean coefficients for optically thin gaseous radiation," *International Journal of Heat and Mass Transfer*, vol. 10, pp. 1291–1292, 1967.

175. Tien, C. L., and W. H. Giedt: "Experimental determination of infrared absorption of high-temperature gases," in *Advances in Thermophysical Properties at Extreme Temperatures and Pressures*, ASME, pp. 167–173, 1965.
176. Tanner, D. B., and R. P. McCall: "Source of a problem with Fourier transform spectroscopy," *Applied Optics*, vol. 23, no. 14, pp. 2363–2368, 1994.
177. Tripp, C. P., and R. A. McFarlane: "Discussion of the stray light rejection efficiency of FT-IR spectrometers: The effects of sample emission on FT-IR spectra," *Applied Spectroscopy*, vol. 48, no. 9, pp. 1138–1142, 1994.
178. Anderson, R. J., and P. R. Griffiths: "Determination of rotational temperatures of diatomic molecules from absorption spectra measured at moderate resolution," *Journal of Quantitative Spectroscopy and Radiative Transfer*, vol. 17, pp. 393–401, 1977.
179. Gross, L. A., and P. R. Griffiths: "Temperature estimation of carbon dioxide by infrared absorption spectrometry at medium resolution," *Journal of Quantitative Spectroscopy and Radiative Transfer*, vol. 39, no. 2, pp. 131–138, 1988.
180. Medvecz, P. J., K. M. Nichols, D. T. Clay, and R. Atalla: "Determination of gas temperatures at 295–1273 K using CO vibrational–rotational absorption spectra recorded with an FT-IR spectrometer," *Applied Spectroscopy*, vol. 45, no. 8, pp. 1350–1359, 1991.
181. Goldstein, R. J.: "Measurements of infrared absorption by water vapor at temperatures to 1000 K," *Journal of Quantitative Spectroscopy and Radiative Transfer*, vol. 4, pp. 343–352, 1964.
182. Oppenheim, U. P., and A. Goldman: "Spectral emissivity of water vapor at 1200 K," in *Tenth Symposium (International) on Combustion*, The Combustion Institute, pp. 185–188, 1965.
183. Abu-Romia, M. M., and C. L. Tien: "Spectral and integrated intensity of CO fundamental band at elevated temperatures," *International Journal of Heat and Mass Transfer*, vol. 10, pp. 1779–1784, 1967.
184. Edwards, D. K.: "Thermal radiation measurements," in *Measurements in Heat Transfer*, eds. E. R. G. Eckert and R. J. Goldstein, ch. 10, Hemisphere, Washington, DC, 1976.
185. Eckert, E. R. G.: "Messung der Gesamtstrahlung von Wasserdampf und Kohlensäure in Mischung mit nichtstrahlenden Gasen bei Temperaturen bis 1300°C," *VDI Forschungshefte*, vol. 387, pp. 1–20, 1937.
186. Bevans, J. T., R. V. Dunkle, D. K. Edwards, J. T. Gier, L. L. Levenson, and A. K. Oppenheim: "Apparatus for the determination of the band absorption of gases at elevated pressures and temperatures," *Journal of the Optical Society of America*, vol. 50, pp. 130–136, 1960.
187. Edwards, D. K.: "Absorption by infrared bands of carbon dioxide gas at elevated pressures and temperatures," *Journal of the Optical Society of America*, vol. 50, pp. 617–626, 1960.
188. Ferriso, C. C., and C. B. Ludwig: "Spectral emissivities and integrated intensities of the 2.7 μm H_2O band between 530 and 2200 K," *Journal of Quantitative Spectroscopy and Radiative Transfer*, vol. 4, pp. 215–227, 1964.
189. Postlethwait, M. A., K. K. Sikka, M. F. Modest, and J. R. Hellmann: "High temperature normal spectral emittance of silicon carbide based materials," *Journal of Thermophysics and Heat Transfer*, vol. 8, no. 3, pp. 412–418, 1994.
190. Postlethwait, M. A., M. F. Modest, M. A. Botch, and J. R. Hellmann: "Normal spectral emittance of alumina based materials," in *Radiative Heat Transfer: Current Research; 6th AIAA/ASME Thermophysics and Heat Transfer Conference*, vol. HTD-276, ASME, pp. 73–77, 1994.
191. Challingsworth, M. J., J. R. Hellmann, and M. F. Modest: "Tailoring the spectral emittance of rare earth oxides via doping," *Proceedings of the 97th Annual Meeting and Exposition of the American Ceramic Society*, 1995.
192. Richardson, H. H., V. W. Pabst, and J. A. Butcher: "A novel infrared spectrometer using a linear array detector," *Applied Spectroscopy*, vol. 44, no. 5, pp. 822–825, 1990.
193. Alawi, S. M., T. Krug, and H. H. Richardson: "Characterization and application of an infrared linear array spectrometer for time-resolved infrared spectroscopy," *Applied Spectroscopy*, vol. 47, no. 10, pp. 1626–1630, 1993.
194. Keltner, Z., K. Kayima, A. Lanzarotta, L. Lavalle, M. Canepa, A. E. Dowrey, G. M. Story, C. Marcott, and A. J. Sommer: "Prism-based infrared spectrographs using modern-day detectors," *Applied Spectroscopy*, vol. 61, no. 9, pp. 909–915, 2007.
195. Ji, J., J. P. Gore, Y. R. Sivathanu, and J. Lim: "Fast infrared array spectrometer with a thermoelectrically cooled 160-element pbse detector," *Review of Scientific Instruments*, vol. 75, no. 2, pp. 333–339, 2004.
196. Barlow, R. S.: *International Workshop on Measurement and Computation of Turbulent Nonpremixed Flames (TNF)* website: http://www.sandia.gov/TNF/abstract.html.
197. Zheng, Y., R. S. Barlow, and J. P. Gore: "Measurements and calculations of spectral radiation intensities for turbulent non-premixed and partially premixed flames," *ASME Journal of Heat Transfer*, vol. 125, pp. 678–686, 2003.
198. Zheng, Y., R. S. Barlow, and J. P. Gore: "Spectral radiation properties of partially premixed turbulent flames," *ASME Journal of Heat Transfer*, vol. 125, pp. 1065–1073, 2003.
199. Zheng, Y., and J. P. Gore: "Measurements and inverse calculations of spectral radiation intensities of a turbulent ethylene/air jet flame," in *Thirtieth Symposium (International) on Combustion*, The Combustion Institute, pp. 727–734, 2005.
200. Brosmer, M. A., and C. L. Tien: "Thermal radiation properties of propylene," *Combustion Science and Technology*, vol. 48, pp. 163–175, 1986.
201. Griffiths, P. R., and J. A. de Haseth: *Fourier Transform Infrared Spectrometry*, vol. 83 of *Chemical Analysis*, John Wiley & Sons, New York, 1986.

Problems

11.1 Estimate the eigenfrequency for vibration, ν_e, for a CO molecule.

11.2 A certain gas at 1 bar pressure has a molecular mass of $m = 10^{-22}$ g and a diameter of $D = 5 \times 10^{-8}$ cm. At what temperature would Doppler and collision broadening result in identical broadening widths for a line at a wavenumber of 4000 cm^{-1}?

11.3 Water vapor is known to have spectral lines in the vicinity of $\lambda = 1.38\,\mu$m. Consider a single, broadened spectral line centered at $\lambda_0 = 1.33\,\mu$m. If the water vapor is at a pressure of 0.1 atm and a temperature of 1000 K, what would you expect to be the main cause for broadening? Over what range of wavenumbers would you expect the line to be appreciable, i.e., over what range is the absorption coefficient at least 1% of its value at the line center?

11.4 Compute the half-width for a spectral line of CO_2 at 2.8 μm for both Doppler and collision broadening as a function of pressure and temperature. Find the temperature as a function of pressure for which both broadening phenomena result in the same half-width. (Note: The effective diameter of the CO_2 molecule is 4.0×10^{-8} cm.)

11.5 Methane is known to have a vibration-rotation band around 1.7 μm. It is desired to measure the Doppler half-width of a spectral line in that band at room temperature ($T = 300$ K). In order to make sure that collision broadening is negligible, the pressure of the CH_4 is adjusted so that the expected collision half-width is only 1/10 of the Doppler half-width. What is this pressure? (For methane: $D = 0.381$ nm.)

11.6 Repeat Problem 11.4 for CO at a spectral location of 4.8 μm (Note: The effective diameter of the CO molecule is 3.4×10^{-8} cm.)

11.7 A certain gas has two important vibration–rotation bands centered at 4 μm and 10 μm. Measurements of spectral lines in the 4 μm band (taken at 300 K and 1 bar = 10^5 N/m^2) indicate a half-width of $\gamma_\eta = 0.5\,\text{cm}^{-1}$. Predict the half-width in the 10 μm band for the gas at 500 K, 3 bar. (The diameter of the gas molecules is known to be between 5 Å $< D <$ 40 Å.)

11.8 It is desired to measure the volume fraction of CO in a hot gas by measuring the transmissivity of a 10 cm long column, using a blackbody source and a detector responsive around 4.7 μm. The conditions in the column are 1000 K, 1 atm, and properties for CO around 4.7 μm are known to be $S = 0.8\,\text{cm}^{-2}\text{atm}^{-1}$, $\gamma = 0.02\,\text{cm}^{-1}$, and $d = 0.05\,\text{cm}^{-1}$. Give an expression relating measured transmissivity to CO volume fraction.

11.9 A polyatomic gas has an absorption band in the infrared. For a certain small wavelength range the following is known:

Average line half-width: $0.04\,\text{cm}^{-1}$,
Average integrated absorption coefficient: $2.0 \times 10^{-4}\,\text{cm}^{-1}/(\text{g/m}^2)$,
Average line spacing: $0.25\,\text{cm}^{-1}$,
The density of the gas at STP is $3 \times 10^{-3}\,\text{g/cm}^3$.

For a 50 cm thick gas layer at 500 K and 1 atm calculate the mean spectral emissivity for this wavelength range using

(*a*) the Elsasser model,

(*b*) the statistical model.

Which result can be expected to be more accurate?

11.10 Consider a gas for which the semistatistical model is applicable, i.e., $\bar{\epsilon}_\eta = 1 - \exp(-W_\eta/d)$. To predict $\bar{\epsilon}_\eta$ for arbitrary situations, a band-averaged (or constant) value for γ_η/d must be known. Experimentally available are values for $\alpha = \int_{\Delta\eta} (S_\eta/d)\,d\eta$ and $\bar{\epsilon}_\eta = \bar{\epsilon}_\eta(\eta)$ (for optically thick situations) for given p_e and T. It is also known that

$$\frac{\gamma_\eta}{d} \simeq \left(\frac{\gamma_\eta}{d}\right)_0 p_e \left(\frac{T_0}{T}\right)^{1/2}.$$

Outline how an average value for $(\gamma_\eta/d)_0$ can be found.

11.11 The following is known for a gas mixture at 600 K and 2 atm total pressure and in the vicinity of a certain spectral position: The gas consists of 80% (by volume) N_2 and 20% of a diatomic absorbing

gas with a molecular weight of 20 g/mol, a mean line half-width $\gamma = 0.01\,\text{cm}^{-1}$, a mean line spacing of $d = 0.1\,\text{cm}^{-1}$, and a mean line strength of $S = 8 \times 10^{-5}\,\text{cm}^{-2}/(\text{g/m}^3)$. (*a*) For a gas column 10 cm thick determine the mean spectral emissivity of the gas. (*b*) What happens if the pressure is increased to 20 atm? (Since no broadening parameters are known you may assume the effective broadening pressure to be equal to the total pressure.)

11.12 Repeat Problem 11.11 for a four-atomic gas.

11.13 1 kg of a gas mixture at 2000 K and 1 atm occupies a container of 1 m height. The gas consists of 70% nitrogen (by volume) and 30% of an absorbing species. It is known that, at a certain spectral location, the line half-width is $\gamma = 300\,\text{MHz}$, the mean line spacing is $d = 2000\,\text{MHz}$, and the line strength is $S = 100\,\text{cm}^{-1}\,\text{MHz}$. (*a*) Calculate the mean spectral emissivity under these conditions. (*b*) What will happen to the emissivity if the sealed container is cooled to 300 K?

11.14 A 50 cm thick layer of a pure gas is maintained at 1000 K and 1 atm. It is known that, at a certain spectral location, the mean line half-width is $\gamma = 0.1\,\text{nm}$, the mean line spacing is $d = 2\,\text{nm}$, and the mean line strength is $S = 0.002\,\text{cm}^{-1}\,\text{nm}\,\text{atm}^{-1} = 2\times10^{-10}\,\text{atm}^{-1}$. What is the mean spectral emissivity under these conditions? ($1\,\text{nm} = 10^{-9}\,\text{m}$)

11.15 The following data for a diatomic gas at 300 K and 1 atm are known: The mean line spacing is $0.6\,\text{cm}^{-1}$ and the mean line half-width is $0.03\,\text{cm}^{-1}$; the mean line strength (= integrated absorption coefficient) is $0.8\,\text{cm}^{-2}\,\text{atm}^{-1}$ (based on a pressure absorption coefficient). Calculate the mean spectral emissivity for a path length of 1 cm. In what band approximation is the optical condition?

11.16 The average narrow band transmissivity of a homogeneous gas mixture has, at a certain wavenumber η, been measured as 0.70 for a length of 10 cm, and as 0.58 for a length of 20 cm. What is the expected transmissivity for a gas column of 30 cm length, assuming the Malkmus model to hold?

11.17 1 kg of a gas mixture at 2000 K and 1 atm occupies a container of 1 m height. The gas consists of 70% nitrogen (by volume) and 30% of an absorbing species. It is known that, at a certain spectral location, the nitrogen-broadening line half-width at STP (1 atm and 300 K) is $\gamma_{n0} = 0.05\,\text{cm}^{-1}$, the self-broadening line half-width is $\gamma_{a0} = 0.02\,\text{cm}^{-1}$, the mean line spacing is $d = 0.4\,\text{cm}^{-1}$, and the density and mean line strength (for the given mixture conditions) are $\rho = 0.800\,\text{kg/m}^3$ and $\bar{S} = 4 \times 10^{-3}\,\text{cm}^{-1}/(\text{g/m}^2)$, respectively. Under these conditions collision broadening is expected to dominate.

(a) Calculate the mean spectral emissivity based on the height of the container.

(b) What will happen to the emissivity if the sealed container is cooled to 300 K at constant pressure (with fixed container cross-section and sinking top end)?

Note: The mean line intensity is directly proportional to the number of molecules of the absorbing gas and otherwise constant. The line half-width is given by

$$\gamma = [\gamma_{n0} p_n + \gamma_{a0} p_a] \sqrt{\frac{T_0}{T}} \qquad (p \text{ in atm}, T_0 = 300\,\text{K}),$$

where p_n and p_a are partial pressures of nitrogen and absorbing species.

11.18 A certain gas is known to behave almost according to the rigid-rotor/harmonic-oscillator model, resulting in gradually changing line strengths (with wavenumber) and somewhat irregular line spacing. Calculate the mean emissivity for a 1 m thick layer of the gas at 0.1 atm pressure. In the wavelength range of interest, it is known that the integrated absorption coefficient is equal to $0.80\,\text{cm}^{-2}\,\text{atm}^{-1}$, the line half-width is $0.04\,\text{cm}^{-1}$ and the average line spacing is $0.40\,\text{cm}^{-1}$.

11.19 A narrow band of a certain absorbing gas contains a single spectral line of Lorentz shape at its center. For a narrow band width of $\Delta\eta = 10\gamma$, determine the corresponding reordered k vs. g distribution. Hint: This can be achieved without a lot of math.

11.20 Consider the spectral absorption coefficient for a narrow band range of $\Delta\eta$ as given by the sketch. Carefully sketch the corresponding k-distribution. Determine the mean narrow band emissivity of a layer of thickness L from this k-distribution.

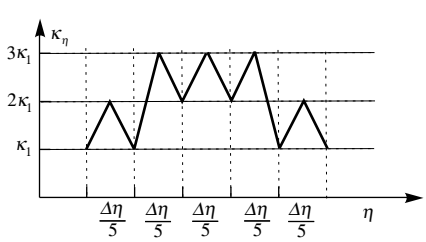

11.21 Consider the spectral absorption coefficient for a narrow band range of $\Delta\eta$ as given by the sketch. Carefully sketch the corresponding k-distribution. Verify your sketch through calculations.

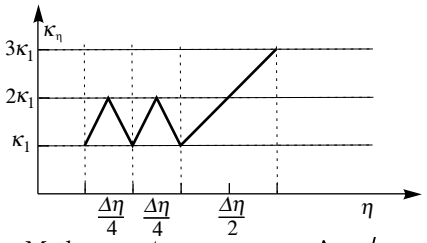

11.22 Consider the (highly artificial) absorption coefficient shown. Mathematically, this may be expressed as

$$\kappa_\eta = A[\eta + 3h(\eta)] \qquad 0 < \eta < \infty$$

where $h(\eta)$ is a periodic function of period $2d$, defined by

$$h(\eta) = \begin{cases} \eta, & 0 < \eta < d, \\ 2d - \eta, & d < \eta < 2d. \end{cases}$$

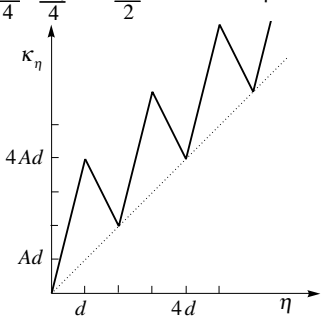

For a narrow band of $\Delta\eta = 10d$ and $0.5d < \eta < 10.5d$,

(a) find the k-distribution as well as the cumulative k-distribution,

(b) determine the narrow band average absorption coefficient $\bar{\kappa}_\eta$ by direct ($\eta-$) integration, and also from the k-distribution,

(c) determine the narrow band average transmissivity for a slab of thickness L from the k-distribution; compare with the gray-gas value (using $\overline{\kappa}_\eta$).

11.23 Consider again the gas of Problem 11.15, but replace the line intensity by

$$S_{p\eta} = S_{p\eta_0}\, e^{-|\eta-\eta_0|/\omega}, \quad S_{p\eta_0} = 0.02\,\mathrm{cm^{-2}\ atm^{-1}}, \quad \omega = 20\,\mathrm{cm^{-1}}.$$

In what regime is this optical condition? What is the total band absorptance?

11.24 A mixture of nitrogen and sulfur dioxide (with 0.05 volume-% SO_2) is at 1 atm and 300 K. For the strong ν_3 band of SO_2, centered at $\eta_3 = 1361\,\mathrm{cm^{-1}}$, it is known that

$$\frac{\gamma_\eta}{d} \simeq 0.06, \quad \frac{S_\eta}{d} = 17\,\mathrm{cm^{-1}\ atm^{-1}}\ \exp\left[-\left(\frac{\eta-\eta_3}{25\,\mathrm{cm^{-1}}}\right)^2\right].$$

For a 10 cm thick gas-mixture layer:

(*a*) Develop an expression for the average spectral emissivity.

(*b*) Calculate the total band absorptance.

(*c*) For comparison, calculate the total band absorptance from the wide band model. (Hint: For 300 K it is known that $\beta^*/\beta_0^* > 1$.)

Note: Under these conditions collision broadening is the predominant broadening mechanism.

11.25 A gas mixture at 1500 K and 1 atm is known to contain a small amount of CO_2. To remotely determine the partial pressure of CO_2 the band absorptance of the CO_2 4.3 μm band is measured and is found to be $100\,\mathrm{cm^{-1}}$ for a path length of 1 m. Assuming that the gas may be treated as a nitrogen–CO_2 mixture, determine the partial pressure of the CO_2.

11.26 Nitrogen at 2000 K and 1 atm contains a small amount of water vapor. To remotely determine the water vapor concentration the contribution of the 6.3 μm band toward the total emissivity is measured, and is found to be $\epsilon_{6.3} = 0.012$ for a 1 m thick isothermal gas layer. Determine the mole fraction of water vapor.

11.27 A large moon in the outer solar system has a thin atmosphere of pure methane. In order to determine average temperatures of the atmosphere, a satellite measures the total band absorptance of the 3.3 μm fundamental band at an altitude where the atmospheric pressure is 100Pa. If the total band absorptance for a 100 km thick layer is measured as $A_{3.3} = 259\,\mathrm{cm^{-1}}$, determine the temperature of the atmosphere (this may be left in the form of an implicit expression).
Note: At the expected cold temperature (< 200K) you may assume $\gamma \simeq \gamma_0 \neq \gamma(T)$.

11.28 A mixture of nitrogen and sulfur dioxide is at 1 atm total pressure. To measure the partial pressure of the sulfur dioxide in a furnace environment, an instrument is used that measures total band absorptance for the strong SO_2 band centered at $\eta_c = 1361\,\text{cm}^{-1}$. For that band it is known that $\alpha = 2340\,(T_0/T)\,\text{cm}^{-2}\,\text{atm}^{-1}$, $\beta = 0.357\sqrt{T/T_0}P_e$, $\omega = 8.8\sqrt{T/T_0}\,\text{cm}^{-1}$, $b = 1.28$, and $n = 0.65$. What is the partial pressure of the sulfur dioxide if the total band absorptance has been measured as $142\,\text{cm}^{-1}$ for a 1 m thick gas layer at $T = 1600\,\text{K}$?

11.29 An optical device to determine NO_x content in the combustion products powering a gas turbine measures the transmissivity of NO for its 5.3 μm band. The device consists of a blackbody source ($T_{bb} = 2000\,\text{K}$), two ports, a filter/detector combination (with flat response $1750\,\text{cm}^{-1} < \eta < 2000\,\text{cm}^{-1}$, and zero response elsewhere), and a chopper (such that the detector registers radiation from the blackbody source, but not the emission from the combustion gases). Two measurements are taken: one with an inert gas in the turbine (signal S_0), and another with combustion gases present (assume $T_g = 1600\,\text{K} = \text{const}$, $p_g = 5\,\text{bar} = \text{const}$, light path through gas $L = 1\,\text{m}$; signal S).

(a) Show that the measured transmissivity, t, is

$$\tau \equiv \frac{S}{S_0} = 1 - \frac{\omega}{\Delta\eta}A^*(T_g, p_g, L, x_{\text{NO}}), \qquad \Delta\eta = 250\,\text{cm}^{-1},$$

where x_{NO} is the volume or mole fraction of NO, and assuming that the Planck function is constant across $\Delta\eta$.

(b) If the transmissivity is measured as $\tau = 0.7$, what is the NO volume fraction, x_{NO}?

Note: For NO at 1600 K, $\beta^*/\beta_0^* = 0.827$.

11.30 It is desired to predict the fraction of the sunlight absorbed by the nitrous oxide (N_2O) contained in the atmosphere. You may assume that the atmosphere is a 20 km high layer of N_2–N_2O mixture, that the atmosphere is isothermal with a linear pressure variation from 1 atm at the ground to zero at the top of the atmosphere, and that N_2O makes up 10^{-4}% by volume of the mixture everywhere.

N_2O has two vibration–rotation bands with the following wide band coefficients (at the temperature of the atmosphere):

	α	β^*	ω	n	b
4.5 μm band	$2035\,\text{cm}^{-2}\,\text{atm}^{-1}$	0.145	$22\,\text{cm}^{-1}$	0.6	1.12
7.8 μm band	$161\,\text{cm}^{-2}\,\text{atm}^{-1}$	0.377	$18.5\,\text{cm}^{-1}$	0.6	1.12

(*a*) Show that the influence of the 7.8 μm band is negligible.

(*b*) Calculate the total absorptivity for this atmosphere assuming a constant average pressure of 0.5 atm.

(*c*) Show that the absorptivity is the same as in (*b*) if the linear pressure variation is taken into account. Hint: You may assume that the pressure-based absorption coefficient, $\kappa_{p\eta}$, is independent of pressure.

11.31 Nitrous oxide (N_2O) is contained in the Earth's atmosphere with a partial pressure of 10^{-6} atm. While N_2O causes pollution, it may also be employed for remote sensing applications. N_2O has two vibration–rotation bands with the wide band coefficients (at the temperature of the atmosphere) given in Problem 11.30.

(*a*) It is known that, for a distance of $L_1 = 1$ km through the atmosphere, the 4.5 μm band has a certain total band absorptance A_1. What length through the atmosphere, L_2, is required to obtain the same band absorptance with the 7.8 μm band, $A_2 = A_1$?

(*b*) Would this ratio L_2/L_1 increase, decrease, or stay the same if L_1 was decreased?

11.32 In a combustor the air–fuel ratio is controlled by measuring the total band absorptance of the fuel (methane) for its 3.3 μm band. The mixture's inlet conditions are 1 atm total pressure, temperature is 400 K, combustor diameter is $L = 10\,\text{cm}$, and the design mole fraction for methane is 25%. If the total band absorptance across the diameter is measured as $A_{3.3} = 112\,\text{cm}^{-1}$, what is the exact methane mole fraction at that time?

11.33 A 1 m thick layer of a mixture of nitrogen and methane (CH_4) at T = 300 K and $p = 1\,\text{atm}$ has a measured total emissivity of $\epsilon = 0.010$. Estimate the partial pressure of the methane ($R_{\text{CH}_4} = 5.128 \times 10^{-6}\,\text{atm}\,\text{m}^3/\text{g}\,\text{K}$). It is known that $p_{\text{CH}_4} \ll p$.

11.34 A mixture of water vapor and nitrogen at a total pressure of 1 atm and a temperature of 300 K is found to have a total band absorptance of 100 cm^{-1} for the 6.3 μm band for a geometric path length of 50 cm. Determine the partial pressure of the water vapor.

11.35 One method of measuring the temperature of a high-temperature gas is to determine the total band absorptance of a vibration–rotation band of the gas under the prevailing conditions. Consider a 20 cm thick layer of pure methane, CH_4, at 1 atm pressure. If the total band absorptance of the 3.3 μm band is 587 cm^{-1}, what is the temperature of the CH_4?
Note: Such instruments are generally used only for $T > 1000°C$.

11.36 Estimate the total band absorptance of the 2.7 μm CO_2 band at 833 K, a total pressure of 10 atm, a partial pressure of 1 atm, and a mass-path length of $\rho_{CO_2} L = 2440$ g/m^2, from Fig. 1-16. Compare with the result from the exponential wide band model.

11.37 A mixture of nitrogen and sulfur dioxide (with 5% SO_2 by volume) is at 1 atm total pressure. To measure the temperature of the mixture in a furnace environment ($T > 1000$ K), an instrument is used that measures total band absorptance for the strong SO_2 band centered at $\eta_c = 1361$ cm^{-1}. For that band it is known that $\alpha = 2340\,(T_0/T)$ cm^{-2} atm^{-1}, $\beta = 0.357\sqrt{T/T_0}P_e$, $\omega = 8.8\sqrt{T/T_0}$ cm^{-1}, $b = 1.28$ and $n = 0.65$. What is the temperature of the mixture if the total band absorptance has been measured as 142 cm^{-1} for a 1 m thick gas layer?

11.38 The Earth's pollution with sulfur dioxide (SO_2)is determined by measuring the transmission of a light beam from a satellite. Assuming that the band absorptance of the 7.3 μm band has been measured as 10.0 cm^{-1}, and that the atmosphere may be approximated as a 10 km thick isothermal layer of nitrogen (with a trace of SO_2) at 0.5 atm and $-10°C$, determine the volume fraction of SO_2. Use `wbmso2` from Appendix F to calculate the overlap parameter β or use $\beta \simeq 0.357\sqrt{T/T_0}P_e$.

11.39 To determine the average atmospheric temperature on a distant planet, the total band absorptance for the 3.3 μm CH_4 band has been measured as $A_{3.3} = 100$ cm^{-1}. It is known from other measurements that methane is a trace element in the atmosphere (which contains mostly nitrogen and whose total pressure is 2 atm), and that the absorption path length for methane on that planet, for which $A_{3.3}$ was measured, is 4.14 g/m^2. What is the temperature?

11.40 Using the exponential wide band model, evaluate the total emissivity of a 1 m thick layer of a nitrogen–water vapor mixture at 2 atm and 400 K if the water vapor content by volume is (*a*) 0.01%, (*b*) 1%, or (*c*) 100%. Compare with Leckner's model using subroutine `totemiss`.

11.41 Using the exponential wide band model, evaluate the total emissivity of a 1 m thick layer of a nitrogen–CO_2 mixture at 0.75 atm and 600 K if the CO_2 content by volume is (*a*) 0.01%, (*b*) 1%, or (*c*) 100%. Compare with Leckner's model using subroutine `totemiss`.

11.42 Evaluate the Planck-mean absorption coefficients for the two gases in Problems 11.40 and 11.41, based on the data given in Table 11.3. Compare the results with Fig. 11-31.

11.43 Write a small computer program that calculates the total emissivity of a CO_2–inert gas mixture, based on wide band property data from Table 11.3, as a function of temperature, pressure, CO_2 volume fraction, and path length. For a given set of pressure, volume fraction, and length, compare with values obtained from Leckner's model using subroutine `totemiss` and plot the emissivity as a function of temperature.

11.44 Repeat Problem 11.40 for a path with a temperature profile given by $T = 300\,\text{K}[1 + 4s(L-s)/L^2]$, where s is distance across the gas layer.

11.45 Develop a simple box model for the evaluation of the effective band width, i.e., $A = \int_0^\infty \epsilon_\eta \, d\eta = \bar{\epsilon}_\eta \, \Delta\eta$, based on an average emissivity (rather than absorption coefficient). You may assume that the line spacing and line intensity are constant across the band. Calculate the total band absorptance of water vapor at 0.1 atm and 400 K for path lengths of 1 mm and 1 m, assuming that $\Delta\eta \approx \omega$, where ω is the band width parameter from the exponential wide band model. Compare with results from that model.